DOCTOR OF PHILOSOPHY

Modelling of physical vapour deposition (PVD) process on cutting tool using response surface methodology (RSM)

Abd Rahman, Md Nizam

Award date:
2009

Awarding institution:
Coventry University

MODELLING OF PHYSICAL VAPOUR DEPOSITION (PVD) PROCESS ON CUTTING TOOL USING RESPONSE SURFACE METHODOLOGY (RSM)

Md Nizam Abd Rahman

A thesis submitted in partial fulfilment of the University's requirements for the Degree of Doctor of Philosophy

September 2009

Coventry University
in collaboration with
the Universiti Teknikal Malaysia Melaka

ACKNOWLEDGEMENTS

First and foremost, my deepest appreciation to my main supervisor and Director of Studies, Dr Philip Swanson not only for the invaluable guidance, ideas and support but also for going the extra miles in ensuring this split site PhD program logistical issues being addressed in timely manner. Your efficiency and responsiveness in reviewing my work through email communication would make any research student envious. I am also appreciative of your willingness to supervise me late in my PhD program, taking over the responsibility from my previous Director of Studies, Professor Ashraf Jawaid.

My appreciation also to Professor Dr Mohd Razali bin Muhamad for his guidance and for giving me enough freedom to define the direction of my research. My deepest gratitude for your help to somehow come up with enough fund to purchase the PVD machine and save this research when everything else fell apart. I would also like to acknowledge Dr Paul Briskham for his advice and critical review of my research proposal.

I am indebted to UTeM and the Government of Malaysia for providing the financial support throughout my study.

My journey in pursuant of this research program will not be possible if not for the sacrifice and constant prayers from my family especially my parents, Abd Rahman Abd Hadi and Hatijah Abdullah, my wife, Liza Suryani Ilias, and my wonderful children, Lutfi, Hanna, Najwa, Alya, Muhammad and Ahmad. Without them, the journey would become less meaningful.

I pray to Allah, whom I owed the knowledge, strength and determination to complete this research, to bless us all.

ABSTRACT

The Physical Vapour Deposition (PVD) magnetron sputtering process is one of the widely used techniques for depositing thin film coatings on substrates for various applications such as integrated circuit fabrication, decorative coatings, and hard coatings for tooling. In the area of coatings on cutting tools, tool life can be improved drastically with the application of hard coatings. Application of coatings on cutting tools for various machining techniques, such as continuous and interrupted cutting, requires different coating characteristics, these being highly dependent on the process parameters under which they were formed. To efficiently optimise and customise the deposited coating characteristics, PVD process modelling using RSM methodology was proposed. The aim of this research is to develop a PVD magnetron sputtering process model which can predict the relationship between the process input parameters and resultant coating characteristics and performance. Response Surface Methodology (RSM) was used, this being one of the most practical and cost effective techniques to develop a process model. Even though RSM has been used for the optimisation of the sputtering process, published RSM modelling work on the application of hard coating process on cutting tool is lacking.

This research investigated the deposition of TiAlN coatings onto tungsten carbide cutting tool inserts using PVD magnetron sputtering process. The input parameters evaluated were substrate temperature, substrate bias voltage, and sputtering power; the out put responses being coating hardness, coating roughness, and flank wear (coating performance). In addition to that, coating microstructures were investigated to explain the behaviour of the developed model. Coating microstructural phenomena assessed were; crystallite grain size, XRD peak intensity ratio I111/I200 and atomic number percentage ratio of Al/Ti.

Design Expert 7.0.3 software was used for the RSM analysis. Three process models (hardness, roughness, performance) were successfully developed and validated. The modelling validation runs were within the 90% prediction interval of the developed models and their residual errors compared to the predicted values were less than 10%. The models were also qualitatively validated by justifying the behaviour of the output responses (hardness, roughness, and flank wear) and microstructures (Al/Ti ratio, crystallographic peak ratio I111/1200, and grain size) with respect to the variation of the input variables based on the published work by researchers and practitioners in this field. The significant parameters that influenced the coating hardness, roughness, and

performance (flank wear) were also identified. Coating hardness was influenced by the substrate bias voltage, sputtering power, and substrate temperature; coating roughness was influenced by sputtering power and substrate bias; and coating performance was influenced by substrate bias.

The analysis also discovered that there was a significant interaction between the substrate temperature and the sputtering power which significantly influenced coating hardness, roughness, and performance; this interaction phenomenon has not been reported in previously published literature. The correlation study between coating characteristics, microstructures and the coating performance (flank wear) suggested that the coating performance correlated most significantly to the coating hardness with Pearson coefficient of determination value (R^2) of 0.7311. The study also suggested some correlation between coating performance with atomic percentage ratio of Al/Ti and grain size with R^2 value of 0.4762 and 0.4109 respectively.

TABLE OF CONTENTS

CHAPTER	TITLE	PAGE
	ACKNOWLEDGEMENTS	i
	ABSTRACT	ii
	TABLE OF CONTENTS	iv
	LIST OF TABLES	vii
	LIST OF FIGURES	ix
	LIST OF ABBREVIATION AND SYMBOLS	xii
	LIST OF APPENDICES	xiv
1.0	Introduction	1
1.1	Problem Statement	5
1.2	Research objectives	6
1.3	Scope	6
2.0	Literature Review	8
2.1	PVD DC Magnetron Sputtering	9
2.1.1	Sputtering process	10
2.1.2	Bombardment of ions, neutral, and electrons on growing film	12
2.1.3	Sputtering of alloys and reactive sputtering	13
2.1.3.1	Sputtering of alloy	13
2.1.3.2	Reactive sputtering	14
2.2	Critical PVD magnetron sputtering process parameters	15
2.2.1	Substrate bias voltage	17
2.2.2	Sputtering power	20
2.2.3	Substrate temperature	22
2.2.4	Gas pressure	25
2.2.5	Summary and discussion of process parameter selection to be studied	27
2.2.5.1	Parameters to be selected as inputs to the model	27
2.2.5.2	Contradiction on trend of process parameters and resultant coating characteristics and performance	28
2.3	Coating characterization method	29

2.3.1 Selection of elemental composition analysis technique 30
2.3.2 Selection of hardness analysis technique 31
2.4 Empirical modelling technique: Response Surface Methodology (RSM) 32
2.4.1 Response Surface Methodology (RSM) 32
2.4.2 Application of RSM in process optimisation and modelling 34

3.0 Methodology 37
3.1 PVD modeling experiment 39
3.1.1 Experimental matrix 42
3.2 Coating Characterization Methods 44
3.2.1 Scanning Electron Microscopy (SEM) –Energy Dispersive X-ray (EDX) 45
3.2.2 X-ray diffraction (XRD) 47
3.2.3 Atomic force microscopy (AFM) 50
3.2.4 Nano-indenter test 51
3.2.5 Turning test to determine coating performance 53
3.3 RSM data analysis 56
3.4 Validation of the process model 59
3.5 Correlation between coating performance and coating characteristic and coating microstructure 60

4.0 Results and Discussions 62
4.1 Modelling of the deposited TiAlN coating hardness, roughness, and wear performance 63
4.1.1 RSM modelling of TiAlN hardness with respect to PVD magnetron sputtering process parameters. 63
4.1.2 RSM modelling of TiAlN coating surface roughness with respect to PVD magnetron sputtering process parameters 74
4.1.3 RSM modelling of TiAlN coated tool wear performance during turning operation with respect to PVD magnetron sputtering process parameters 83
4.1.4 Modelling summary 94

4.2 Microstructural analysis of the developed TiAlN coating as a function of substrate bias voltage, substrate temperature and sputtering power variation 96

4.2.1 Analysis on the effect of substrate bias voltage variations 98
4.2.2 Analysis on the effect of substrate temperature variations 102
4.2.3 Analysis on the effect of sputter power variations 106
4.3 The interaction between sputtering power and substrate temperature
4.4 Correlation between coating performance, coating characteristics and microstructures 115
4.5 Summary of experimental results 122
5.0 Conclusions 124
5.1 New contributions to body of knowledge 126
5.2 Future work 127

REFERENCES 128

APPENDICES 139

LIST OF TABLES

TABLE	TITLE	PAGE
2.1	Literature on the study of the influence of coating parameters on coating characteristics and performance	16
2.2	A list of published studies on the impact of negative substrate bias on coating characteristics and performance. The evaluated range of substrate bias is also indicated.	19
2.3	List of published studies on the impact of sputtering power on coating characteristics and performance. The evaluated power range is also indicated.	21
2.4	A list of published studies on the impact of substrate temperature and sputtering power on coating characteristics and performance. The evaluated temperature range is indicated.	24
2.5	List of published studies on impact of gas pressure on coating characteristic and performance and the evaluated range.	26
2.6	Thin film coating characterization techniques	29
2.7	Characterization and analysis techniques	30
2.8	The optimization and modelling applications of RSM	35
3.1	Sumitomo SPGN120308S cutting tool dimensions	40
3.2	Extreme operating window for respective process parameters	43
3.3	PVD process modelling experimental matrix based on RSM central composite design approach	44
3.4	The characterization equipment used with the respective intended coating characteristic/performance data to be collected.	45
3.5	AISI D2 steel chemical composition	55
3.6	Summary of single point turning conditions	56
3.7	Experimental matrix and the output response table	59
4.1	Experimental run and results of coating hardness	64
4.2	Sequential model sum of squares (SMSS) analysis for hardness model	65
4.3	Lack of fit test for hardness model	65
4.4	ANOVA analysis of the quadratic model for coating hardness	66
4.5	ANOVA analysis of the Reduced Cubic Model for coating hardness	67
4.6	Validation data of coating hardness model	73
4.7	Experimental run and results of coating roughness	74
4.8	Sequential model sum of squares for coating roughness model	75
4.9	Lack of fit test for coating roughness model	75
4.10	ANOVA for coating roughness model	76
4.11	Summary of validation run for surface roughness model	82
4.12	Experimental run and results of cutting tool performance (flank wear)	83
4.13	Sequential model sum of squares to determine the appropriate polynomial model for coating wear performance	84

4.14	Lack of fit test to determine the appropriate polynomial model for coating wear performance	85
4.15	The ANOVA analysis for the quadratic model of coating wear performance	86
4.16	The ANOVA analysis for the reduced cubic model of coating wear performance	87
4.17	Summary of validation run for coating wear performance	93
4.18	Polynomial equations to represent the developed models	94
4.19	The PVD parameters and interactions that significantly influence the respective developed models	95
4.20	Experimental run with variation in substrate bias voltage and constant substrate temperature and sputtering power	96
4.21	Experimental run with variation in substrate temperature and constant substrate bias voltage and sputtering power	96
4.22	Experimental run with variation in sputtering power, constant substrate temperature and substrate bias voltage	96
4.23	TiAlN coating characteristics and microstructure data as substrate bias voltage varies	98
4.24	TiAlN coating characteristics and microstructure data as substrate temperature varies	102
4.25	The quantitative data from the XRD and EDX analysis for TiAlN coating as the sputtering power increases	108
4.26	Compilation of TiAlN coating performance, characteristics, and microstructure data for correlation study.	116
4.27	Summary of coefficient of determination values for the correlation studies between flank wear and coating characteristic/ microstructure data.	118
4.28	Summary of the behaviour of the deposited TiAlN coating with changes PVD process parameters	123

LIST OF FIGURES

FIGURE	TITLE	PAGE
2.1	Schematic representation of the magnetron sputtering process	12
2.2	Cross-sectional TEM micrograph obtained from the middle portion of a 3.5-microns thick TiN layer grown by reactive magnetron sputtering deposition on a steel substrate at 300 °C (Petrov et al. 2003)	18
2.3	Thornton model (Mattox 1998).	23
3.1	Methodology of PVD process modelling development	37
3.2	Overall approach of PVD process modelling study	38
3.3	(a) PVD unbalanced magnetron sputtering system VACTEC Korea model VTC PVD 1000. (b) Substrate holder inside coating chamber	39
3.4	Tungsten carbide cutting tool insert commercially made by Sumitomo	40
3.5	RSM Central Composite Design for 3 factors at two levels	42
3.6	SEM/EDX LEO 1525 apparatus.	46
3.7	Signals produced when an electron beam interacts with the sample	46
3.8	Schematic illustration of an x-ray diffraction setup	47
3.9	Schematic illustration of diffraction according to Bragg's law	48
3.10	Bruker D-8 XRD apparatus with GIA capability	49
3.11	AFM Shimadzu model SPM-9500J2 apparatus	51
3.12	A typical loading/unloading curve for nano-indentation test	52
3.13	NanoTest nano-indentation system	53
3.14	Flank wear measurement method for tool insert in single point turning operation based on ISO 3685:1993(E) standard.	54
3.15	GATE-Precision milling machine and lathes model G-410-TCV	55
3.16	Summary of RSM analysis flow	57
4.1	Behaviour of coating hardness in response to variation of substrate bias voltage	68
4.2	Behaviour of coating hardness in response to variation in substrate temperature.	69
4.3	Behaviour of coating hardness in response to variation of sputtering power	70
4.4	Interaction between sputtering power and substrate temperature with respect to coating hardness	71
4.5	Influence of quadratic function of substrate bias and significant influence of sputtering power on coating hardness	72
4.6	Behaviour of coating roughness in response to variation of sputtering power	77
4.7	Behaviour of coating roughness in response to variation of substrate bias voltage	78
4.8	Behaviour of coating roughness relative to interaction between sputtering power and substrate temperature	79

4.9	Response surface model holding substrate temperature at constant 400°C	80
4.10	Significant influence of quadratic term of substrate bias while holding sputtering power at 6 kW	81
4.11	Influence of substrate bias voltage on the tool wear performance of the coated cutting tool	89
4.12	Interaction between sputtering power and substrate temperature Influencing wear performance of TiAlN coating	90
4.13	Response surface model for flank wear while holding substrate temperature constant at 400°C	91
4.14	Response surface model for flank wear while holding substrate bias at -175V	92
4.15	Response surface model for flank wear while holding sputtering power constant at 6 kW	92
4.16	Effect of substrate bias variation on the hardness, roughness, and tool wear performance	98
4.17	2θ vs. intensity curves for the XRD analysis for substrate bias voltage of -50 V, -175 V and -300 V	99
4.18	AFM image (with imbedded SEM image) indicating the transformation of grain size and morphology of TiAlN coating as the substrate bias increases	101
4.19	Effect of substrate temperature variation on the hardness, roughness, and tool wear performance	102
4.20	The 2θ vs. intensity XRD curves for substrate temperature of 200 °C, 400 °C and 600 °C	103
4.21	AFM images reflecting the change in grain size as the substrate temperature (Ts) changes from 200 °C to 600 °C	105
4.22	Effect of sputtering power variation on the hardness, roughness, and tool wear performance	106
4.23	The 2θ vs. intensity XRD curves for sputtering power of 4 kW,6 kW and 8 kW	108
4.24	AFM images reflecting the reduction in grain size as the sputtering power (Ps) changes from 4 kW to 8 kW	109
4.25	Interaction behaviour of substrate temperature and sputtering power	111
4.26	XRD curves to compare the effect of interaction between sputtering power and substrate temperature	112
4.27	Interaction effect between substrate temperature and sputtering power on the TiAlN coating morphology.	114
4.28	Correlation between flank wear and I111/1200 ratio	116
4.29	Correlation between flank wear and atomic percentage ratio of aluminium to titanium in the TiAlN coating	117
4.30	Correlation between flank wear and grain size of TiAlN coating	117
4.31	Correlation between flank wear and roughness of TiAlN coating	117
4.32	Correlation between flank wear and TiAlN coating hardness	118
4.33	A typical flank wear image from the experiment	119

4.34 Diffusion wear on the minor cutting edge of the cutting tool 120
4.35 SEM and EDX analysis performed on the diffusion wear area 121
4.36 SEM and EDX analysis performed on wear area associated to friction 121
.

LIST OF ABBREVIATION AND SYMBOLS

Å	Ångstrom
ω	Angle of the incident beam
θ	Diffraction angle
λ	Wavelength of the x-ray radiation
2FI	Two factor of interaction
AFM	Atomic force microscopy
ANOVA	Analysis of variance approach
a_p	Depth of cut
Ar	Argon
A_r	Residual indentation area during nano-indenter test
d	Interplanar spacing of the diffracting atomic planes
B	Line broadening at half the maximum intensity in radians
C	Carbon
CCD	Central Composite Design
Cr	Chromium
CVD	Chemical vapour deposition
D	Grain size
DOE	Design of experiment
e	Elementary charge
E_p	Energy per deposited atom
E_i	Energy of ions
EDX	Energy Dispersive X-ray
FWHM	Full Width Half the Maximum intensity
GPa	Giga Pascal
L_c	Cutting length
Mbar	Millibar
Mo	Molybdenum
MQL	Minimum Quantity Lubrication
P	Maximum load on nano-indenter test
PI	Predictive interval
P_s	Sputtering power

PVD	Physical Vapour Deposition
R	Pearson product moment correlation coefficient
Rpm	Revolutions per minute
RSM	Response Surface Methodology
Sccm	Standard Cubic Centimeters per Minute
SEM	Scanning Electron Microscopy
SME	Small and medium enterprises
SMSS	Squares sequential model
SNMS	Secondary neutral-mass spectrometry
TEM	Transmission electron microscopy
T_s	Substrate temperature
TiO_2	Titanium Dioxide
TiAl	Titanium Aluminium
TiN	Titanium nitride
TiAlN	Titanium aluminium nitride
V	Vanadium
V_p	Plasma potential
V_c	Cutting speed
V_s	Substrate bias voltage
V_{wp}	Volume of workpiece material removed
V_i/V_m	Ratio of flux ion to flux particle bombarding the growing film
XPS	X-ray photoelectron spectroscopy
XRD	X-ray diffraction

LIST OF APPENDICES

APPENDIX	TITLE	PAGE
A	Nano-indenter hardness data	A-1
B	AFM coating surface roughness data	B-1
C	Flank wear measurement data	C-1
D	XRD data	D-1
E	EDX Data	E-1

CHAPTER 1

INTRODUCTION

Background of study

This research project is part of a programme funded by the Malaysian Government to enable the cutting tool coating industry among small and medium enterprises (SME's) in Malaysia. One of the "help needed areas" identified is to develop a method for practical and cost effective coating process optimization that potentially gives cost competitiveness and process flexibility advantages.

1.0 Introduction

The main objective of thin film coating applications is to improve the surface properties of an artefact while maintaining its bulk properties. The application of thin film coatings on cutting tools is to improve cutting tool performance by enhancing the surface properties of the tool. The improved performance of coated cutting tools has been proven and documented. Some of the published works supporting this claim are Laing et al. 1999, Gekonde and Subramanian 2002, Byrne and Scholta 1993, and Tuffy et. al. 2004. One particular study done by Tuffy et. al. (2004) indicated that coated tool wear performance was forty times better than the uncoated tools. Aside from prolonging tool life, coated tools can also enable the implementation of Minimum Quantity Lubrication (MQL) and pursuant of dry machining. This can drastically reduce manufacturing costs associated with cutting fluids, which attribute ~15% of metal cutting manufacturing costs

and minimize environmental impacts associated with disposal of cutting fluid (Byrne and Scholta 1993).

One of the main challenges in surface coating technologies is to develop cost efficient coating processes such that the improvement in performance can offset the coating process cost. (Bradbury and Huyanan, 2000). If this can be accomplished, the end users' adoption of coated cutting tools can be ensured.

Other than cost, having the capability to customize coating properties for intended machining applications can also provide value added advantages to the industry. Different cutting applications might require different coating characteristics as indicated by the following studies: Settineri and Faga (2006) suggested that for the interrupted cutting process; coating adhesion and toughness were more important than hardness in determining cutting tool performance; Weber et al.(2004) indicated that compressive stresses in the deposited coating influence drilling performance; Bouzakis et al. (2007) indicated that for continuous cutting operations such as milling, coating impact strength and hardness could be correlated to the cutting tool performance.

One approach to address both the cost and customization of coating process needs is by developing a process model. Having developed a process model that can predict the output response of the coating process based on the input parameters, process optimization can be performed efficiently. Resource wastage such as material, equipment utilization plus human resources related to a trial and error experimental

approach, can be minimized. By virtue of the developed process model, the desired coating characteristic for its specific application can also be predicted.

Modelling work in PVD thin film coating processes can be categorized into two groups; theoretical method and empirical methods. The theoretical methods are mainly based on the Monte Carlo method (Han and Lee 2005) and direct mathematical modelling (Song et. al 2005). The Monte Carlo modelling approach requires extensive investment in computing hardware and highly specialized skills; direct mathematical modelling requires highly specialized skills in conducting process characterization of the coating, substrate, and process combination. These requirements can be a hindrance for SME companies for practical day-to-day operational application.

Empirical process optimization and modelling work on PVD processes, reported in the literature, follow methodologies such as full factorial design of experiment (Deng et al. 2006), Taguchi method (Keles et al. 1999; Chou et al. 2003; Yu et al. 2008), and response surface modelling (RSM) (Axelevitch and Golan 2007). The full factorial method is more suitable for process optimization. The Taguchi method cannot detect interaction effects in the process (Bisgaard and Diamond 1990). The RSM approach meets the requirement for both optimization and modelling needs. It uses mathematical and statistical techniques to represent the domain of all feasible solutions for the process model (Box et al. 1978) and is the best method for an empirical study of the relationships between one or more of the measured response functions.(Voznesensky 1974). The work

on RSM by Axelevitch and Golan (2007) was focused on microelectronic applications, looking at the transparency and resistivity characteristics of thin films.

In order to assist the SME companies, especially in Malaysia, that are involved in PVD thin film coating technology, a study of process modelling for PVD through the utilization of Response Surface Methodology (RSM) approach was proposed. It is the most practical solution compared to the theoretical approach and meets the need to both optimize and develop process modelling. The RSM analysis was done using Design Expert 7.0.3 software, which is very affordable for SMEs.

In developing coating processes, understanding factors that influence coating performance is imperative. Musil and Vlcek (1998) and Mayrhofer et al. (2006) stated that the three main factors that significantly influence coating characteristics and performance are: particle bombardment of growing film, substrate temperature, and composition of elements in coating material. This research focuses on ion bombardment and temperature effects only. Since ion bombardment is influenced by process parameters (Smith 1995) and substrate temperature is also one of PVD process parameters, the modelling work will only focus on these process parameters as the input variables to the model.

1.1 Problem Statement

A cost efficient PVD process modelling technique is imperative in pursuant of hard coating process optimisation and customisation. The Monte Carlo method and direct mathematical modelling of PVD processes for hard coating applications require resources, both capital and human, which might be prohibitive for operational application (Han and Lee 2005, Song et. al 2005). Empirical modelling techniques such as full factorial design of experiment (DOE) and Taguchi's methods are lacking in their ability to predict the output response in non-linear systems and interaction phenomena respectively (Anderson and Whitcomb 2005, Bisgaard and Diamond 1990).

RSM meets both cost efficient optimization and the customization of coating process needs. Application of RSM in modelling and optimisation has been proven in various fields ranging from food products to electronic technology (Deshpande et al. 2008, Lofty et al. 2007, Axelevitch and Golan 2007). Its wide adoption is due to its practicality, its economy, and its relative ease of use (Shokuhfar et al. 2008). Some of the process optimization or modelling works using RSM approach on PVD sputtering process have been published (Adamczyk et al. 2008, Axelevitch and Golan 2007); however these works focus on the microelectronic application with the transparency, resistivity, and crystal preferred orientation as the output responses. Published work of RSM modelling on PVD sputtering technique for hard coating application is lacking.

1.2 Research objectives

The purpose of this research is to develop a PVD coating process model using RSM to predict the relationship between the input parameters of the PVD coating process and characteristics and performance of the coated cutting tools so that customization of process optimization can be done cost efficiently.

Specific objectives of this research are:

- To develop a model in the form of predictive mathematical equations that define the relationships between the PVD coating process parameters and the characteristics and performance of the coated cutting tools using RSM.
- To identify PVD process parameters that influence coating performance.
- To identify interaction phenomena between the input process parameters.
- To validate the mathematical model prediction against actual coating performance and characteristics.
- To define the coating characteristics and microstructures that correlate with its machining performance.

1.3 Scope

The scope of this research is to develop empirical modelling of PVD magnetron sputtering process of TiAlN coating onto the tungsten carbide cutting tool inserts. The modelling work is based on the response surface methodology (RSM). The TiAlN coating is selected for this study because it was one of the widely used coatings for

machining applications, due to its superior performance at elevated temperature compared to TiN coating (Razali et al. 2006). The RSM statistical analysis used in developing the model is carried out using Design Expert 7.0.3 software which is widely used for RSM analysis in various research areas (Zinatizadeh et al. 2006, Benyounis et al. 2005, Kalavathy M. 2009, Aktas et al. 2006).

CHAPTER 2

LITERATURE REVIEW

2.0 Literature Review

In this section a critical review of published work is carried out to achieve the following objectives:-

• To provide a general review of the PVD magnetron sputtering process.

• To identify the critical PVD process parameters so that appropriate parameters can be chosen as the input parameters of the modelling work.

• To identify critical coating characteristics and microstructures that correlate with improved coating performance. The identified coating characteristics and microstructures will be designated as the output responses of the modelling and the behaviour of the developed models will be explained.

• To review the response surface methodology (RSM) as the selected experimental approach for this modelling study.

2.1 PVD DC Magnetron Sputtering

Two main techniques in vacuum coating process are physical vapour deposition (PVD) and chemical vapour deposition (CVD). The fundamental difference between the two processes is the vapour source. As the name indicates, the vapour source for PVD originates from a solid target from which atoms are displaced and vapour source for CVD originates from a chemical vapour precursor. In PVD process, the vapourization of the solid target may be done through heating or sputtering; this work focuses on the PVD sputtering process only.

The PVD sputtering process involves the ejection of particles from target material due to the collision of highly energetic projectile particles (e.g. argon ions) with the target surface (Bunshah 1994). Some of the earliest sputtering experiments were reported by W R Grove in 1852, M Faraday in 1854, and Julius Pluker in 1958 (Mattox 2003). Since then many advances in sputtering processes have been achieved. Advances in magnetron sputtering, controlled reactive sputtering, and controlled ion bombardment, rapidly increased the application of sputtered deposition coatings in the area of semiconductor, optical coating, decorative, and cutting tools (Mattox 2003).

The microstructure, crystallographic texture, and the state of residual stress in the thin film coating dictate performance of the coating; due to this, it is imperative to be able to control and manipulate the above characteristics to produce desired coating performance (Anon 1983, Mayrhofer et al. 2006). Studies have also shown that coating process parameters significantly influence the microstructure, crystallographic texture, and the

state of stress of the deposited coating (Smith 1995). To provide a clearer picture on these linkages, this review focuses on the PVD DC magnetron sputtering process, its process parameters, and the effect of the process parameters on characteristics and performance of the deposited coating.

2.1.1 Sputtering process

In the PVD sputtering technique, the vapourization of target material is done through bombardment of the target materials using positive, high-energy noble gas ions such as argon. It requires vacuum conditions and it is used to deposit very thin films on substrates for a wide variety of commercial and scientific purposes. The process requires very low chamber pressures in the range of 10^{-5} to 10^{-7} mbar. Two main purposes necessitating this condition before initiation of sputtering process are contamination minimization and maximization of particle mean free path. Once the vacuum condition is satisfied, a noble gas such as argon (Ar) is backfilled inside the chamber to a pressure of 10^{-3} mbar to fulfil the role of the bombarding particles. Ar is often used as the source of the bombarding particles because of its inertness, relatively high atomic mass, and low cost (Bunshah 1994).

At this stage, inside the chamber there are neutral atoms, electrons, and ions. The presence of the magnetron system local to the target/ cathode creates a magnetic field close to the cathode and parallel to the target surface. This magnetic field traps electrons close to the surface of the target, refer to Figure 2.1. Argon atoms that collide with electrons turn into positively charged argon ions and are accelerated towards the

target/cathode that is negatively biased. During the impact, momentum exchange between the Ar ions and atoms in the target material occurs resulting in ejection of one or several target material atoms. The number of atoms ejected from the surface per incident ion is called the sputter yield and is a measure of the efficiency of the sputtering process (Mattox 1998). During impact, the positively charged noble gas ions will also eject a secondary electron. This electron will again produce ions through impact ionization resulting in a self-sustaining process. Visually, a glow discharge phenomena can be seen near the cathode region. This glow is due to the collision between argon atoms and electrons resulting in transformation from argons atoms to argon ions. During this transformation process, energy in the form of photons, is released and can be seen visibly as a glow discharge. Within this glow-discharge region, also known as a plasma region, there exists a quasi-neutral mixture of electrons and gas ions in a high-energy state.

The sputtered atoms, those ejected into the gas phase, are not in their thermodynamic equilibrium state. Therefore, they tend to condense back into the solid phase, in the form of metastable materials, upon colliding with any surface in the sputtering chamber. In magnetron sputtering process most of the sputtered particles are neutrals, in the range of 95% to 99% (Lugscheider 1996).

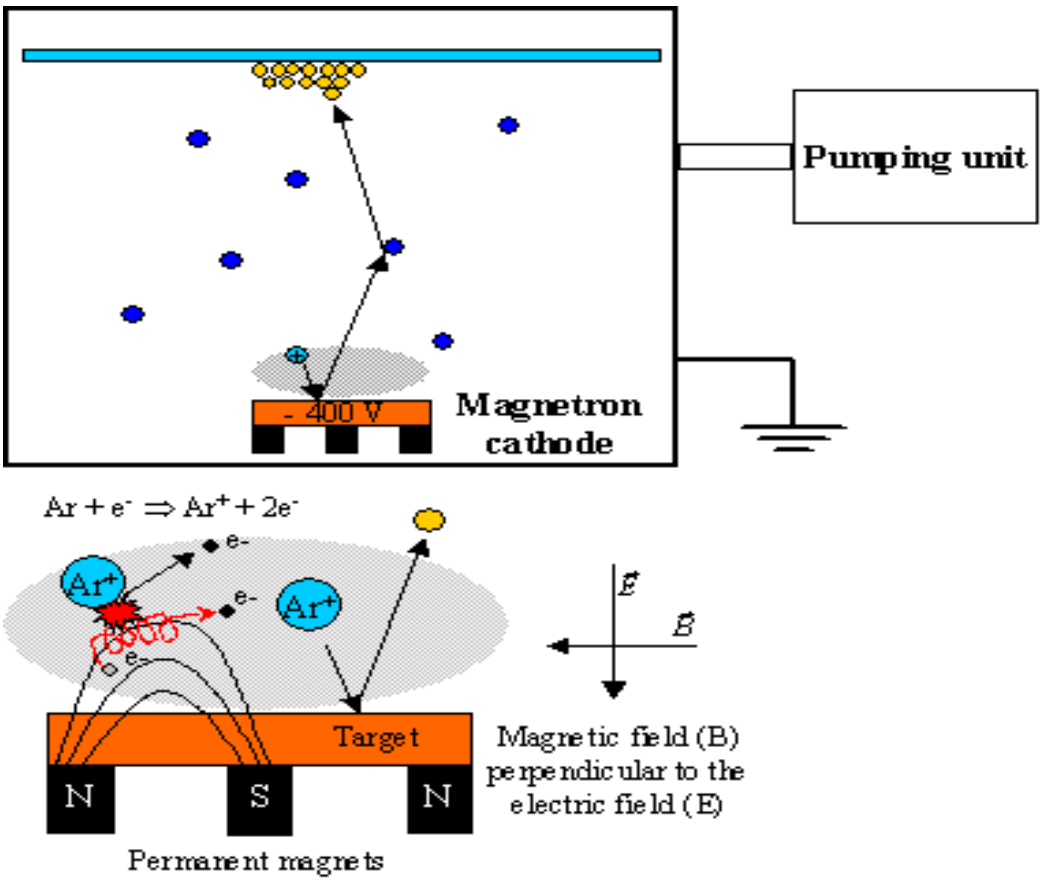

Figure 2.1. Schematic representation of the magnetron sputtering process.

2.1.2 Bombardment of ions, neutral, and electron on growing film

Back sputtering occurs when the substrate is bombarded by neutral atoms of inert gas and of ions of inert gas (if the substrate is negatively biased). This can significantly impact the properties of coating. The rate of back sputtering due to ions of inert gas increases with the application of negative potential on the substrate (bias).

This phenomenon should be controlled because it has both desirable and undesirable impacts with respect to the characteristics of the growing film. Some of the undesirable consequences of back sputtering are the decrease in deposition rate due to the re-

sputtering of the coating layer established on the substrate surface. Therefore the resulting composition of the growing coating may be different from the target material, and there may be a significant increase in substrate temperature. This will occur if the energy of the bombarding particles is excessively high such as in the influence of high substrate bias voltage condition (Petrov et al. 2003). There are also desirable effects of back sputtering such as improvement in coating density, adhesion, and hardness. This is the result of changes in microstructure of the growing film where the grain size becomes smaller and the absence of columnar structure. The higher substrate temperature also aids faster diffusion of deposited atoms into the substrate for better adhesion (Nissim et.al., 2007).

2.1.3 Sputtering of alloys and reactive sputtering

The deposited coating layer can be of pure material, a compound or an alloy. There are two common ways of sputtering compound materials onto a substrate surface, sputtering of an alloy and reactive sputtering.

2.1.3.1 Sputtering of alloy

In this method, the intended compound coating material is used as the target. The target is then sputtered and the atomized compound material deposits itself onto the substrate surface. Since the sputtering yield is a function of the atomic weight of the atom, and the compound material (target) consists of several different types of atoms, the initial coating will not have the same composition of the target material. This is due to different sputter yields for different species of atoms from the target alloy. However, by virtue of the

sputtering mechanism where only surface atoms can be sputtered; when equilibrium is reached, the composition of the coating on the substrate surface will be the same as the target's composition.

In ensuring the composition of the coating on the substrate surface is the same as the target material, the target temperature has to be controlled, usually with chilled water, so that no significant diffusion can take place from the interior of the target. If the afore mentioned diffusion happens, variation in the coating material composition is expected. The deposited coating from a target containing volatile constituents is more likely to have a different composition compared with the target. This is due to loss of lighter and more volatile constituents during the transport between the target and the substrate. For example, in the sputtering of TiO_2, oxygen is the more volatile constituent and would preferentially get lost during the transport to the substrate. The developed coating would be generally enriched by titanium, the less volatile constituent. In case of such compound, reactive sputtering is recommended (Mattox, 1998).

2.1.3.2 Reactive sputtering

Reactive sputtering is the process where the intended coating compound material is achieved through the reaction between the ejected particles from the target material and the chemically reactive gases (e.g. nitrogen) (Safi 2000). The reactive sputtering process can be used to deposit coatings of elements and alloys as well as compounds (Mattox 1998). Coatings such as TiAlN are commonly deposited by sputtering of a Ti-Al alloy (the target material) in the presence of nitrogen gas within the coating chamber.

Reactive sputtering is a complex process since a compound forms at the target surface as well as at the substrate surface. The compound formation at the target surface is called target poisoning; this causes the deposition rate on the substrate to decrease as the supply of reactive gas increases (Berg and Nyberg 2005). The reactively sputtered thin film characteristics were found to be greatly influenced by process parameters such as magnetron power, discharge current density, argon gas pressure or flow rate, reactive gas pressure or flow rate, substrate bias, substrate temperature, and target to substrate distance. (Farooq and Lee 2002, Xu et al. 2006, Chou et al. 2003, Evans et al. 2007, Choi 2004).

2.2 Critical PVD magnetron sputtering process parameters

A deposited thin film's characteristics and service performance are determined by its microstructure, crystallographic texture, state of stress, and chemical composition. In turn, those factors are greatly influenced by particle bombardment of the growing film, deposition temperature, and composition of elements in the coating material (Musil and Vlcek 1998, Mayrhofer et al. 2006). The scope of this literature review is to look into the effect of particle bombardment and deposition temperature. Chemical composition of the thin film and its influence on coating characteristics and performance are out of the scope of this study because the focus of this study is in the area of PVD magnetron sputtering process only.

Particle bombardment and deposition temperature are influenced significantly by the PVD process parameters. As tabulated in Table 2.1, researchers in this field have studied

influence of PVD process parameters on thin film coatings extensively. The parameters identified are bias voltage (V_s), sputtering power, substrate temperature (T_s), nitrogen partial pressure, and distance between substrate and the target. Subsequent chapters of this literature review look on how these parameters influence coating characteristic and performance.

Table 2.1: Literature on the study of the influence of coating parameters on coating characteristics and performance

Author	**Parameter evaluated**	**Affected coating characteristics**
Wang et al. (1999)	Bias Voltage (Vs)	Hardness & adhesion
Choi, et al. (2004)	Substrate Temp (Ts) Bias Voltage (Vs)	Elastic modulus & hardness.
Schneider et al. (2000)	Substrate bias(Vs)	Density
Evans et al. (2007)	Bias Voltage (Vs)	Crystallite size, compressive stress and hardness
Matsue et al(2004)	Bias Voltage	Preferred orientation
Ahlgren and Blomqvist (2005)	Biased Voltage	Residual stress, crystallographic direction, hardness
Weber et al. (2004)	Biased Voltage	Tool life, compressive stress
Barshilia and Rajam (2004)	Bias voltage	Surface roughness, hardness, crystallite size
	N_2 partial pressure	Hardness
Chou et al. (2003)	DC Power N_2 partial pressure Specimen Distance Specimen height	Power influence hardness (sputtering)
	Substrate Temperature Substrate bias Argon flow rate Nitrogen flow rate	Hardness (ion-plating)
Farooq and Lee (2002)	Chamber pressure Sputtering Power	Thickness and composition
González et al. (2007)	Substrate temperature	Thickness, crystalline grain size, hardness
Xu et al.(2006)	Substrate temperature Sputter Current N_2/Ar ratio	Crystal orientation, roughness.
Kim and Jeong (2001)	Sputter voltage Distance	Crystal orientation
Wuhrer and Yeung (2002)	Sputter Power of target	Grain size, porous, hardness, crystal structure
Gredic and Zlatanovic (1991)	Magnetron Power	Hardness, density, residual stress
Mubarak, et al. (2006)	N_2 flow rate	Hardness, crystal orientation, elemental composition, roughness, adhesion
Ding et al. (2008)	Sputtering current	Composition (atomic ratio) and crystalline structure

2.2.1 Substrate bias voltage

Substrate bias is one of the most evaluated parameters in the PVD process. This is due to its direct influence on the energy of ion bombardment on the growing film. The relationship between substrate bias voltage (V_s) and the energy of ion bombardment (E_i) on a growing film for simple sputtering process can be defined as,

$$E_p = E_i V_i / V_m = e(V_p - V_s) V_i / V_m \quad (2.1)$$

Where E_p is the energy per deposited atom, E_i is the energy of ions, V_p is plasma potential, V_s is substrate bias, e is elementary charge, and V_i/V_m is the ratio of flux ion to flux particle bombarding the growing film. From equation 2.1 above, the greater the V_s (usually V_s is negative in value), the greater the E_i (Musil and Vlcek 1998). The magnitude of the ion's energy (E_i) determines the magnitude of acceleration of the ion onto the growing film, which transfers energy to the growing film upon impact. Schneider et al. (2000) also reported that ion energy at the substrate is equal to the difference of plasma potential to the substrate bias plus the initial kinetic energy of the depositing ion, meaning that energy of depositing ions forming the thin film coating can be directly controlled by substrate bias.

Work by Petrov et al. (2003) illustrated clearly the change in the microstructure of a growing coating as the E_i changes. Transmission electron microscopy (TEM), was used to produce images of film sections of TiN grown using magnetron sputtering with increasing E_i values (40-160eV), as shown in Figure 2.2. As E_i increases, the microstructure changes from a columnar structure with porosity to a dense columnar

structure with open boundaries and finally to a dense structure without boundaries. In general, dense structures without porosity are desirable for protective and wear resistant coatings. However, beyond certain V_s level, it can induce undesirable effects such as re-sputtering and lattice defects (Medjani et al. 2006).

Figure 2.2: Cross-sectional TEM micrograph obtained from the middle portion of a 3.5μm thick TiN layer grown by reactive magnetron sputter deposition on a steel substrate at 300 °C (Petrov et al. 2003)

Table 2.2: A list of published studies on the impact of negative substrate bias on coating characteristics and performance. The evaluated range of substrate bias is also indicated.

Author	**Range**
Wang et al. (1999)	150V-300V
Choi, et al. (2004)	0-500 V
Evans et al. (2007)	0-300V
Matsue et al. (2004)	0-100V
Ahlgren and Blomqvist (2005)	40-200V
Weber et al. (2004)	30-125 V
Barshilia and Rajam (2004)	0-240V

Published studies addressing the effect of substrate bias (V_s) on thin film coating characteristics and performance, are tabulated in Table 2.2. From a review of those studies, general trends with respect to the effect of V_s on thin film coatings can be summarized as:

- Increase of V_s creates finer and denser microstructure due to greater ion bombardment energy. Denser microstructure resulted in higher hardness and compressive stress values.
- However, some studies indicated that beyond certain value of V_s, the hardness and compressive stress value either stabilized or reduced. Study by Ahlgren and Blomqvist (2005) indicated that this critical V_s value was -100V, beyond which the hardness and compressive stress remain constant. However, Weber et al. (2004) and

Choi, et al. (2004) reported reduction of compressive stress beyond -100 V_s due to microstructure changes brought about by re-sputtering of deposited coating.

- In contradiction to this, Barshilia and Rajam (2004) reported steady increases in hardness over the evaluated V_s range of -50 V to -250 V.
- Substrate bias also influenced the crystallographic orientation of deposited thin film coating. Ahlgren and Blomqvist (2005) reported that the crystal orientation of TiAlN at low V_s was {200} and changing to {111} structure at higher voltages, -140V to -200V. However, Weber et al (2004) reported that no change of structure orientation was observed within substrate range of -30V to -125V.

2.2.2 Sputtering power

Sputtering power is one of the most important process parameters that influences the growth and properties of the deposited film. Two components of sputtering power are voltage and current which dictate the sputtering rate and consequent bombardment of the growing film. Sputtering current influences the rate of the deposition process which influences nucleation and growth process within the forming film; coating formation mechanisms being based primarily on either surface diffusion and agglomeration on existing growth centres or nucleation with other adatoms. The sputter voltage mainly determines the energy of sputtered particles. Studies listed in Table 2.3 have shown that the sputter power (current or voltage) have a significant influence on coating characteristics and microstructure.

The importance of sputtering power relative to other sputtering parameters was indicated by a study performed by Chou et al. (2003). In that study, the influences of four sputtering process parameters, sputtering power, nitrogen partial pressure, specimen height, and specimen distance, were evaluated using Taguchi design of experiments methodology. The results indicated that sputtering power was the most influential factor in determining hardness of the deposited thin film coating.

Table 2.3: List of published studies on the impact of sputtering power on coating characteristics and performance. The evaluated power range is also indicated.

Author	**Parameter evaluated**	**Range**
Chou et al. (2003)	DC Power	0.7-0.9Amps
Farooq and Lee (2002)	Sputtering Power	100W-1400W
Xu et al. (2006)	Sputter Current	0.8- 1.6 A
Kim and Jeong (2001)	Sputter voltage	300-360 to 400-480V
Wuhrer and Yeung (2002)	Sputter Power density	0- 0.6 W/cm2
Gredic and Zlatonovic (1991)	Sputtering Power	2.65-4.65 kW

The influence of sputtering power upon thin film microstructure and characteristics based on reported studies listed in Table 2.3 can be summarized as below:-

- The crystallographic orientation of the developing film was influenced by changes in sputtering power as reported by Wuhrer and Yeung (2002) where an increase of sputtering power density by 0.6 Watts/cm^2 changed TiAlN crystal orientation from {111} to {200}. Changes in power components, current and voltage can also

influence crystallographic orientation. Xu et al. (2006) reported that as the sputtering current varied from 0.8 A to 1.6 A, the TiN {200} peak value increased significantly (by almost three fold). Variation of sputtering voltage, the other component of sputtering power, also influenced crystallographic orientation as reported by Kim and Jeong (2001) where the AlN crystallographic orientation changed from {100} to {002} as the voltage increased by about 100 volts.

- The change in the microstructure of growing film due to sputtering power variation, as reported earlier, affected its physical characteristics. Based on a reported studies on deposition of TiAlN thin film by Wuhrer and Yeung (2002) and by Gredict and Zlatanovic(1991), increased sputtering power brought about an increase in the thin film coating hardness. This increase in hardness was attributed to a denser microstructure and increase in compressive residual stresses. Xu et al.(2006) and Wuhrer and Yeung (2002) reported decrease in roughness with the increase in sputtering power.

2.2.3 Substrate temperature

Substrate temperature has a strong influence on the growth behaviour and microstructure of thin film (Musil and Vlcek 1998). An increase in substrate temperature can lead to an increase in hardness due to the denser microstructure produced, due to better atomic surface mobility. At lower substrate temperature the depositing particles do not have enough kinetic energy, hence mobility, to reach lower potential energy before being covered by other particles (Patsalas et al. 2000). However beyond a certain temperature, hardness will reduce due to grain growth (Choi et al. 2004). Normally, the substrate

temperature is regulated by the heater installed inside the coating chamber, however, it can also be affected by the heat from the target due to sputtering and energy from the secondary electrons (Wasa et.al., 2004).

The role of substrate temperature in determining coating microstructure was illustrated by the widely used Thornton structure zone model shown in Figure 2.3. The model illustrates the relationship between the coating morphology, the deposition temperature, and the pressure (Mattox, 1998). For a given argon partial pressure, as the substrate temperature increases, the structure of the deposited film changes from porous (zone 1) to dense structure (zone T). Beyond that point, the structure becomes columnar (zone II) and further increase in substrate temperature resulting in recrystalization of grain structure (zone III).

.

Figure 2.3: Thornton model (Mattox 1998).

Table 2.4: A list of published studies on the impact of substrate temperature and sputtering power on coating characteristics and performance. The evaluated temperature range is indicated.

Author	**Temperature range**
Choi, et al. (2004)	Room-300C
Chou et al. (2003)	300-430C
González et al.(2007)	22- 120 C
Xu et al.(2006*)*	20-500 C

Some specific studies on the effect of substrate temperature on the microstructure and characteristics of thin films deposited using PVD process are listed in Table 2.4, and summarized below.

- The effect of substrate temperature on the crystallography of growing films was reported by Xu et al.(2006). That study indicated that as substrate temperature increased from 20°C to 500°C, the crystallographic orientation of TiN film changed from combination of {111} and {200} to {200}.
- The impact of substrate temperature on the hardness of thin film was reported by Choi, et al. (2004), Chou et al. (2003), and González et al. (2007). The findings from those studies were consistent; the hardness of thin film increased with increased substrate temperature even with different thin films being evaluated.
- González et al. (2007) also reported significant reductions in grain size as temperature increased from 22°C to 120°C.

2.2.4 Gas pressure

The quantity of gases in the deposition chamber can be regulated by means of regulating the flow rate or partial pressure. In the reactive sputtering process normally there are two types of gases involved. One for the sputtering process, usually argon, and the other one being the reactive gas, such as nitrogen. The sputtering gas is usually inert and of high atomic mass. The influence of sputtering gas pressure on the deposited film microstructure was clearly shown by the Thornton structure-zone model, as shown in Figure 2.3. For a given substrate temperature, changes in sputtering gas pressure can result in formation of different microstructural zones in the surface film (see Thornton model in Figure 2.3). This is quite prevalent at T/Tm ratios lower than 0.3. However, looking at the Thornton model, the influence of sputtering gas pressure on microstructure is much less compared to that of temperature (Mattox 1998).

The reactive gas partial pressure plays an important role in determining the stoichiometry of the film developed. Low reactive gas flow will result in formation of an under-stiochiometric film and excessive flow rate will result in poisoning of targets.

The other effect that gas pressure has during sputtering process is on the thermalisation distance of energetic particles, thermalisation being the process of particles reaching thermal equilibrium through mutual interaction. As the gas pressure increases, the

thermalisation distance becomes shorter. A shorter thremalisation distance equates to a reduction in the frequency and energy of particles or ions bombarding the growing film.

Listed in Table 2.5 are published works on the influence of nitrogen flow rate on the deposited thin film coating. Studies done by Barshilia and Rajam (2004) indicated that an increase in nitrogen flow rate from 0.6 to 3 sccm[1] resulted in a reduction of hardness. As the nitrogen flow rate increases, the composition of the developing TiN film shifted further away from its stiochiometric value hence reducing its hardness. Studies by Chou et al. (2003) on TiN coatings indicated that the increase in nitrogen flow rate from 0.75 to 1.25 sccm did not have a significant influence on the hardness of developing TiN thin film.

The studies listed in Table 2.5 indicate that while gas pressure is an important factor to be considered in optimizing the sputtering process, the general trend indicated the optimum setting for reactive gas partial pressure or flow rate is one that can generate a stoichiometric coating composition.

Table 2.5: List of published studies on impact of gas pressure on coating characteristic and performance and the evaluated range

Author	Parameter evaluated	Range
Barshilia and Rajam (2004)	Nitrogen flow rate	0.6-3 **sccm**
Chou et al. (2003)	Nitrogen flow rate	0.75-1.25 **sccm**
Xu et al(2006)	N_2/Ar ratio	1:9 – 5:5

2.2.5 Summary and discussion of process parameters selection to be studied

[1] sccm: Standard Cubic Centimeters per Minute

Key points of the literature review on the coating process parameters that have influence on the coating characteristics and performance can be summarized as below

- Four main PVD process parameters that have significant influence on coating characteristics and performance are substrate bias, substrate temperature, sputtering power, and reactive gas pressure.
- Many contradictions were reported on the trend between the process parameters and resultant coating characteristics and performance especially the substrate bias and sputtering power.
- It was consistently reported that the optimum nitrogen gas flow rate or pressure with respect to the resultant coating performance is one that resulted in coating with stoichiometric composition

2.2.5.1 Parameters to be selected as input to the model

As mentioned earlier four main process parameters were identified as being significant influential parameters that most likely dictate the characteristics and performance of the developed coating. Out of the four significant parameters, optimum levels of nitrogen gas pressure were consistently reported as generating a stoichiometric coating composition. Due to this, nitrogen gas pressure will not be included in this study as one of the input parameters. For this study, nitrogen pressure will be optimized before the experiment. By that reasoning, the PVD process parameters selected as the input to the model are substrate temperature, substrate bias, and sputtering power.

2.2.5.2 Contradiction on trend of process parameters and resultant coating characteristics and performances.

The contradictory findings reported on the effect of process parameters and the resultant coating properties, especially for substrate bias and sputtering power, could be due to either interaction phenomena between process parameters or the different process range being evaluated. In all the works reviewed, one aspect that has not been looked at is the possibility of interaction factors. For a complex process such as the PVD process, interaction factors cannot be ignored because it can muddle the results and generate contradictory findings compared to other work. Due to this, the modelling work performed here addresses the interactions between process parameters.

2.3 Coating characterization method

In order to develop a PVD sputtering process model, relationships between microstructure, characteristics, and performance of the developing film in relation to process parameters need to be ascertained. Table 2.6 lists some of the characterization techniques utilized by researchers to determine coating microstructure, characteristics, and performance.

Table 2.6: Thin film coating characterization techniques.

Author	**Measured characteristic**	**Method/Equipment**
Choi, et al. (2004)	Elastic Modulus, Hardness	Nanoindenter
Evans et al. (2007)	Crystallite size , Compressive stress, Hardness	XRD Nanoindenter
Matsue et al(2004)	Crystal orientation Composition	XRD, X-ray photoelectron spectroscopy(XPS)
Ahlgren and Blomqvist (2005)	Comp. Residual stress, Hardness Edge line delamination	XRD,SEM, Nanoindenter, Machining turning
Weber et al. (2004)	Tool Life, Crystal orientation Compressive stress Composition	Machining –turning, XRD, Secondary neutral-mass spectrometry(SNMS)
Barshillia and Rajam (2004)	Surface roughness Hardness Crystallite size , Composition	AFM, Nanoindenter XRD, EDX
Chou et al. (2003)	Hardness	Nanoindenter
González et al. (2007)	Thickness Crystalline grain size, Hardness	SEM, XRD Microhardness tester
Xu et al(2006).	Crystal orientation Roughness	XRD AFM
Kim and Jeong (2001)	Crystal orientation, Microstructure	XRD SEM
Wuhrer and Yeung (2002)	Microstructure, Roughness Grain size, Hardness, Crystal structure	SEM XRD
Gredic and Zlatanovic (1991)	Hardness Power Ti:Al ratio, Residual stress	Microhardness EDX, SEM
Mubarak, et al. (2006)	Hardness, Crystal orientation Elemental composition, Surface roughness, Microstructure	Micro Vickers hardness tester, XRD, EDX, AFM SEM
Ding et al. (2008)	Composition (atomic ratio) Crystalline structure	EDX XRD

The listed characterization methods can be grouped into coating properties and analysis techniques shown in Table 2. 7.

Table 2.7: Characterization and analysis techniques

Coating property	**Analysis technique**
Microstructure	Scanning electron microscopy (SEM)
Surface roughness	Atomic Force Microscopy (AFM)
Phase composition/ crystal orientation/residual stress/ crystal size	X-ray diffraction (XRD)
Elemental composition	Energy dispersive x-ray (EDX), X-ray photoelectron spectroscopy (XPS) Secondary neutral-mass spectrometry (SNMS)
Hardness	Nanoindenter, Micro hardness tester
Coating performance	Machining (Turning operation)

Based on Table 2.7, the analysis techniques for microstructure, surface roughness, phase composition/ crystal orientation/residual stress/ crystal size, adhesion, and coating performance are straightforward. However some discussion is needed to select the analysis techniques for the elemental composition and hardness, as there are several techniques suggested by the literature.

2.3.1 Selection of elemental composition analysis technique

EDX analysis is not really a discrete surface analysis technique. The information gathered is based on about 0.5 microns of the sample depth. Limitations of this analysis are poor sensitivity to light elements and the detection sensitivity is limited to about 1% atomic of the sample (Grasserbauer and Werner 1995). XPS analysis is able to gather elemental information of the topmost atomic layer of a surface and its detection

sensitivity is 0.1% atomic, which is much better than that of EDX. The advantage of SNMS over both EDX and XPS analysis is that the detection sensitivity is at parts per million (PPM) or part per billion (PPB) level and it is a depth profiling analysis technique (Criegern et al. 1997).

For the thin film coating analysis conducted in this research, the elemental analysis is performed on the fractured surface of the coating. It is not surface analysis, rather the average elemental composition of the coating. Due to this, EDX analysis can meet the intended requirement. One of the concerns mentioned earlier on EDX analysis limitation is poor sensitivity to light elements. This concern is negated as the elemental analysis data gathered are composition of titanium and aluminium.

2.3.2 Selection of hardness analysis technique

One of the main concerns in thin film coating hardness analysis is the influence of substrate hardness on the measurement. Because of this concern, Oliver and Pharr (1992) suggested that the indentation depth should not exceed 10-20% the coating thickness. This finding is also supported by Hainsworth and Soh (2003) who suggested indentation depth should not exceed 10% of coating thickness. The thickness of coating investigated in this research is in the range of 1-2 microns, implying that conservatively penetration depth of the indenter during hardness analysis must not exceed 0.2 micron. To able to control such penetration depth, a nanoindenter that has much lower load range capability is selected to be the instrument of choice for hardness analysis.

2.4 Empirical modelling technique: Response Surface Methodology (RSM)

Based on the objectives, scope, and problem statement, the modelling method must be practical, able to cater for multiple output responses, able to identify interaction between input parameters, and be able to predict the input parameters based on desired output responses. Some of the empirical experimentation methods used by researchers to study the relationships between inputs and outputs of PVD processes are Taguchi approach (Chou et al. 2003), full factorial design of experiment (Chou et al 2003), and RSM (Keles et al.2003), (Axelevitch and Golan 2007). Both the full factorial design and Taguchi approach do not meet the requirement mentioned above. Full factorial design is good if the input and output relationship of the process is linear and the Taguchi approach cannot detect interaction phenomena (Anderson and Whitcomb 2005). The RSM approach can meet the stated requirements but published studies on RSM modelling work on PVD hard coating for cutting tool applications is lacking.

RSM is one of the best methods for an empirical study of the relationships between one or more of the measured response functions (Voznesensky 1974). It uses mathematical and statistical techniques to represent the domain of all feasible solutions for the process model and once the model is developed, process optimization can be done without a trial and error approach (Box et al. 1978).

2.4.1 Response Surface Methodology (RSM)

Response Surface Methodology (RSM) is a collection of mathematical and statistical techniques to model and analyse problems in which responses (output) are influenced by

several input variables (Montgomery 2005). The relationship between the input parameters and output responses is defined using regression analysis in form of a polynomial equation. A regression is performed to describe the data collected based on a estimated response variable, y, and one or more input variables x_1, x_2, . . ., xi. Depending on the behaviour of the model, the polynomial equation can be of a linear or non-linear form. Equation 2.2 and equation 2.3 are examples of first-order and second-order polynomial equations respectively.

$$y = \beta_0 + \beta_1 x_1 + \beta_2 x_2 + \beta_3 x_3 + \ldots + \beta_k x_k + \varepsilon \qquad (2.2)$$

$$y = \beta_0 + \sum_{i=1}^{k} \beta_i x_i + \sum \beta_{ii} x_i^2 + \sum_{i<j} \sum \beta_{ij} x_i x_j + \varepsilon \qquad (2.3)$$

If the relationship can be described by a linear function then the approximating function is the first-order model otherwise it is a second-order model if there is curvature in the relationship. The developed polynomial function can only be used to describe the relationship within the range of the independent variables specified during the development of the function.

To ensure that the selected polynomial equation best represents the model, a least square technique is used to minimize the residual error measured by the sum of square deviations between the actual and the estimated responses. This involves the calculation of estimates for the regression coefficients, i.e. the coefficients of the model variables including the intercept or constant terms. The calculated coefficients of the model

equation(s) need to however be tested for statistical significance. This is done using analysis of variance approach (ANOVA), where tests for significance of the regression model, significance of individual model coefficient, and lack of it are performed (Steppan et al. 1998).

2.4.2 Application of RSM in process optimisation and modelling.

Application of RSM in modelling and optimisation has been proven in various fields ranging from food products to electronic technology. Its wide adoption is due to its practicality, economy and relative ease of use (Shokuhfar et al. 2008). The main advantage of RSM is the economy in the number of experimental trials needed to evaluate multiple parameters and their interactions (Chen et al. 2005, Karacan et al. 2007). RSM is utilized for two main purposes, modelling and optimization, as indicated in Table 2.8. The optimization work done using RSM covers wide research areas such as waste treatment (Sharma et al. 2009, Aktas et al. 2006, Zinatizadeh et al. 2006), the food industry (Deshpande et al. 2008, Lofty et al. 2007), welding processes (Benyounis et al. 2005), and sputtering processes (Axelevitch and Golan 2007). RSM is also being used in the areas of process modelling of wire electrical discharge machining (Hewidy et al. 2005), adsorption for H_3PO_4 activated rubber wood sawdust in water treatment application (Kalavathy M et al. 2009), palm oil mill effluent treatment (Zinatizadeh et al. 2006), and sputtered thin film coatings for electronic applications (Adamczyk et al. 2008). Some of the optimization and modelling applications of RSM are tabulated in Table 2.8.

Table 2.8: The optimization and modelling applications of RSM

Author	Area of research	Statistical Software Used
Shokuhfar et al. 2008	Shape memory alloy	NCSS 2000 statistical software
Sharma et al., 2009	Waste treatment	Design-Expert
Lofty et al. 2007	Enzyme production	*
Hewidy et al. 2005	Wire electrical discharge machining	*
Kalavathy M et al. 2009	Waste treatment	Design Expert 5.0.7
Aktas et al. 2006	Waste water treatment	Design-Expert 6.0
Ahmad et al. 2009	Membranes technology	Design Expert 6.0.6
Benyounis et al. 2005	Laser welding	Design-expert
Zinatizadeh et al. 2006	Waste treatment	Design Expert
Deshpande et al. 2008	Chocolate-flavoured peanut–soy beverage	STATISTICA, Version 6.0
Nambiar & Ramamurthy 2006	Foam concrete technology	Statistical Analysis Software (SAS)
Adamczyk et al. 2008	Sputtering thin film coating for electronic application	NEMRODW
Axelevitch and Golan 2007	Sputtering of thin film coating	*

* Information not available

Even though the RSM has been used for the optimisation and modelling of sputtering process (Adamczyk et al. 2008, Axelevitch and Golan 2007), these examples were for electronic applications where the output responses of interest were electrical properties of the developed thin film coating. However, application of RSM for modelling and

optimisation of sputtering process for the hard coating applications where mechanical properties of the developed coating were the output responses of interest, is lacking.

Table 2.8 also indicates the software used for the RSM analysis of various applications such as NCSS 2000, Design Expert, STATISTICA, Statistical Analysis Software, and NEMRODW. The proposed software for this research, Design Expert, is one of the more widely used software for RSM analysis as reflected by Table 2.8.

CHAPTER 3

METHODOLOGY

3.0 Methodology

This chapter describes the approach and methodology adopted for this project. The activities involved and research flow are summarized in Figure 3.1. Detailed explanations of the process steps are covered in subsequent sub-chapters.

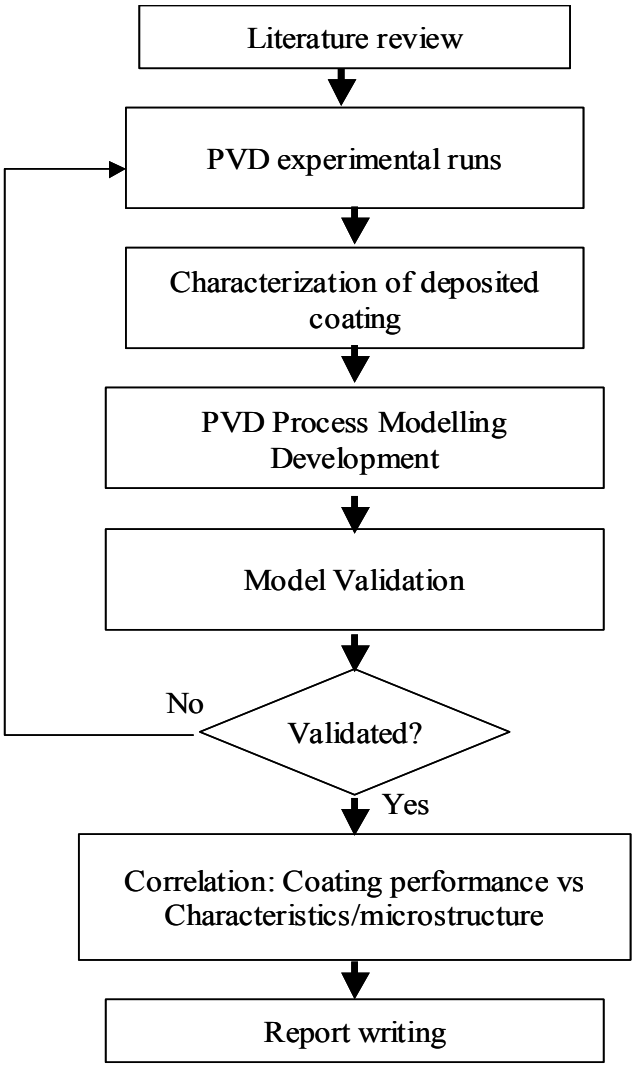

Figure 3.1: Methodology of PVD process modelling development

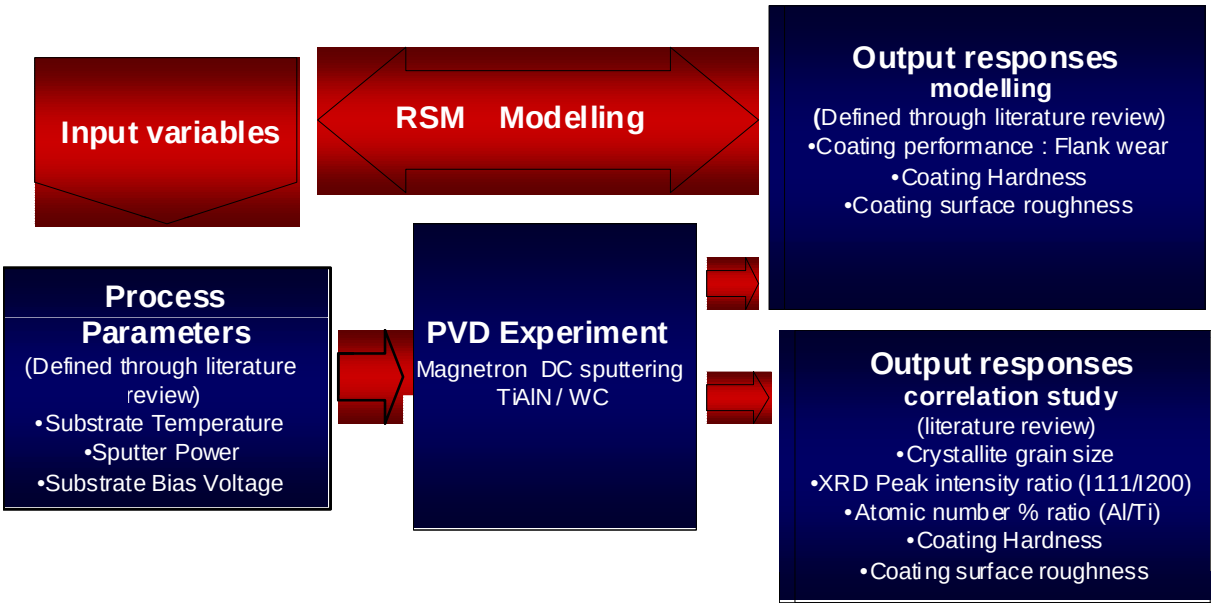

Figure 3.2: Overall approach of PVD process modelling study

The overall approach of this research is depicted in Figure 3.2. The input variables, process parameters, and the output responses for both modelling and correlation studies are selected based on the literature review. PVD experimentation was executed based on the experimental matrix defined using RSM central composite design approach. The relationship between the output responses (flank wear, coating hardness, and coating roughness) and the input process variables (substrate temperature, sputter power, and substrate bias voltage) are defined using RSM modelling approach. The correlation studies to indicate if there is any relationship between coating performance (flank wear) and the coating characteristics and microstructures (hardness, roughness, crystallite grain size, XRD peak intensity ratio I111/I200, atomic number % ratio Al/Ti) are performed using the Pearson coefficient of correlation approach.

3.1 PVD modelling experiment

Experiments were conducted using an unbalanced closed field magnetron sputtering system made by VACTEC Korea, model VTC PVD 1000. The system comprises of two vertically mounted Ti-Al alloy targets (50 % Ti: 50 % Al) with dimensions of 600mm x 100mm x 30mm. The substrate holder has an adjustable planetary rotation capability with two axis rotation, refer to Figure 3.3. The thermocouple to detect substrate temperature was located on the top of the chamber approximately about 2 cm from the substrate holder. It has feed back loop capability to regulate induction heater power in order to maintain the required temperature. There might be gradient of temperature between the thermocouple temperature and the substrate temperature. However, this gradient should be the same for all experimental runs, hence relative temperature comparison between experimental runs can still be made.

(a) (b)

Figure 3.3: (a) PVD unbalanced magnetron sputtering system VACTEC Korea model VTC PVD 1000. (b) Substrate holder inside coating chamber.

The intended TiAlN coatings were deposited on the substrate reactively, in the presence of nitrogen gas inside the coating chamber. The sputtering of target material, TiAl, was induced by the bombardment of argon ions. The substrate is a tungsten carbide cutting tool insert commercially made by Sumitomo as shown in Figure 3.4, the tool insert specification is shown in Table 3.1.

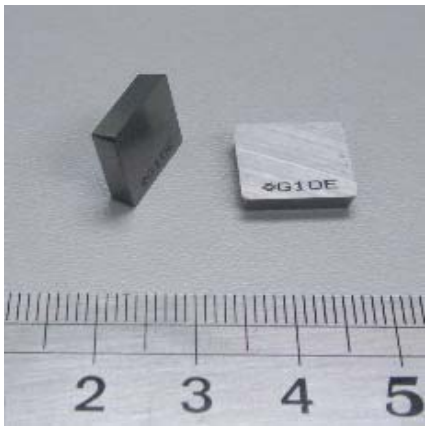

Figure 3.4: Tungsten carbide cutting tool insert commercially made by Sumitomo

Table 3.1: Sumitomo SPGN120308S cutting tool dimensions

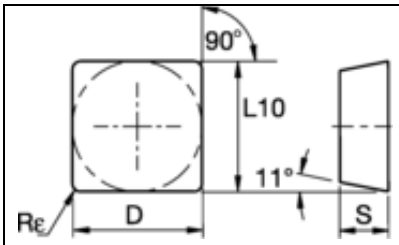	**Sumitomo SPGN120308S** Dimensions: • D = 12.7 mm • S = 3.18 mm • R_E = 0.8 mm

Prior to coating, the substrates were cleaned using an ultrasonic cleaner with alcohol bath for 20 minutes. The substrates were loaded in the rotating substrate holder inside the coating chamber. The shortest distance between substrate and target was 5 cm and the substrate holder rotation speed was set at 5 rpm.

The coating process throughout the experiment consisted of three stages; substrate etching (ion cleaning), interlayer coating (TiAl), and coating deposition (TiAlN). The

base pressure before the initiation of coating process was set at 5.0 x 10^{-5} mbar. Process settings for the three stages were:

- Substrate ion cleaning

  Purpose: This in-situ cleaning process was to clean surface of the substrate by means of argon ions bombardment onto the substrate surface. During this process, the ion source was activated to increase ionisation of argon gases going through the ion source. The magnetron shutters were activated to protect the targets from argon ions bombardment and also contamination due to etching of substrate.

  Process settings:

  Argon pressure: 5.5 x 10^{-3} mbar

  Ion source power: 0.24 kV/ 0.4 A

  Substrate bias: -200V

  Duration: 30 minutes

- Interlayer coating deposition (TiAl)

  Purpose: The purpose of the TiAl interlayer coating was to minimize the coefficient of thermal expansion gradient between tungsten carbide and TiAlN coating.

  Process settings:

  Ar pressure: 4.0 x 10^{-3} mbar

  Duration: 5 minutes (0.2 microns)

  Other settings: based on experimental matrix (Table 8)

- TiAlN deposition

Ar partial pressure: 4.0x 10-3 mbar

N_2 pressure 0.4 x 10-3 mbar

Duration: 90 minutes

Other settings: based on experimental matrix

3.1.1 Experimental matrix

The experimental matrix was developed based on the on RSM centre cubic design, using Design Expert version 7.0.3 software. It consisted of 8 factorial points, 4 axial points and 6 central points to enable an estimation of process variability as illustrated by Figure 3.5.

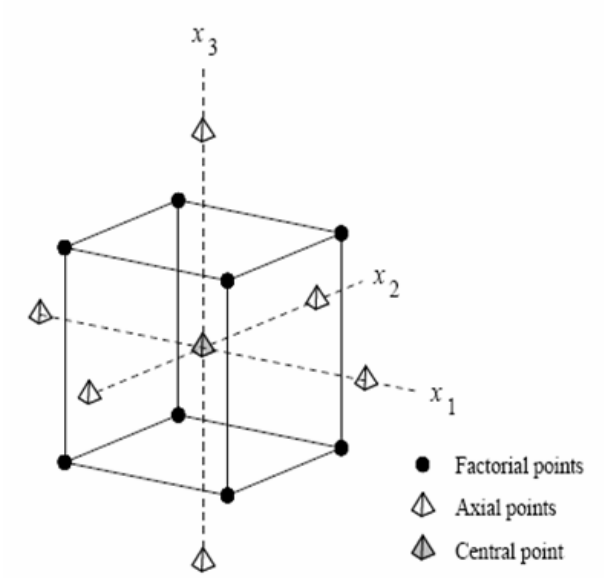

Figure 3.5: RSM Central Composite Design for 3 factors at two levels

Central Composite Design (CCD) is the most common RSM design used for process modelling. A CCD has three groups of design points:

(a) Two-level factorial design points.

(b) Axial points: The axial points have all of the factors set to 0, the midpoint, except one factor, which has the value +/- Alpha. The value for Alpha is calculated in each design for both "rotatability" and "orthogonality" of blocks. (6 points)

(c) Center points: Center points were repeated 6 times to get a good estimate of experimental error (pure error).

The experimental matrix was designed based on assigning the extreme points (operating window) as the +/- Alpha value, refer to Table 3.2. Based on the defined extreme point values, the software then assigned the high and low settings for the factorial points. This was to ensure the modelling could be performed covering the widest range of operating window possible for respective parameters. Because of this the values of factorial points were not nicely rounded.

Table 3.2: Extreme operating window for respective process parameters

	Substrate temperature (°C)	Substrate bias voltage (V)	Sputter power (kW)
- Alpha	200	-50	4
+ Alpha	600	-300	8

The developed experimental matrix based on the RSM central composite design and the +/- Alpha values defined in Table 3.2, are as shown in Table 3.3. Each experimental run consisted of three samples and the sequence of experiment following the randomly assigned run number as reflected in Table 3.3.

Table 3.3: PVD process modelling experimental matrix based on RSM central composite design approach

Run	A:Sputter Power (kW)	B:Substrate Bias Voltage (V)	C:Substrate Temperature (°C)
1	6	-50	400
2	4.81	-100.67	518.92
3	4.81	-249.33	281.08
4	6	-175	400
5	6	-175	200
6	4.81	-100.67	281.08
7	7.19	-249.33	281.08
8	6	-175	400
9	6	-175	400
10	4.81	-249.33	518.92
11	7.19	-100.67	281.08
12	6	-175	600
13	7.19	-249.33	518.92
14	6	-175	400
15	8	-175	400
16	6	-300	400
17	7.19	-100.67	518.92
18	4	-175	400
19	6	-175	400
20	6	-175	400

3.2 Coating Characterization Methods

The developed coatings from the experiment were analyzed for their characteristics, microstructure, and performance. This chapter describes the equipment, procedure, and specific data that were collected from each analysis. Table 3.4 describes the characterization equipment and corresponding coating characteristic/microstructure data/ performance that was measured. As indicated in Figure 3.2 some of the output data (results) were used to develop the respective models and some were used to understand and explain the behaviour of the developed model.

Table 3.4: The characterization equipment used with the respective intended coating characteristic/performance data to be collected.

Characterization equipment	Measured coating characteristic/ performance indicators	Purpose	
		Output response to develop model	To explain model behaviour
SEM/ EDX	Microstructure Atomic number % ratio (Al/Ti)		X
AFM	Roughness	X	X
XRD	Crystal orientation Crystal grain size Peak intensity ratio I111/I200		X
Turning machine	Tool wear (crater wear)	X	
Nano-indenter	Hardness	X	X

3.2.1 Scanning Electron Microscopy (SEM) –Energy Dispersive X-ray (EDX)

The specific data collected from this analysis were the coating growth structure (porous, dense, columnar, or recrystallized) for qualitative data, and titanium to aluminium ratio for the quantitative data. The analysis was performed using FESEM LEO 1525 scanning electron microscope equipped with electron dispersive x-ray (EDX; Oxford) as shown in Figure 3.6. Samples were fractured to expose the cross sectional view of the developed coating. The specific data collected from this analysis were the coating growth structure (porous, dense, columnar, recrystallized) for qualitative data, and titanium to aluminium ratio for the quantitative data

SEM images are a result of interaction between electron beam and surface of materials (samples). The interaction produces many signals such as Auger electrons, backscattered electrons, secondary electrons and characteristic X-rays as shown in Figure 3.7. The SEM uses secondary electron emitted from the sample surface to form an image.

Figure 3.6: SEM/EDX LEO 1525 apparatus.

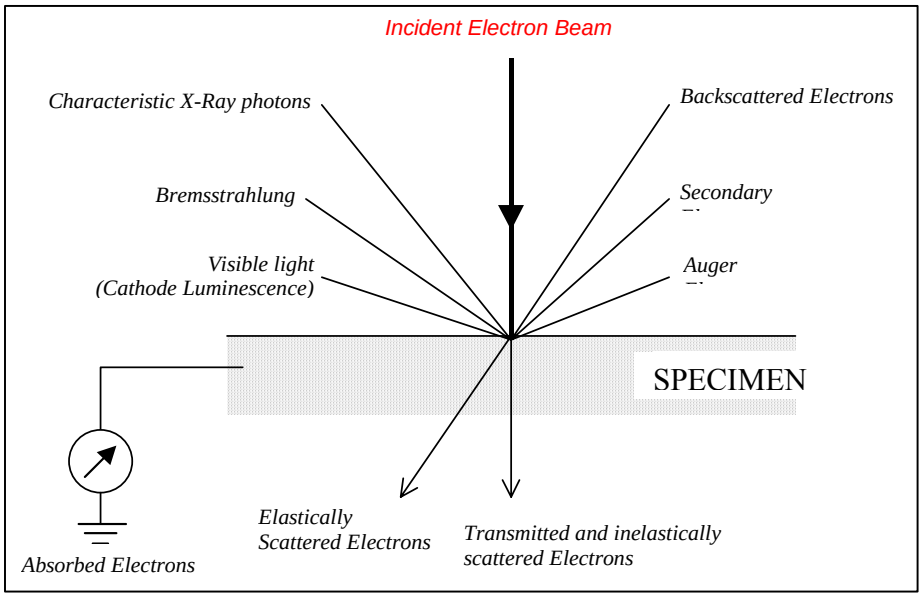

Figure 3.7: Signals produced when electron beam interact with the sample (Grasserbauer and Werner 1995)

All the samples were characterized using SEM and EDX under these conditions:

Magnification	= 10000 times
Working distance	= 15 mm
Signal A	= Secondary electron 2
EHT	= 15 kV

3.2.2 X-ray diffraction (XRD)

In x-ray diffraction (XRD), an x-ray beam is incident onto the sample and the diffracted beam is detected. The intensity of the diffracted radiation is dependent on the interaction of the beam with the sample. An illustration of XRD setup is shown in Figure 3.8.

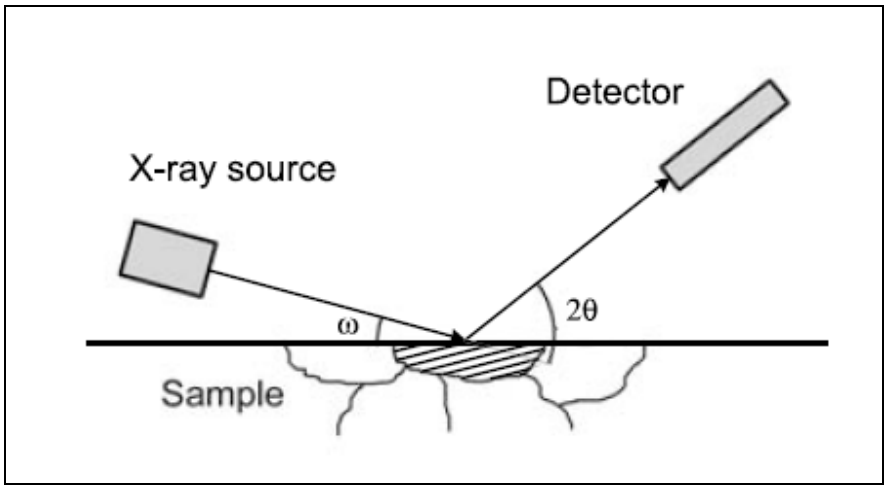

Figure 3.8: Schematic illustration of an x-ray diffraction setup

Principle of XRD analysis is based on Bragg's law depicted in Figure 3.9. The intensity of the diffracted radiation is dependent on the interaction of the beam with the sample and, in particular, the orientations of, and distances between, different crystallographic planes. Bragg's law can be described based on equation 3.1

$$2d \sin\theta = n\lambda, \qquad (3.1)$$

where n is an integer, λ is the wavelength of the x-ray radiation, and d is the interplanar spacing of the diffracting atomic planes. When λ and θ are known then d value can be calculated. From this calculation the crystal structure of material can be determined.

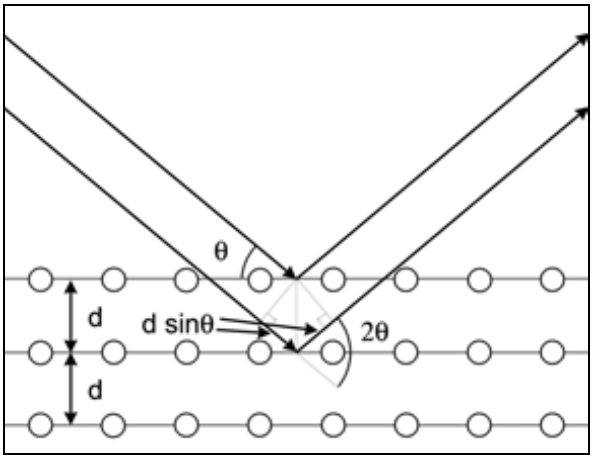

Figure 3.9: Schematic illustration of diffraction according to Bragg's law

For normal analysis the angle of the incident beam, ω, and the diffraction angle, 2θ, are scanned simultaneously where only planes parallel to the sample surface are probed. However, for the study of thin film coatings as in the present work, grazing incidence angle technique is necessary. In this method, the angle of the incident beam, ω , is kept at a small angle relative to the sample surface, and only the diffraction angle, 2θ , is varied. This is to reduce the penetration depth of the beam resulting in a relative increase in the diffracted intensity from the near-surface part of the sample.

In present study, the crystal structure of samples was characterized using Bruker D-8 XRD diffraction system, as shown in Figure 3.10, and the data was analysed using X'pert PRO software. The x-ray source used was CuKα radiation with λ = 0.15406 nm and all samples were characterized under following conditions:

2θ scanning range : 30° to 60°

Grazing angle : 1°

Step size : 0.020°

Dwell time : 1 second.

Voltage : 40 kV

Current : 40 mA

Figure 3.10: Bruker D-8 XRD apparatus with GIA capability

The grain size (D) of the coating is calculated by using the Scherrer formula shown in equation 3.2 (Chakrabarti et al., 2002),

$$D = \frac{0.9\lambda}{B\cos\theta} \qquad (3.2)$$

where B is the line broadening at half the maximum intensity (FWHM) in radians.

3.2.3 Atomic force microscopy (AFM)

Atomic force microscopy, AFM, is a technique to determine the morphology of a surface with minimal sample preparation requirements. The morphology of a surface is detected based on the force interaction between a sample surface and a sharp tip mounted on a flexible cantilever, and produces, in such a way, topographic images of a surface with

atomic resolutions in all three dimensions. When the tip is brought close to sample surface, by a few Å, the repulsive Van der Waals forces between the atoms of the tip and those of the sample cause the cantilever to deflect. The magnitude of the deflection depends on the distance between the tip and the sample. Normally the lateral AFM resolution is about 1 nm. However, with a highly sharp tip and a flat sample higher resolutions could be obtained (Brundle et al. 1992).

The AFM analysis in this study was performed using a Shimadzu model SPM-9500J2 apparatus as shown in Figure 3.11. The detection mode is contact mode using a commercial Si_3N_4 cantilever. The AFM scanning areas are set 5x 5 microns (25 μm^2). Specific data collected from this analysis being surface roughness; images of the coating surface morphology were also generated.

Figure 3.11: AFM Shimadzu model SPM-9500J2 apparatus

3.2.4 Nano-indenter test

In the traditional indentation method, a hard tipped indenter is pressed into a sample with a known load. After a set period of time the load is removed and the area of the residual indentation in the sample is measured. The hardness, H, can be defined using equation 3.3,

$$H = P/A_r \tag{3.3}$$

where P is the maximum load and A_r is the residual indentation area.

In nano-indentation, the hardness measuring process involves the indenting a specimen by a very small load up to a maximum set value using a high precision instrument, which records the load and displacement continuously. The mechanical properties of thin films coatings can be derived from the measured load-displacement loading/unloading curve through appropriate data analysis. A typical loading/unloading curve is shown in Figure 3.12. By using this curve, the hardness and Young's modulus can be calculated. The calculation details can be found from work performed by Oliver and Pharr (1992).

Figure 3.12: A typical loading/unloading curve for nano-indentation test (Oliver and Pharr, 1992)

For this research, the hardness of the TiAlN was determined using nano-indentation system, NanoTest, as shown in Figure 3.13. All the samples were tested using Berkovitch indenter with maximum load set at 50mN and the dwell time at maximum load was set at 10 seconds. For each sample, six measurements were taken and the average value was calculated and used as the hardness value for the particular sample. With the said load, if the indentation depth was more than 10% of the thickness of the

coating, the measured hardness value would be influenced by the substrate hardness. Since all the experimental runs used the same substrate, the comparison of relative hardness between different runs would still be valid for the construction of the response surface modelling.

Figure 3.13: NanoTest nano-indentation system

3.2.5 Turning test to determine coating performance

The performance of coated cutting tool insert can be determined by assessing its tool wear after machining. The most common tool wear measurement value to determine the tool wear is the flank wear. Flank wear of cutting tool insert in single point turning operation can be determined as indicated in Figure 3.14 based on ISO 3685:1993(E) standard. For current research maximum flank wear value was used as the coating performance indicator.

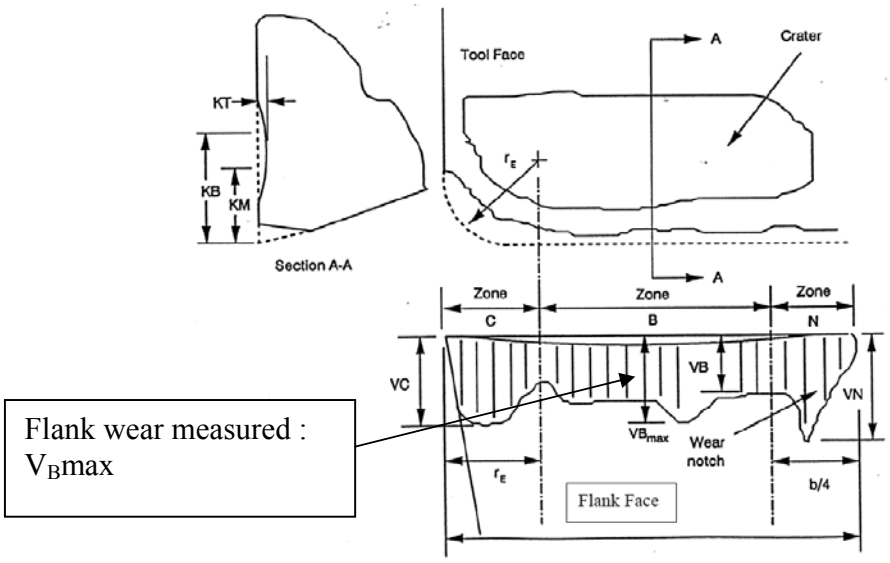

Figure 3.14: Flank wear measurement method for tool insert in single point turning operation based on ISO 3685:1993(E) standard.

The single point turning operation in this study was conducted using GATE-Precision milling machine and lathes model G-410-TCV as shown in Figure 3.15. The work piece material used was KRUPP 2379X155 CrVMo121 AISI D2 steel with diameter of 100 mm and length of 250 mm. The chemical composition of the work piece is listed in Table 3.5. The turning process was done under dry conditions (without coolant) that suits well the TiAlN coating characteristic of high hardness and wear resistance at elevated temperatures (Schramm et al. 2004).

Figure 3.15: GATE-Precision milling machine and lathes model G-410-TCV

Table 3.5: AISI D2 steel chemical composition

Element	Composition (%)
C	1.55
Cr	12.0
V	1.0
Mo	0.70

To compare performance of TiAlN coatings generated under different sputtering conditions, all the coated cutting tools for each of the 20 experimental runs were subjected to removal of same volume of workpiece material (V_{wp}) using same machining conditions. Volume of workpiece material can be calculated based on equation 3.4

$$V_{wp} = L_c\, a_p \tag{3.4}$$

where L_c is cutting length and a_p is depth of cut. Since the a_p is fixed, the volume of material removed is directly a function of L_c. For all experimental runs, L_c is set at 18 meters. The L_c and also cutting speed (V_c) was determined based on a study performed on commercially manufactured TiAlN coated tools by Razali et al. 2009. The L_c and V_c values were selected, as shown in Table 3.6, to ensure that some amount of flank wear could be generated under these cutting conditions. This enabled comparison of coating performances among the experimental runs. The feed rate (f) and depth of cut (a_p) were selected based on ISO 3685:1993(E) standard for a cutting tool with 0.8 mm corner radius and are tabulated in Table 3.6 together with previously mentioned cutting conditions.

Table 3.6: Summary of single point turning conditions

Cutting Length (L_c) m	Cutting Speed (V_c) m/min	Feed rate (f) mm/rev	Depth of cut (a_p) mm
18	200	0.25	1.6

The flank wear for all the samples was measured using an optical microscope (Zeiss Axiomat 2) attached with Axiovision AC measurement software version 4.2.

3.3 RSM data analysis

RSM encompasses a collection of mathematical and statistical techniques that can be used for modelling and optimizing of processes, from which output responses of interest are influenced by several variables (Montgomery 1997). RSM also quantifies relationships among one or more output responses and the significant input factors.

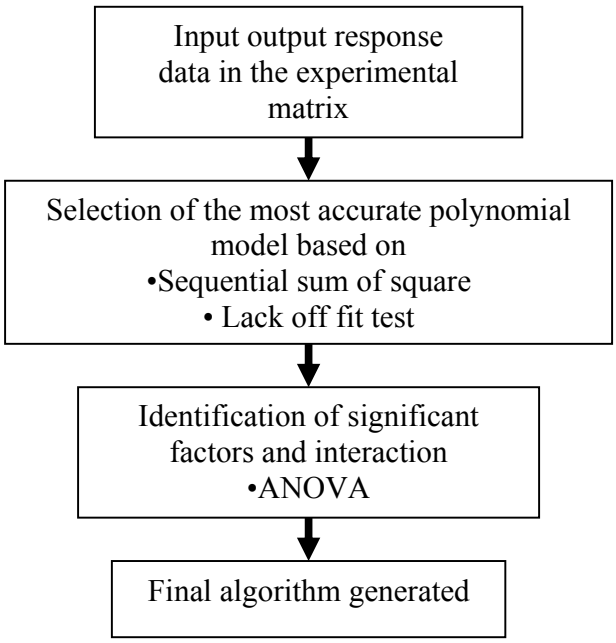

Figure 3.16: Summary of RSM analysis flow

The version 7.03 of the Design Expert software was used to develop the experimental plan for RSM was also used to analyze the data collected by following these steps (Design-Expert Software 2000) and summarized in Figure 3.16:

a) The output response data for each experimental run were keyed into the respective run number matrix as reflected in Table 3.7.

b) For each output response the Design-Expert 7.0.3 software identifies which model to choose for further analysis. The identification of the appropriate model was done using these methods.

- Sequential model sum of squares: This analysis provides comparison of models showing the statistical significance of adding model terms to those already in the model. For example, Liner vs 2FI (factor of interaction) sequential sum of square evaluates the significance of adding an interaction term to the linear model. A small p-value (Prob>F) indicates that adding interaction terms improved the model. The highest degree model that has a p-value less than 0.10 should be chosen as the model to represent the process.
- Lack of Fit: Lack of fit test assesses how well each of the polynomial models fit the data, by comparing the residual error to the pure error from replicated design points. A lack of fit error significantly larger that the pure error indicates that something remains in the residuals that can be removed by more appropriate modelling. Models with significant lack of fit of Prob>F value 0.10 or smaller should not be selected.

c) The selected model based on step (b) was analyzed using ANOVA where the significant of the model, significant parameters, and interaction factors were determined. The F value in the analysis compares model/factor variance with the residual variance (sum of square ratio). If the variance values are close to each other, then F value is close to unity and it is less likely that the model/factor to have significant effect on the output response. If the Prob>F value is small (less than 0.1), the model/ factor is considered to have a significant effect on the output response.

d) Once the model is statistically validated and main factors and interactions identified, the model can be plotted in 3-D surface model or be represented by polynomial equation

Table 3.7: Experimental matrix and the output response table

Run	A:Sputter Power (kW)	B:Substrate Bias Voltage (V)	C:Substrate Temperature (°C)	Output response 1: Hardness (GPa)	Output response 2: Roughness (nm)	Output response 3: Flank wear (mm)
1	6	-50	400			
2	4.81	-100.67	518.92			
3	4.81	-249.33	281.08			
4	6	-175	400			
5	6	-175	200			
6	4.81	-100.67	281.08			
7	7.19	-249.33	281.08			
8	6	-175	400			
9	6	-175	400			
10	4.81	-249.33	518.92			
11	7.19	-100.67	281.08			
12	6	-175	600			
13	7.19	-249.33	518.92			
14	6	-175	400			
15	8	-175	400			
16	6	-300	400			
17	7.19	-100.67	518.92			
18	4	-175	400			
19	6	-175	400			
20	6	-175	400			

3.4 Validation of the process model

The result of the modelling work consists of polynomial mathematical equations to represent relationships between PVD process input parameters (the sputter power, substrate bias voltage, and substrate temperature) and the resultant coating hardness, roughness, and wear performance. Quantitative validations of the developed model were

done by analysing the results of validation runs to assess if they meet the following two conditions:

1. To determine if the model can predict the validation run outcome based on specific input parameters within 90% of its predictive interval. The 90% predictive interval of the output responses were generated by the Design-Expert software using its optimisation analysis mode.
2. Residual error method can be used to assess the accuracy of a process model with respect to the validation run (Nordin et al. 2004). The residual error was calculated based on the percentage difference between validation run value and predicted value over the predicted value. This value should be less than 10% to represent the accuracy of the model.

Qualitative validations of the model were also performed by justifying the relationships between the individual PVD input process parameter and coating roughness, hardness, and wear performance of the developed coating based on published studies.

3.5 Correlation between coating performance (flank wear) and coating characteristic and coating microstructure

One of the objectives of this study is to establish if there is any correlation between coating performance, flank wear, and coating characteristics and microstructures. The method selected to accomplish this is by calculating coefficient of determination, R^2, based on Pearson product moment correlation coefficient method, R. The R^2 value indicates of how well a regression line represents the data. If the regression line passes exactly through every point on the scatter plot, it would be able to explain all of the variation. The further the line is away from the points, the less accurate is the particular

regression line. The coefficient of determination value will be in the range of $0 < R^2 < 1$. R^2 value of 1 means the regression line passes exactly through all points; R^2 value of 0 means denotes that no correlation at all between the two variables being investigated (Milton et al., 1997).

All the data obtained from the modelling experimental runs were compiled for the use of this correlation study. Respective coating characteristics and microstructure data were plotted against flank wear in form of scatter plot using EXCEL software. The regression line to best fit the data and the R^2 were also generated using the EXCEL software.

CHAPTER 4

RESULTS AND DISCUSSIONS

4.0 Results and Discussions

The results and discussion of this research are structured under these headings

- Modelling of the deposited TiAlN coating hardness, roughness, and wear performance.
- Microstructure analysis of the coating to explain the behaviour of the developed models.
- The interaction phenomenon of PVD process parameters affecting coating hardness, roughness, and wear performance.
- Quantitative correlation analysis between coating performance and the coating microstructure and characteristics.

4.1 Modelling of the deposited TiAlN coating hardness, roughness, and wear performance

The results of the modelling work consists of the RSM analyses to define the polynomial mathematical equations to represent relationships between PVD process input parameters (the sputter power, substrate bias voltage, and substrate temperature) and the resultant coating hardness, roughness, and wear performance. The quantitative validations of the developed model are presented by analysing the results of validation runs to assess if they meet the following two conditions:

1. To determine if the model can predict the validation run outcome based on specific input parameters within 90% of its predictive interval.
2. To calculate residual error between validation run roughness value and predicted roughness value based on specific input parameters. This value should be less than 10% to represent the accuracy of the model.

Qualitative validations of the model are also performed by justifying the relationships between individual PVD process parameters and coating roughness, hardness, and wear performance, in relation to published studies.

4.1.1 RSM modelling of TiAlN hardness with respect to PVD magnetron sputtering process parameters

Twenty experimental runs were carried out as listed in Table 4.1. The hardness of the developed TiAlN thin film coating for each experimental run was analysed using a NanoTest nano-hardness tester. The hardness data was obtained using a load of 50 mN with indentation depth of less than 10% of coating thickness. Six hardness measurements were collected per sample and the average hardness were calculated and used as the output response of the process as tabulated in Table 4.1.

Table 4.1: Experimental run and results of coating hardness

Run	Factor 2 A:Sputter Power (kW)	Factor 2 B:Bias Voltage (Volts)	Factor 3 C:Substrate Temperature (°C)	Response 1 Hardness (GPa)
1	6	-50	400	3.54
2	4.81	-100.67	518.92	5.27
3	4.81	-249.33	281.08	13.17
4	6	-175	400	10.96
5	6	-175	200	8.06
6	4.81	-100.67	281.08	4.33
7	7.19	-249.33	281.08	4.04
8	6	-175	400	16.12
9	6	-175	400	7.77
10	4.81	-249.33	518.92	3.53
11	7.19	-100.67	281.08	9.76
12	6	-175	600	7.48
13	7.19	-249.33	518.92	15.26
14	6	-175	400	8.91
15	8	-175	400	22.64
16	6	-300	400	14.14
17	7.19	-100.67	518.92	8.88
18	4	-175	400	15.69
19	6	-175	400	11.27
20	6	-175	400	12.34

Determination of appropriate polynomial equation to represent RSM model

RSM data analysis was carried out using Design Expert software. The determination of appropriate polynomial equations to represent the relationships between the input parameters and the output response (coating hardness) was done by carrying out sum of squares sequential model (SMSS) and lack of fit test shown in Table 4.2 and 4.3 respectively. Both analyses suggested the relationship between input parameters and resultant coating hardness can be modelled using quadratic equations.

Table 4.2: Sequential model sum of squares (SMSS) analysis for hardness model

Sequential Model Sum of Squares						
Source	**Sum of Squares**	**df**	**Mean Square**	**F Value**	**p-value Prob > F**	
Mean vs Total	2063.41	1	2063.41			Suggested
Linear vs Mean	87.82	3	29.27	1.19	0.3467	
2FI vs Linear	50.79	3	16.93	0.64	0.6032	
Quadratic vs 2FI	170.6	3	56.87	3.27	0.0673	Suggested
Cubic vs Quadratic	81.82	4	20.45	1.33	0.3576	Aliased
Quartic vs Cubic	49.43	1	49.43	5.81	0.0609	Aliased
Fifth vs Quartic	0	0				Aliased
Sixth vs Fifth	0	0				Aliased
Residual	42.55	5	8.51			
Total	2546.42	20	127.32			

Table 4.3: Lack of fit test for hardness model

Lack of Fit Tests						
Source	**Sum of Squares**	**df**	**Mean Square**	**F Value**	**p-value Prob > F**	
Linear	352.64	11	32.06	3.77	0.0773	
2FI	301.85	8	37.73	4.43	0.0589	
Quadratic	131.25	5	26.25	3.08	0.1209	Suggested
Cubic	49.43	1	49.43	5.81	0.0609	Aliased
Quartic	0	0				Aliased
Fifth	0	0				Aliased
Sixth	0	0				Aliased
Pure Error	42.55	5	8.51			

ANOVA analysis of the Response Surface Quadratic Model for coating hardness

The ANOVA analysis for the quadratic model is shown in Table 4.4. The "Model F-value" of 1.98 implies the model is not significant relative to the noise. There is a 15.16 % chance that a "Model F-value" this large could occur due to noise. This implies that the model does not represent the data within the required 90% confidence interval.

Table 4.4 ANOVA analysis of the quadratic model for coating hardness

ANOVA for Response Surface Quadratic Model					
Source	**Sum of Squares**	**df**	**Mean Square**	**F Value**	**p-value Prob > F**
Model	309.2	9	34.36	1.98	0.1516
A-Sputter Power	39.84	1	39.84	2.29	0.161
B-Bias Voltage	47.95	1	47.95	2.76	0.1277
C-Substrate Temperature	0.033	1	0.033	1.89E-03	0.9662
AB	5.21	1	5.21	0.3	0.596
AC	45.29	1	45.29	2.61	0.1376
BC	0.29	1	0.29	0.016	0.9003
A_2	56.24	1	56.24	3.24	0.1023
B_2	40.41	1	40.41	2.33	0.1583
C_2	60.67	1	60.67	3.49	0.0913
Residual	173.8	10	17.38		
Lack of Fit	131.25	5	26.25	3.08	0.1209
Pure Error	42.55	5	8.51		
Cor Total	483.01	19			

To improve the model a cubic term ABC is added to the model and the ANOVA analysis of the Reduced Cubic Model is shown in Table 4.5. In the ANOVA analysis “The Model F-value” of 3.07 implies the model is significant and the “Prob > F” value indicated that there is only a 5.31% chance that a "Model F-Value" this large could occur due to noise. The accuracy of this model is also supported by the lack of fit analysis. The "Lack of Fit F-value" of 1.97 implies the Lack of Fit is not significant relative to the pure error. There is a 23.8% chance that a "Lack of Fit F-value" this large could occur due to noise.

Determination of significant factors influencing coating hardness

Determination of the process parameters and potential interactions affecting the surface hardness were done by carrying out analysis of variance (ANOVA) on the quadratic response surface model shown in Table 4.5. Based on the p-value of less than 0.1, bias voltage, interaction between sputter power and substrate temperature,

sputter power quadratic term, and substrate temperature quadratic term are the significant influencing factors of the resultant surface hardness. The interaction among the three input parameters "ABC" p-value is also below 0.1, however the significant of the "ABC" interaction cannot be ascertained due to alias nature of cubic term for this particular experimental set-up.

Table 4.5: ANOVA analysis of the Reduced Cubic Model for coating hardness

ANOVA for Response Surface Reduced Cubic Model					
Source	**Sum of Squares**	**df**	**Mean Square**	**F Value**	**p-value Prob > F**
Model	373.51	10	37.35	3.07	0.0531
A-Sputter Power	39.84	1	39.84	3.27	0.1038
B-Bias Voltage	47.95	1	47.95	3.94	0.0784
C-Substrate Temperature	0.033	1	0.033	2.70E-03	0.9597
AB	5.21	1	5.21	0.43	0.5292
AC	45.29	1	45.29	3.72	0.0858
BC	0.29	1	0.29	0.024	0.8814
A2	56.24	1	56.24	4.62	0.06
B2	40.41	1	40.41	3.32	0.1017
C2	60.67	1	60.67	4.99	0.0524
ABC	64.3	1	64.3	5.29	0.0471
Residual	109.5	9	12.17		
Lack of Fit	66.95	4	16.74	1.97	0.238
Pure Error	42.55	5	8.51		
Cor Total	483.01	19			

To illustrate the influence of parameters on the hardness, the effect of main factors (significant process parameters determined through earlier ANOVA analysis) are discussed below. The behaviour of the coating hardness in response to variation of main factors was also compared to work published by other researchers to support the validity of the model.

- Substrate bias main factor curve in Figure 4.1 indicates that as the sputtering power increases from -100V to -250V, coating hardness increases from 7.8

GPa to 11.6 GPa with a diminishing rate. Beyond -180 V, increase in substrate bias does not affect the hardness of deposited coating. Studies by Evans et al. (2007) on the effect of substrate bias within range of 0V to -300V and Ahlgren and Blomqvist (2005) for the range of -40V to -200V indicated the same trend where the hardness increased as the substrate bias increased before it leveled off at -175V and -100V respectively.

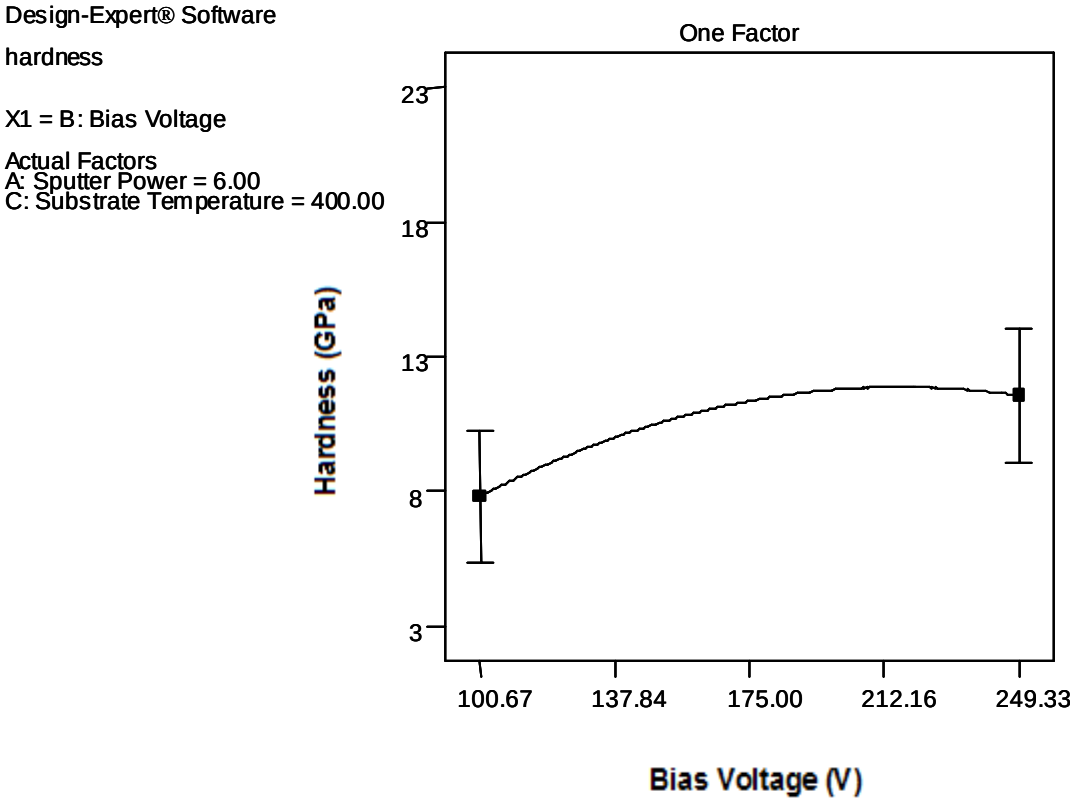

Figure 4.1: Behaviour of coating hardness in response to variation of substrate bias voltage.

- Substrate temperature: As shown in Figure 4.2, increase in substrate temperature from 281°C to 518°C resulted in an insignificant change of coating hardness from 9.3 GPa to 9.4 GPa. However, the quadratic term of substrate temperature in the ANOVA analysis, Table 4.5, indicate a p-value of less than 0.1 reflecting the significance of the quadratic term value. This is also indicated by main effect graph in Figure 4.2, where the highest hardness

value, around 420°C, is 11.4 GPa before it starts to drop. Published studies by Choi et al. (2004), Chou et al. (2003), and González et al.(2007) evaluated the effect of substrate temperature from room temperature up to 430°C; Results indicated an increase in hardness with rising temperature, which is supported by findings from this study. The downward trend of the deposited coating hardness found in this study can be attributed to grain growth (Choi et al. ,2004) which also reflected by Thornton model (Mattox, 1998).

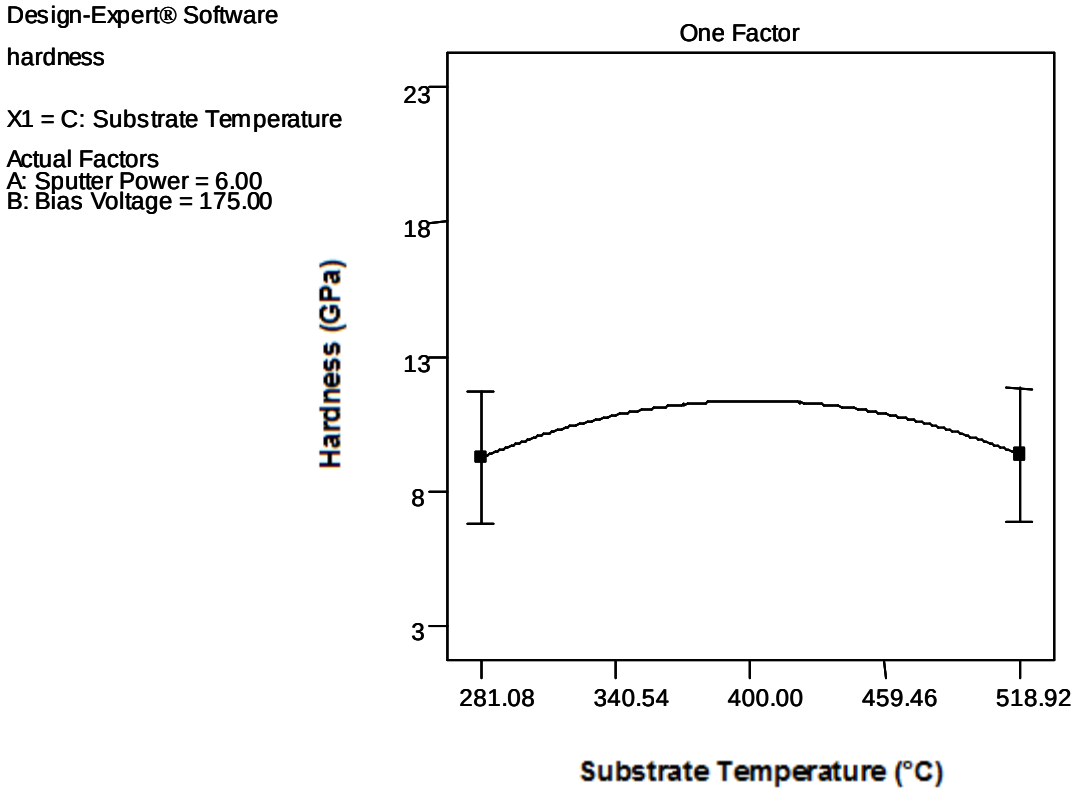

Figure 4.2: Behaviour of coating hardness in response to variation in substrate temperature.

Sputtering power: Figure 4.3 indicates that an increase in sputtering power from 4.8 kW to 9.2 kW resulted in an increase of coating hardness from 11.6 GPa to 15

GPa. This significant increment is support by sputter power p-value of 0.1 in the ANOVA analysis, Table 4. Reported studies on deposition of TiAlN thin films by Wuhrer and Yeung (2002) and by Gredict and Zlatanovic (1991) supported this finding where the increased in sputtering power brought about an increase in the thin film coating hardness. Higher hardness values being attributed to a denser microstructure and increase in compressive residual stresses in the coating.

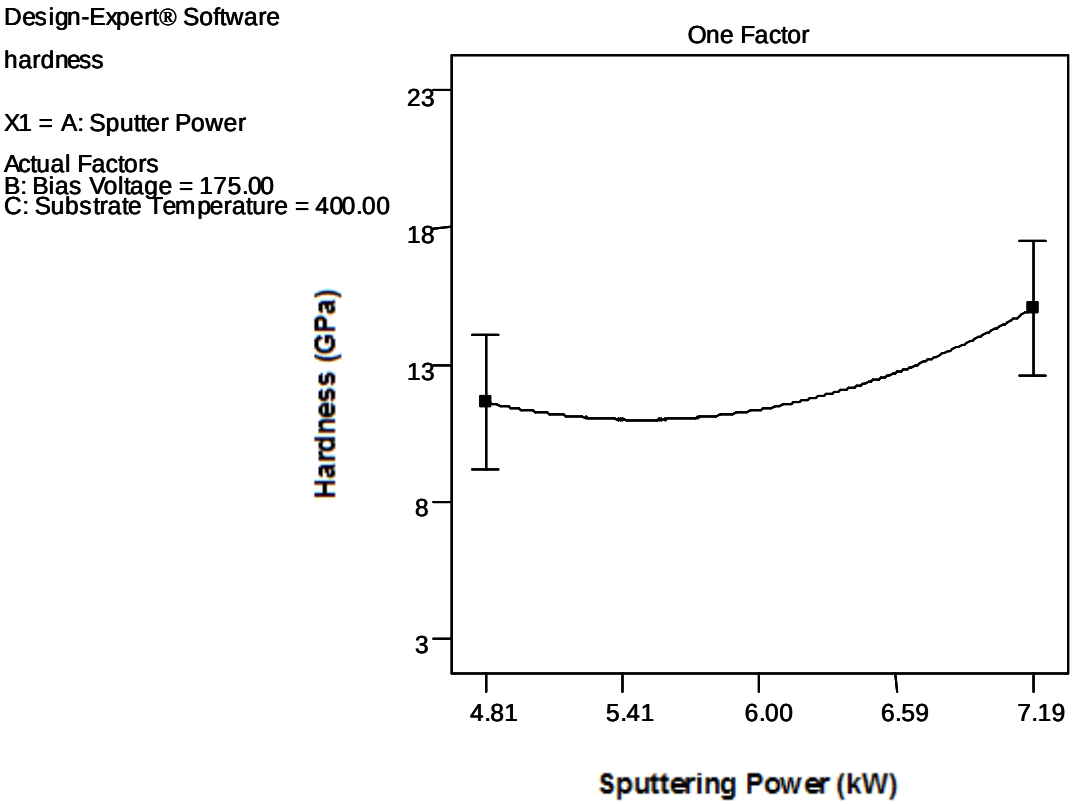

Figure 4.3: Behaviour of coating hardness in response to variation of sputtering power.

- Interaction between substrate temperature and sputtering power: The ANOVA analysis also revealed that one of the significant factors influencing the coating hardness is the interaction between sputtering power and substrate temperature. Figure 4.4 shows the interaction behaviour of sputtering power and substrate temperature with respect to resultant coating hardness. At low substrate temperature, 281°C, the variation in sputtering

power resulted in minimal change in coating hardness. However at high substrate temperature, 518°C, variation in sputter power resulted in significant changes in coating hardness. This indicates strong interaction between the two parameters. There is no published work on the interaction of these two parameters affecting the hardness on the developed coating. Detail discussion on this interaction phenomenon is covered section 4.3.

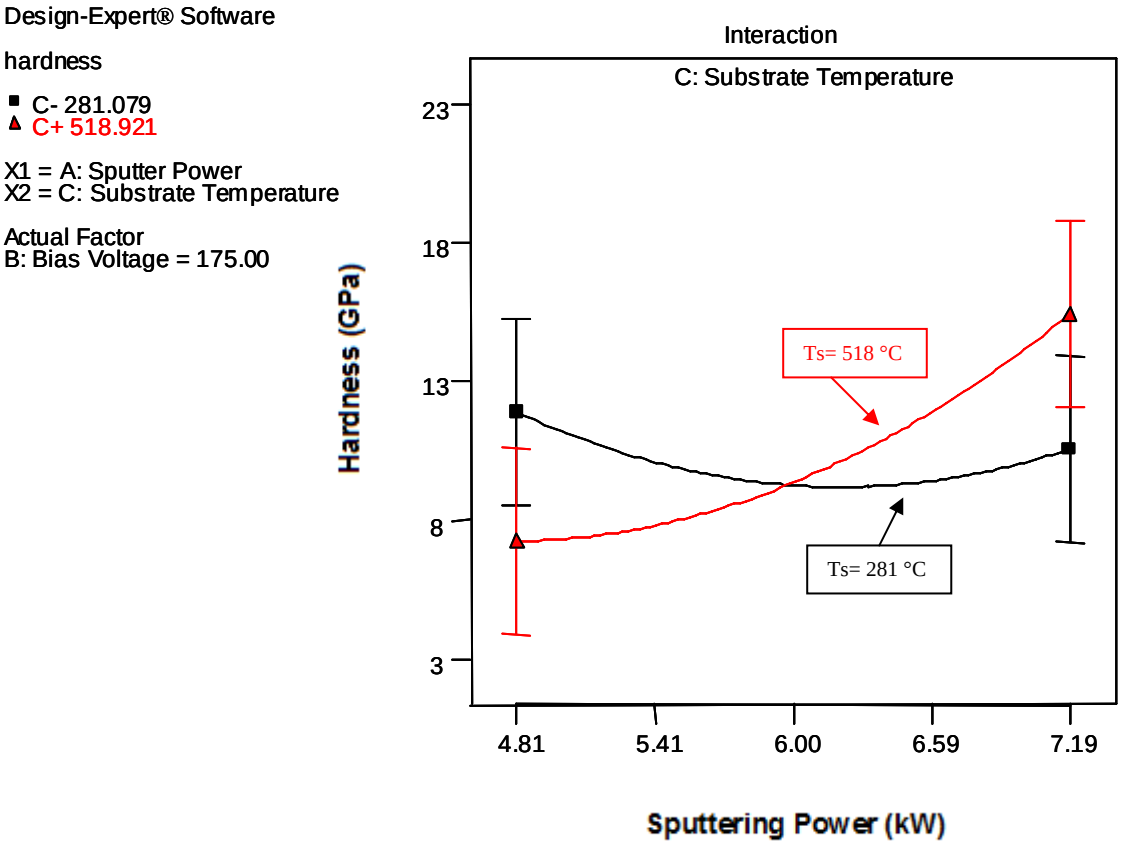

Figure 4.4: Interaction between sputter power and substrate temperature with respect to coating hardness

From the surface response modelling the quadratic polynomial equation developed to relate the input parameters to the coating hardness is shown in Equation 4.1

$$\text{Hardness (GPa)} = -65.04488 - 1.57702P_s + 0.82486V_s + 0.29499T_s - 0.11702P_sV_s - 0.030377P_sT_s - 1.59691E\text{-}003V_sT_s + 1.39684P_s^2 - 3.03132E\text{-}004V_s^2 - 1.45081E\text{-}04T_s^2 + 2.69721E\text{-}004P_sV_sT_s$$

P_s: Sputter Power (kW)
T_s: Substrate temperature (°C)
V_s: Substrate bias voltage (V)

Equation 4.1 Polynomial equation representing the coating hardness model with respect to substrate temperature, substrate bias, and sputter power

Graphically, this equation can be represented by 3D surface response plot and Example of this 3-D plot is shown in Figure 4.5. The plot shows the effect of varying two parameters while holding the other parameter constant at center point. Figure 4.5 shows influence of quadratic function of substrate bias and significant influence of sputtering power on coating hardness.

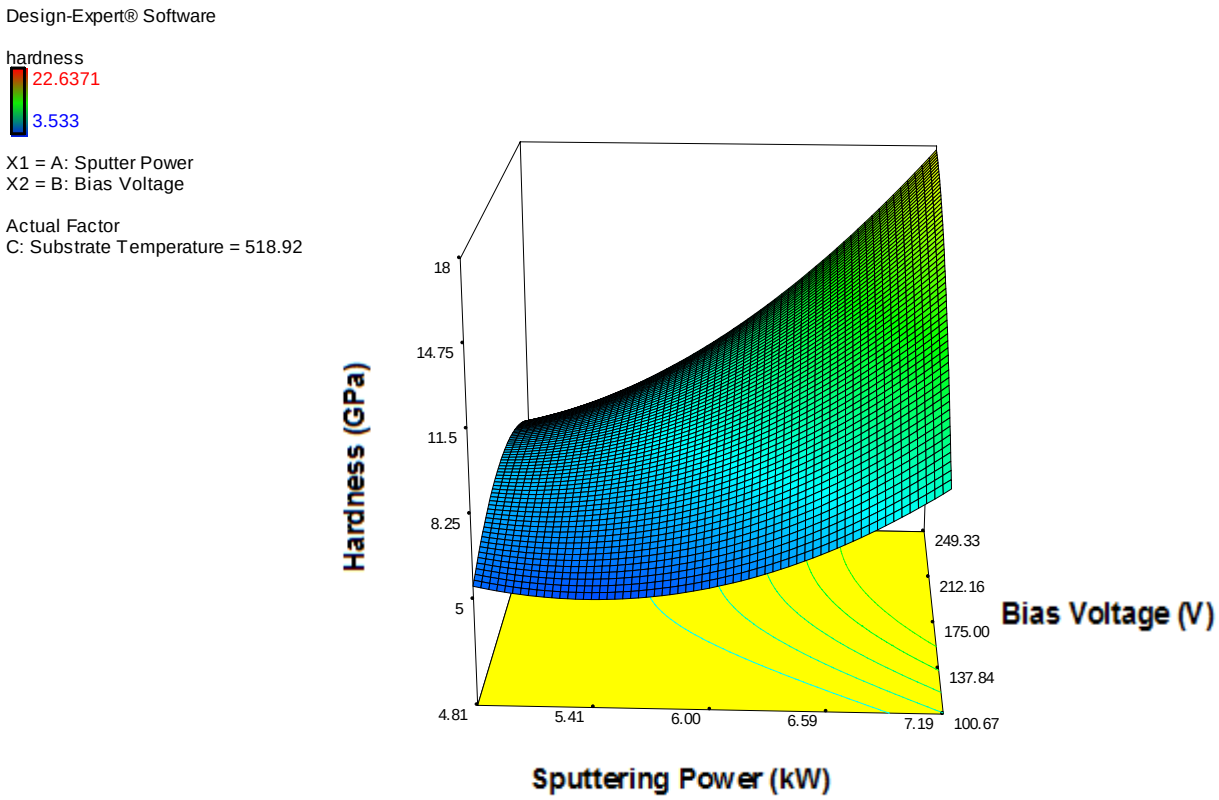

Figure 4.5: Influence of quadratic function of substrate bias and significant influence of sputter power on coating hardness.

Model validation

Validation of model to determine if the developed response surface model can predict the coating process behaviour was successfully performed. Using the point prediction capability of the software, three sets of process parameters were chosen as validation runs. The software, based on the algorithm developed, calculates the predicted hardness values together with their 90% prediction interval values. The residual error comparing predicted and validated hardness values were also calculated to determine the accuracy of the model. If the validation data falls within the 90% prediction interval and the residual errors are less that 10%, the model is considered validated and accurate. The validation results of the three sets of parameter settings are shown in Table 4.6. As shown in Table 4.6 the actual hardness data from three validation runs fall within the 90% prediction interval and the residual errors are ranging from 4.9% to 9.6%. This indicates that the model is accurate enough to predict the resultant coating hardness within 90% CI and the residual error relative to predicted values are less than 10%.

Table 4.6: Validation data of coating hardness model

Input parameters			**Prediction (GPa)**	**90% PI low (GPa)**	**90% PI Hi (GPa)**	**Actual (GPa)**	**Error (%)**
Sputter Power	**Bias Voltage**	**Substrate Temperature**					
5	-100	280	4.7	0	13	5.2	9.6
6.5	-150	350	11.1	4.23	18	10.3	-7.7
7	-145	450	13.5	6.48	20.5	14.2	4.9

4.1.2 RSM modelling of TiAlN coating surface roughness with respect to PVD magnetron sputtering process parameters

Twenty experimental runs were carried out as listed in Table 4.7. The roughness of the developed TiAlN thin film coating for each experimental run was analysed using Shimadzu SPM-9500J2 Atomic Force Microscopy (AFM) apparatus. The detection mode used was contact mode using a commercial Si_3N_4 cantilever and the scanning area was set 5x 5 microns. The roughness data, in nanometres (nm), for the developed coating of each experimental run is tabulated in Table 4.7.

Table 4.7 Experimental run and results of coating roughness

	Factor 2	Factor 2	Factor 3	Response 1
	A:Sputter Power	B:Bias Voltage	C:Substrate Temperature	Roughness
Run	(kW)	(Volts)	(°C)	(nm)
1	6	-50	400	81.00
2	4.81	-100.67	518.92	65.60
3	4.81	-249.33	281.08	81.90
4	6	-175	400	70.30
5	6	-175	200	58.80
6	4.81	-100.67	281.08	75.60
7	7.19	-249.33	281.08	44.30
8	6	-175	400	48.10
9	6	-175	400	43.70
10	4.81	-249.33	518.92	56.10
11	7.19	-100.67	281.08	49.90
12	6	-175	600	56.00
13	7.19	-249.33	518.92	49.10
14	6	-175	400	57.90
15	8	-175	400	40.20
16	6	-300	400	100.00
17	7.19	-100.67	518.92	67.30
18	4	-175	400	47.40
19	6	-175	400	45.00
20	6	-175	400	63.60

The determination of appropriate polynomial equation for the model

The determination of appropriate polynomial equation to represent the relationship between the input parameters and the output response (surface roughness) was

performed by carrying out sequential model sum of squares (SMSS) and a lack of fit test as shown in Table 4.8 and Table 4.9 respectively. Both analyses suggested the relationship between input parameters and resultant coating surface roughness can be modelled using a quadratic equation.

Table 4.8: Sequential model sum of square for coating roughness model

Sequential Model Sum of Squares						
Source	**Sum of Squares**	**df**	**Mean Square**	**F Value**	**p-value Prob > F**	
Mean vs Total	72216.16	1	72216.16			
Linear vs Mean	503.31	3	167.77	0.65	0.5964	
2FI vs Linear	574.37	3	191.46	0.7	0.571	
Quadratic vs 2FI	2541.77	3	847.26	8.18	0.0048	Suggested
Cubic vs Quadratic	410.8	4	102.7	0.99	0.4809	Aliased
Residual	624.73	6	104.12			
Total	76871.14	20	3843.56			

Table 4.9: Lack of fit test for coating roughness model

Lack of Fit Tests						
Source	**Sum of Squares**	**df**	**Mean Square**	**F Value**	**p-value Prob > F**	
Linear	3560.23	11	323.66	2.74	0.1382	
2FI	2985.87	8	373.23	3.16	0.1106	
Quadratic	444.1	5	88.82	0.75	0.6196	Suggested
Cubic	33.3	1	33.3	0.28	0.6184	Aliased
Pure Error	591.43	5	118.29			

Determination of significant factors influencing resultant coating roughness

Determination of the process parameters and the presence of interactions affecting the surface roughness were done by carrying out analysis of variance (ANOVA) on the quadratic response surface model as shown in Table 4.10. Based on the p-value of less than 0.1, sputtering power, interaction between sputtering power and substrate temperature, and substrate bias quadratic term are the significant influencing factors of the resultant surface roughness.

Table 4.10: ANOVA for coating roughness model

ANOVA for Response Surface Quadratic Model

Source	Sum of Squares	df	Mean Square	F Value	p-value Prob > F
Model	3619.45	9	402.16	3.88	0.0229
A-Sputter Power	476.97	1	476.97	4.61	0.0574
B-Bias Voltage	1.8	1	1.8	0.017	0.8978
C-Substrate Temperature	24.55	1	24.55	0.24	0.6368
AB	53.04	1	53.04	0.51	0.4905
AC	420.5	1	420.5	4.06	0.0716
BC	100.82	1	100.82	0.97	0.3471
A^2	299.49	1	299.49	2.89	0.1198
B^2	2058.74	1	2058.74	19.88	0.0012
C^2	0.9	1	0.9	8.67E-03	0.9276
Residual	1035.53	10	103.55		
Lack of Fit	444.1	5	88.82	0.75	0.6196
Pure Error	591.43	5	118.29		
Cor Total	4654.98	19			

To illustrate the influence of parameters on the surface roughness, the main effect and interaction analysis are as follows:

- Sputtering power: as the sputtering power increases from 4.81kW to 7.19kW, coating roughness reduced from 56.2 nm to 44.4 nm. (Fig 4.6). This is aligned with findings by Wuhrer and Yeung (2002) who reported a decrease in roughness with the increase in sputtering power.

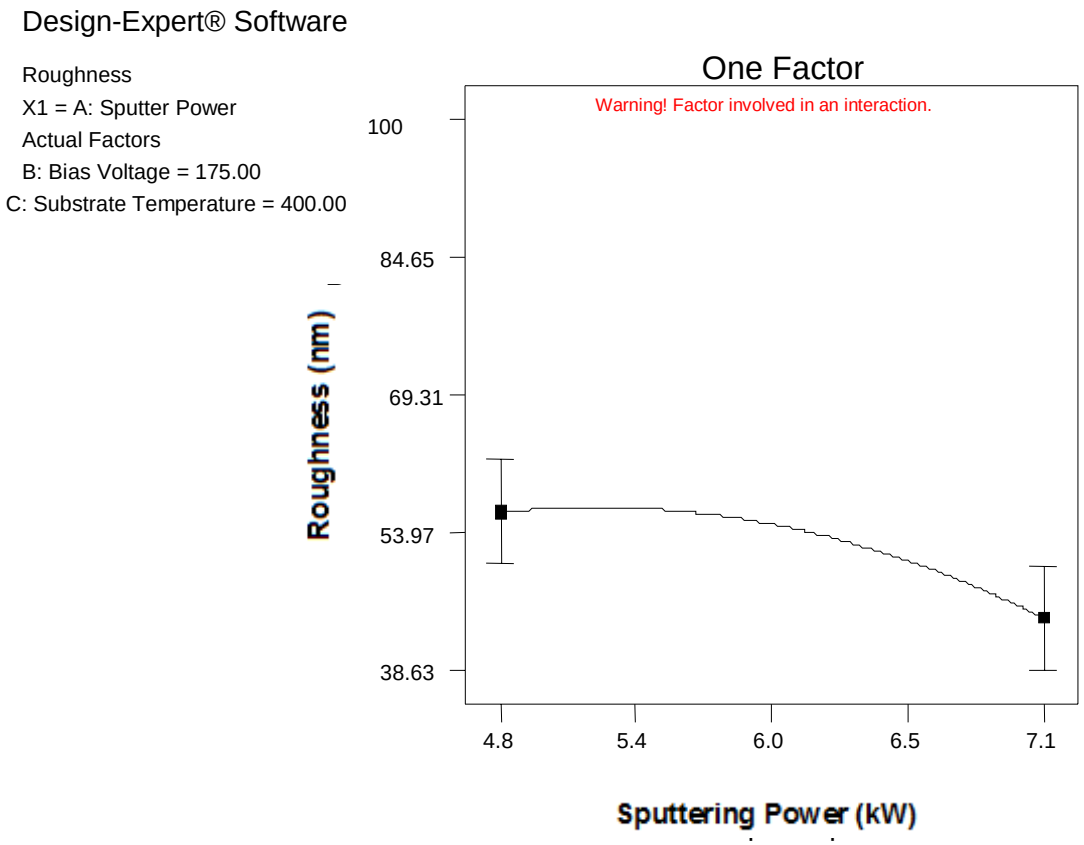

Figure 4.6: Behaviour of coating roughness in response to variation of sputtering power

- Substrate bias: As reflected in Figure 4.7, as the substrate bias increases from -100.67 to -175 V the coating roughness decreases from 66.4nm to 55nm and as the substrate bias increases from -175V to -249V, the coating roughness increases from 55nm to 67nm. This is reflected by the ANOVA analysis in Table 4.10 where the quadratic term of substrate bias is a significant term. This trend is supported by work from Barshilia and Rajam, (2004) that indicated as the substrate bias increased from -0V to -200V, the developed coating roughness reduced significantly. The upward trend of coating roughness beyond certain substrate bias level, as indicated in this study, was also reported by Cheng et al. (2002). This could be due to imperfection of

coating surface caused by bombardment of ions with excessively high energy level above certain substrate bias voltage (Hultman et al. 1987).

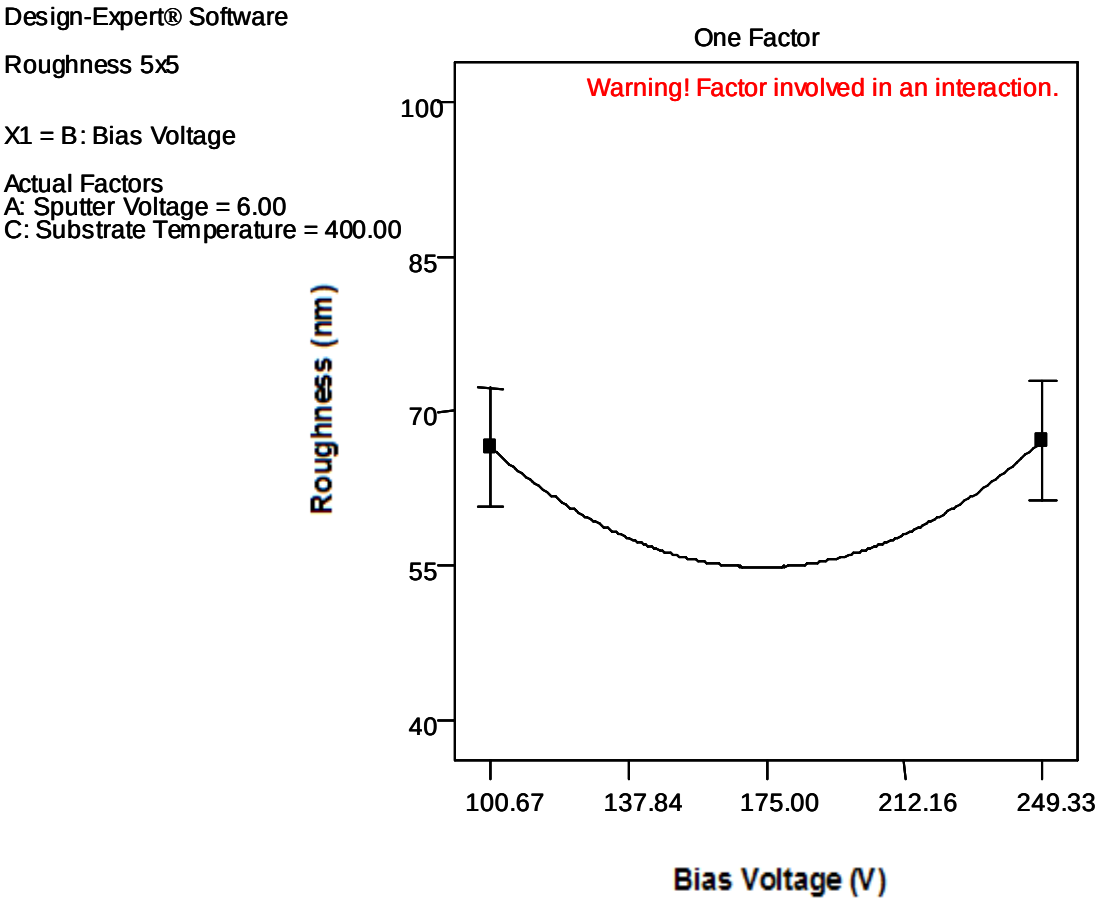

Figure 4.7: Behaviour of coating roughness in response to variation of substrate bias voltage.

- Interaction between sputtering power and substrate temperature: The ANOVA analysis also revealed that one of the significant factors influencing the coating roughness is the interaction between sputtering power and the substrate temperature. As shown in Figure 4.8, at low levels of substrate temperature, changes in sputtering power does not significantly affect coating roughness. However at the high levels of substrate temperature, increases in

sputtering power significantly reduce coating roughness. This indicates strong interaction exists between these two parameters that affect coating roughness. This is similar to findings in the modelling work for hardness of deposited coating in earlier section (4.1.1). Further discussion on these interaction phenomena is covered in section 4.3.

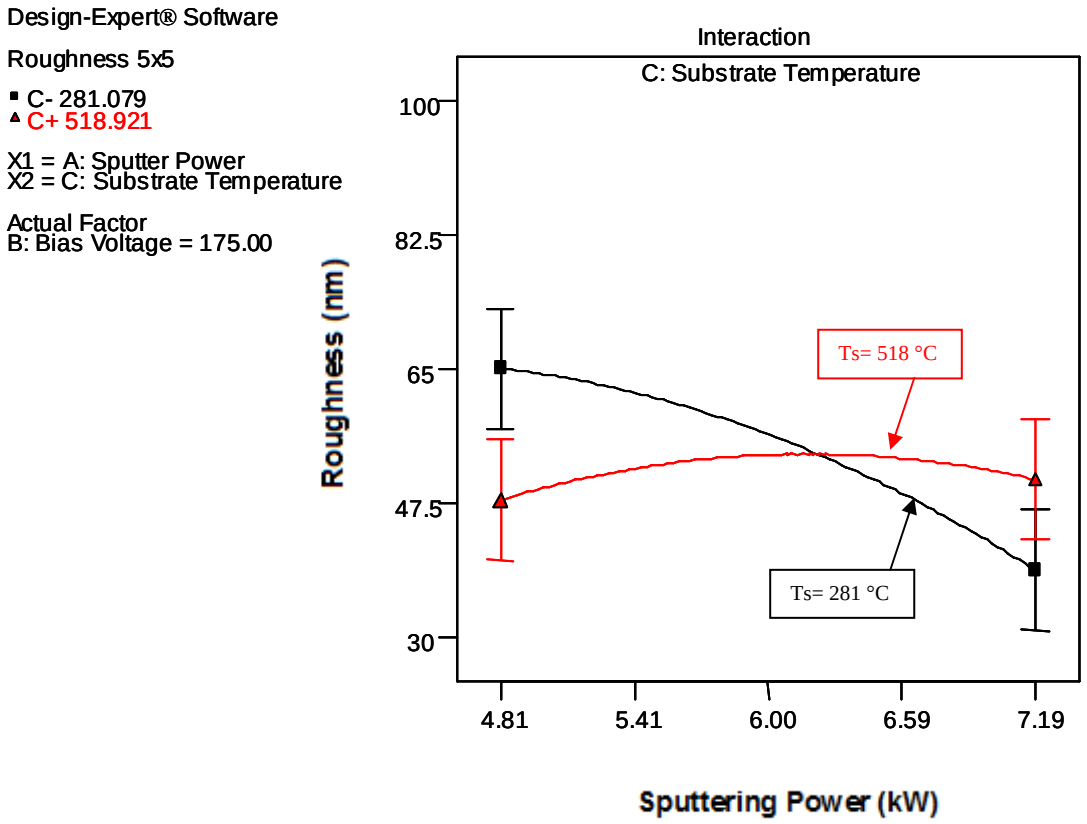

Figure 4.8: Behaviour of coating roughness relative to interaction between sputtering power and substrate temperature.

Polynomial equation of the roughness model

From the surface response modelling the quadratic polynomial equation developed to relate the input parameters to the coating roughness is shown in Equation 4.2.

Roughness (nm) = +105.71410+18.30453P_s -0.41692V_s -0.26270T_s -0.029133P_sV_s+ 0.051265P_sT_s -4.01637E-004V_sT_s -3.22349P_s^2 +2.16359E-003V_s^2+1.76509E-005T_s^2

P_s: Sputter Power (kW)
T_s: Substrate temperature (°C)
V_s: Substrate bias voltage (V)

Equation 4.2: Quadratic polynomial equation representing the coating roughness model with respect to substrate temperature, substrate bias, and sputter power

Graphically, this equation can be represented by 3D surface response plots. Examples of this 3D surface response plot are shown in Figure 4.9 and 4.10. Each plot shows the effect of varying two parameters while holding the other parameter constant at center point. Figure 4.9 shows the influence of quadratic function of substrate bias and significant influence of sputter power on coating roughness and Figure 4.10 shows the significant influence of the quadratic term of substrate bias on coating roughness .

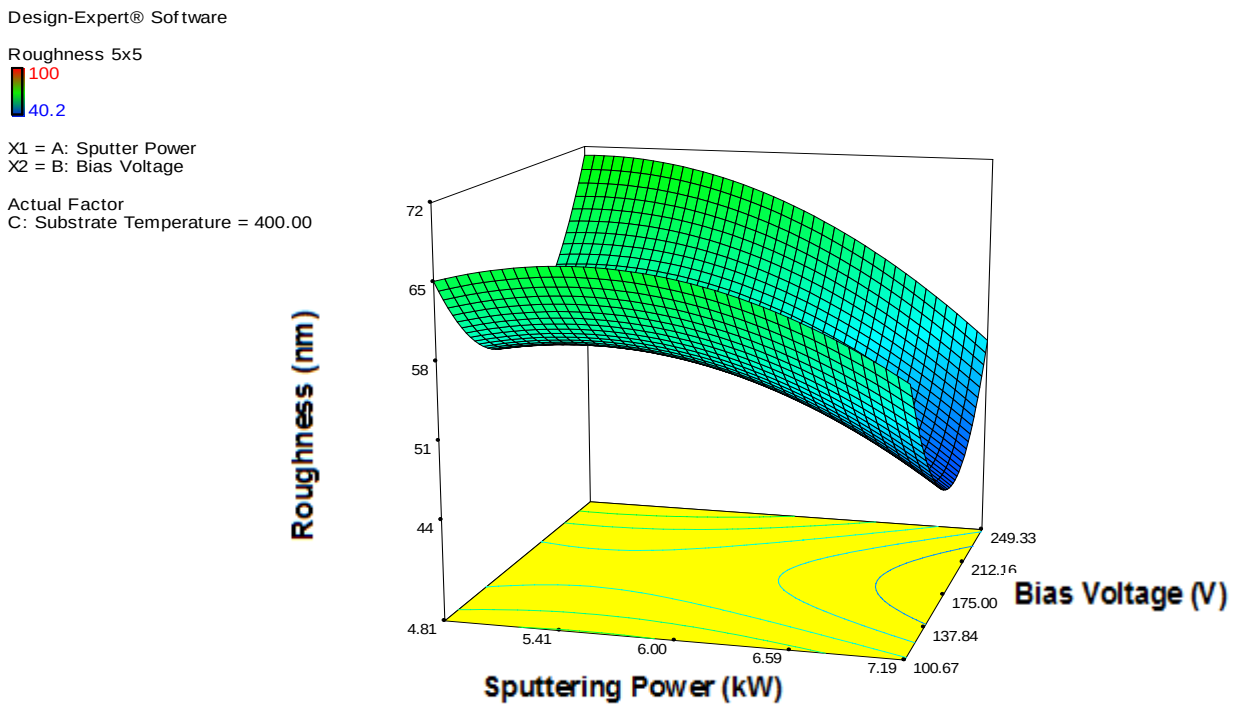

Figure 4.9: Response surface model holding substrate temperature at constant 400°C

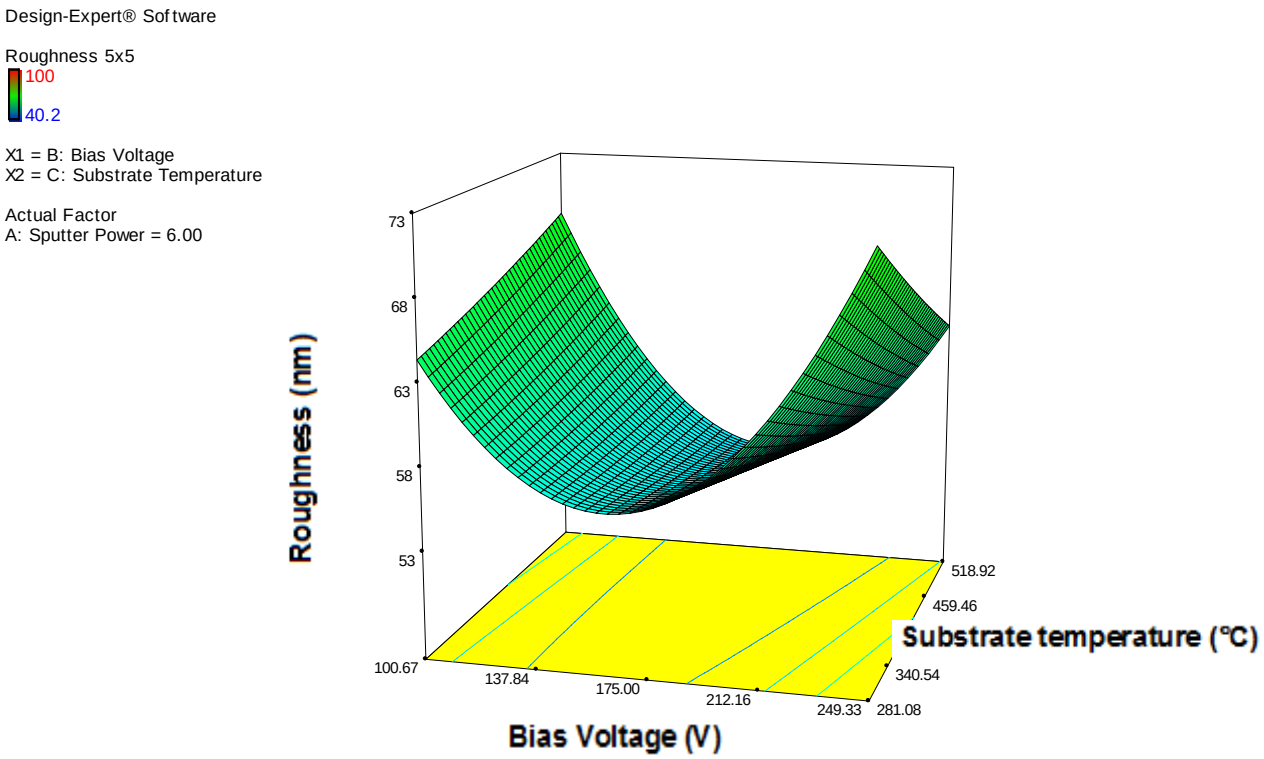

Figure 4. 10: Significant influence of quadratic term of substrate bias while holding sputtering power at 6 kW

Model validation

Validation of model to determine if the developed response surface model can predict the coating process behaviour was successfully done. The validation results of the three sets of parameter settings are shown in Table 4.11. As shown in Table 4.11 the actual roughness data from the validation runs fall within the 90% prediction interval and the residual errors are ranging between 1.28% to 4.98%, which in absolute value is less than 10%. This indicates that the model is accurate enough to predict the resultant coating roughness within 90% CI and the residual error relative to predicted values are less than 10%.

Table 4.11: Summary of validation run for surface roughness model.

Validation run	Input parameters			Prediction	Prediction interval		Validation	Residual Error (%)
	Sputter Power (kW)	Bias Voltage (V)	Substrate Temp. (°C)	Coating roughness (nm)	90% PI low (nm)	90% PI Hi (nm)	Coating roughness (nm)	
1	5	-100	280	70.1001	47.04	93.16	66.3	-3.8001
2	6.5	-150	350	52.0158	32.13	71.9	53.3	1.2842
3	7	-145	450	52.0837	31.87	72.3	47.1	-4.9837

4.1.3 RSM modelling of TiAlN coated tool wear performance during turning operation with respect to PVD magnetron sputtering process parameters

Twenty tungsten carbide cutting tool inserts were coated with TiAlN using process parameters based on the experimental runs listed in Table 4.12. The coated tools were subjected to dry turning of AISI D2 X115Cr VMo121 steel using MOMAC lathe machine model SM 200. The cutting speed was 200m/min, the feed rate was 0.25 mm/rev and the depth of cut was 1.6 mm. The cutting length was fixed at 18 metres for all the experimental runs and the flank wear measurement was performed using Axiomat 2 microscope with Axiovison software. The resultant flank wear values are tabulated in Table 4.12.

Table 4.12 Experimental run and results of cutting tool performance (flank wear)

	Factor 2	**Factor 2**	**Factor 3**	**Response**
Run	**A:Sputter Power**	**B:Bias Voltage**	**C:Substrate Temperature**	**Flank wear**
	(kW)	**(Volts)**	**(°C)**	**(mm)**
1	6	-50	400	2.29
2	4.81	-100.67	518.92	1.08
3	4.81	-249.33	281.08	0.73
4	6	-175	400	1.40
5	6	-175	200	0.94
6	4.81	-100.67	281.08	2.01
7	7.19	-249.33	281.08	1.92
8	6	-175	400	0.57
9	6	-175	400	1.26
10	4.81	-249.33	518.92	1.97
11	7.19	-100.67	281.08	1.18
12	6	-175	600	1.72
13	7.19	-249.33	518.92	0.35
14	6	-175	400	0.86
15	8	-175	400	0.27
16	6	-300	400	1.03
17	7.19	-100.67	518.92	0.93
18	4	-175	400	0.56
19	6	-175	400	0.85
20	6	-175	400	0.83

The determination of appropriate polynomial equation for the flank wear model

The determination of appropriate polynomial equation to represent the relationship between the input parameters and the output response (flank wear) was done by carrying out sequential model sum of squares (SMSS) and lack of fit test shown in Tables 4.13 and 4.14 respectively. Both analyses suggested the relationship between input parameters and resultant coating performance (flank wear) can be modelled using a quadratic equation. Even though the p-value of SMSS for cubic model is less than that of quadratic model, the quadratic model is an aliased model, meaning that not enough experiments have been run to independently estimate all the terms for this model.

Table 4.13: Sequential model sum of square to determine the appropriate polynomial model for coating wear performance

Sequential Model Sum of Squares						
Source	**Sum of Squares**	**df**	**Mean Square**	**F Value**	**p-value Prob > F**	
Mean vs Total	25.87	1	25.87			Suggested
Linear vs Mean	0.67	3	0.22	0.63	0.6078	
2FI vs Linear	0.7	3	0.23	0.6	0.6247	
Quadratic vs 2FI	1.94	3	0.65	2.11	0.1624	Suggested
Cubic vs Quadratic	2.54	4	0.63	7.27	0.0175	Aliased
Quartic vs Cubic	0.05	1	0.05	0.53	0.5012	Aliased
Fifth vs Quartic	0	0				Aliased
Sixth vs Fifth	0	0				Aliased
Residual	0.47	5	0.095			
Total	32.24	20	1.61			

Table 4.14: Lack of fit test to determine the appropriate polynomial model for coating wear performance

Lack of Fit Tests						
Source	**Sum of Squares**	**df**	**Mean Square**	**F Value**	**p-value Prob > F**	
Linear	5.22	11	0.47	5.01	0.0441	
2FI	4.53	8	0.57	5.97	0.0324	
Quadratic	2.59	5	0.52	5.46	0.043	Suggested
Cubic	0.05	1	0.05	0.53	0.5012	Aliased
Quartic	0	0				Aliased
Fifth	0	0				Aliased
Sixth	0	0				Aliased
Pure Error	0.47	5	0.095			

ANOVA analysis of the Response Surface Quadratic Model

The ANOVA analysis for the quadratic model is shown in Table 4.15. The "Model F-value" of 1.20 implies the model is not significant relative to the noise. There is a 38.82 % chance that a "Model F-value" this large could occur due to noise. This implies that the model does not represent the data within the required 90% confidence interval. The lack of fit value also supported the finding where the "Lack of Fit F-value" of 5.46 implies the Lack of Fit is significant. There is only a 4.30% chance that a "Lack of Fit F-value" this large could occur due to noise. Significant lack of fit indicates the model does not fit the data.

Table 4.15: The ANOVA analysis for the quadratic model of coating wear performance

ANOVA for Response Surface Quadratic Model						
Source	**Sum of Squares**	**df**	**Mean Square**	**F Value**	**p-value Prob > F**	
Model	3.31	9	0.37	1.2	0.3882	not significant
A-Sputter Power	0.26	1	0.26	0.85	0.3776	
B-Bias Voltage	0.41	1	0.41	1.33	0.2763	
C-Substrate Temperature	2.99E-03	1	2.99E-03	9.78E-03	0.9232	
AB	0.037	1	0.037	0.12	0.7363	
AC	0.57	1	0.57	1.86	0.2031	
BC	0.091	1	0.091	0.3	0.5982	
A_2	0.4	1	0.4	1.3	0.28	
B_2	1.08	1	1.08	3.51	0.0903	
C_2	0.35	1	0.35	1.15	0.3079	
Residual	3.06	10	0.31			
Lack of Fit	2.59	5	0.52	5.46	0.043	significant
Pure Error	0.47	5	0.095			
Cor Total	6.37	19				

To improve the model a cubic term ABC is added to the model and the ANOVA and lack of fit analysis of the Reduced Cubic Model is shown in Table 4.16. The ANOVA analysis, in Table 4.16, indicates that “The Model F-value” is 2.84 implying that the model is significant and the “Prob > F” value indicated that there is only a 6.59% chance that a "Model F-Value" this large could occur due to noise. The accuracy of this model also supported by the lack of fit analysis. The "Lack of Fit F-value" of 2.79 implies the Lack of Fit is not significant relative to the pure error. There is a 14.51% chance that a "Lack of Fit F-value" this large could occur due to noise.

Table 4.16: The ANOVA analysis for the reduced cubic model of coating wear performance

ANOVA for Response Surface Reduced Cubic Model						
	Sum of		**Mean**	**F**	**p-value**	
Source	**Squares**	**df**	**Square**	**Value**	**Prob > F**	
Model	4.83	10	0.48	2.84	0.0659	significant
A-Sputter Power	0.26	1	0.26	1.53	0.247	
B-Bias Voltage	0.41	1	0.41	2.38	0.157	
C-Substrate Temperature	2.99E-03	1	2.99E-03	0.018	0.8975	
AB	0.037	1	0.037	0.22	0.6535	
AC	0.57	1	0.57	3.34	0.1011	
BC	0.091	1	0.091	0.53	0.4841	
A_2	0.4	1	0.4	2.35	0.16	
B_2	1.08	1	1.08	6.32	0.0331	
C_2	0.35	1	0.35	2.08	0.1836	
ABC	1.53	1	1.53	8.98	0.015	
Residual	1.53	9	0.17			
Lack of Fit	1.06	4	0.26	2.79	0.1451	
Pure Error	0.47	5	0.095			
Cor Total	6.37	19				

The significant process parameters that influence tool wear performance

From ANOVA analysis of the reduced cubic model in Table 4.16, the significant factors that influence the tool wear performance of coated tools, indicated by a " p-value" of less that 0.1, is the interaction between sputtering power and substrate temperature and the squared value of substrate bias voltage. The interaction among the three input parameters "ABC" p-value is also below 0.1, however the significance of the "ABC" interaction cannot be ascertained due to the aliased nature of cubic term for this particular experimental set-up.

To illustrate the influence of the interaction between sputtering power and substrate temperature and the quadratic value of substrate bias voltage on the tool wear performance, the main effects and interaction analysis are as follows:

- Squared value of substrate bias voltage:

Figure 4.11 shows the quadratic curve indicating the influence of substrate bias voltage on the tool wear performance of the coated cutting insert while varying the voltage and holding the sputter power and substrate temperature constant at 6 kW and 400 ^{o}C respectively. Figure 4.11 indicates that as the substrate bias increases from -100.67 V to -175 V the flank wear decreases from 1.40 mm to 0.96 mm and as the substrate bias increases from -175V to -249V, the flank wear increases from 0.96 to 1.06 mm. The decreasing tool wear trend as the substrate bias increases was reported by Weber et al. (2004). Their findings indicated that as the substrate bias increased from -30V to -125V, the tool life increased monotonically. To support the finding of deterioration of coated tool performance as the substrate bias increases beyond certain level is a study done by Ahlgren and Blomqvist (2005) who investigated effect of substrate bias ranging from -40V to -200 V on TiAlN coating. Their result indicated that beyond -100V the tool performance decreased, this being attributed to excessive residual stress in the developed coating resulting in delamination of coating from substrate. The delamination occurs when the coating residual stress is greater than the adhesion strength between the coating and the substrate.

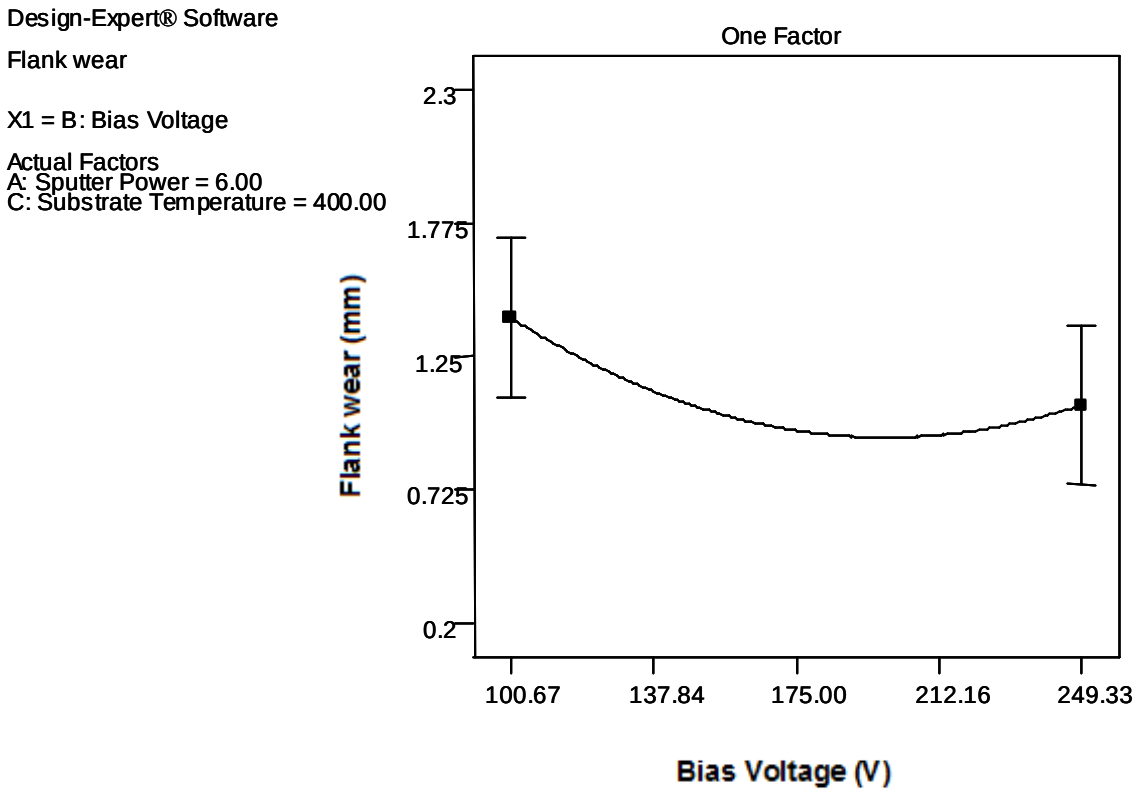

Figure 4.11: Influence of substrate bias voltage on the tool wear performance of the coated cutting tool

- Interaction between sputter power and substrate temperature.

Figure 4.12 shows the influence of interaction between sputtering power and substrate temperature on the flank wear performance of the coated cutting insert. Figure 4.12 indicates that at low substrate temperature, 281°C , as the sputter power increases from 4.8 kW to 7.2 kW , the flank wear performance improves from 1.34 mm to 0.53 mm respectively. However the trend is reversed for high substrate temperature condition, 519 °C, where the flank wear performance deteriorates as the sputter power increases. This indicated the strong existence of interaction between the two process parameters. Further discussion on this interaction phenomenon is covered in chapter 4.3.

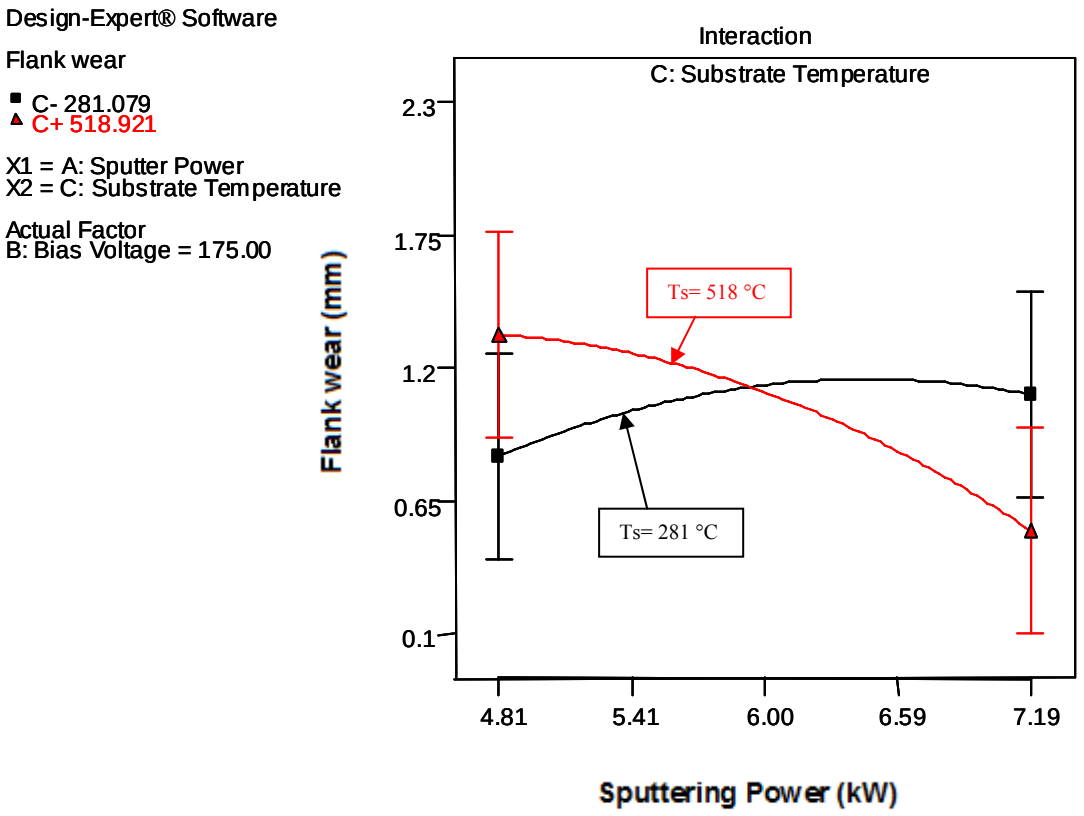

Figure 4.12: Interaction between sputtering power and substrate temperature influencing wear performance of TiAlN coating

Polynomial equation the influence of tool wear model

The response surface reduced cubic model polynomial equation to relate the input parameters to the flank wear performance is shown in Equation 4.3.

$$\text{Flank wear (mm)} = 15.75645 - 0.99562P_s - 0.12889V_s - 0.043465T_s + 0.017406P_s V_s + 5.39529 \times 10^{-3} P_s T_s + 2.61640 \times 10^{-4} V_s T_s - 0.11774P_s^2 + 4.94740 \times 10^{-3} V_s^2 + 1.10758 \times 10^{-5} T_s^2 - 4.15985 \times 10^{-5} P_s V_s T_s$$

P_s: Sputtering Power (kW)
T_s: Substrate temperature (°C)
V_s: Substrate bias voltage (V)

Equation 4.3 : Reduced cubic polynomial equation representing the coating roughness model with respect to substrate temperature, substrate bias, and sputter power

Graphically, this equation can be represented by 3D surface response plots. Examples of these 3 D plota are shown in Figure 4.13, 4.14, and 4.15. Each plot shows the

effect of varying two parameters while holding the other parameter constant at center point.

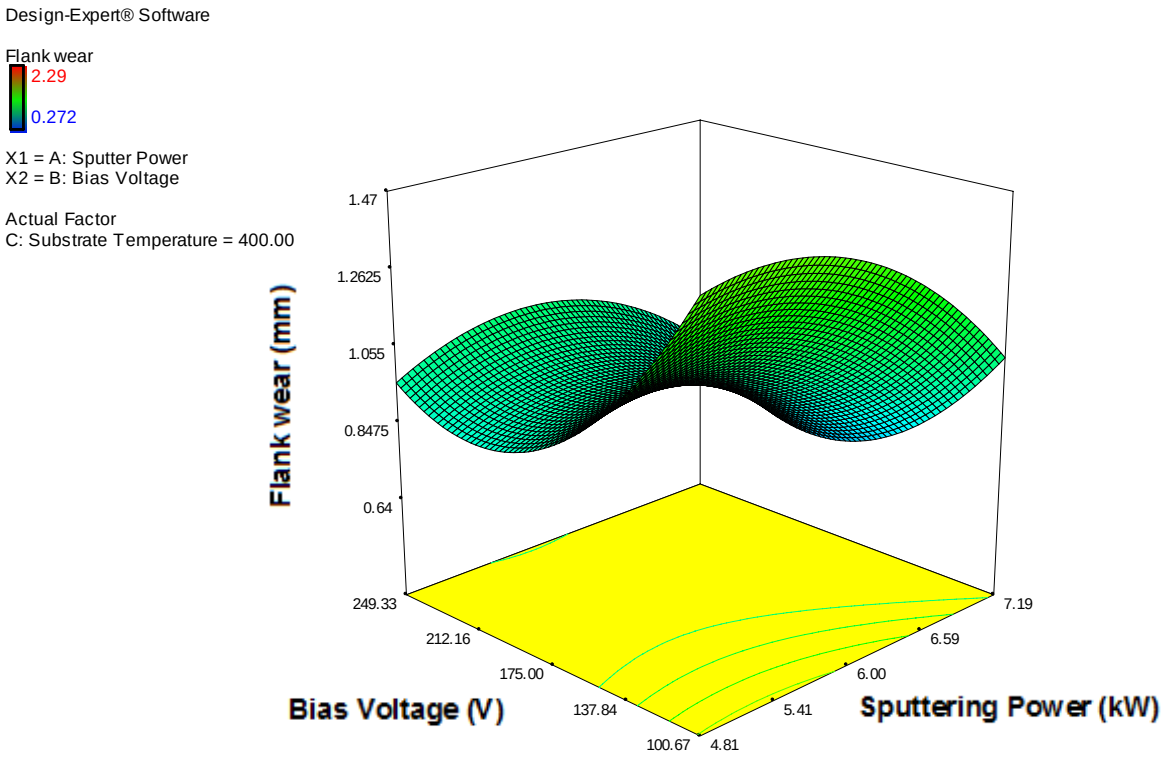

Figure 4.13: Response surface model for flank wear while holding substrate temperature constant at 400°C

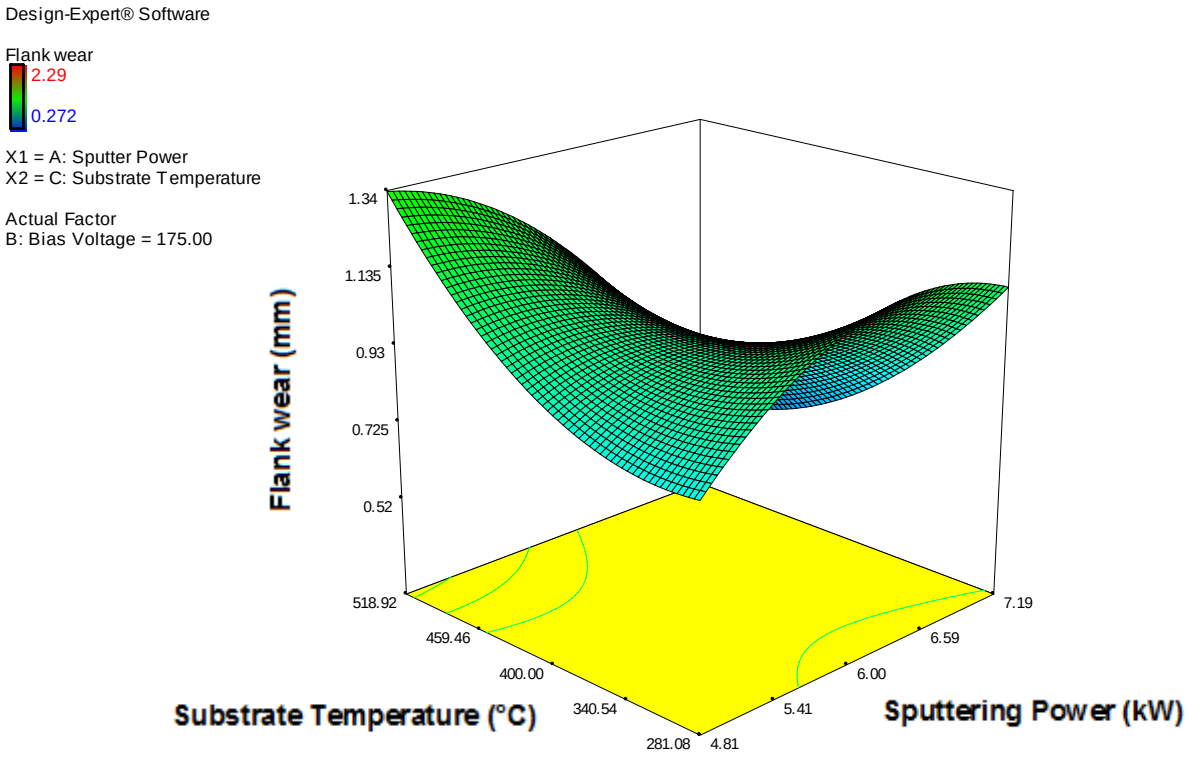

Figure 4.14: Response surface model for flank wear while holding substrate bias voltage at -175 V

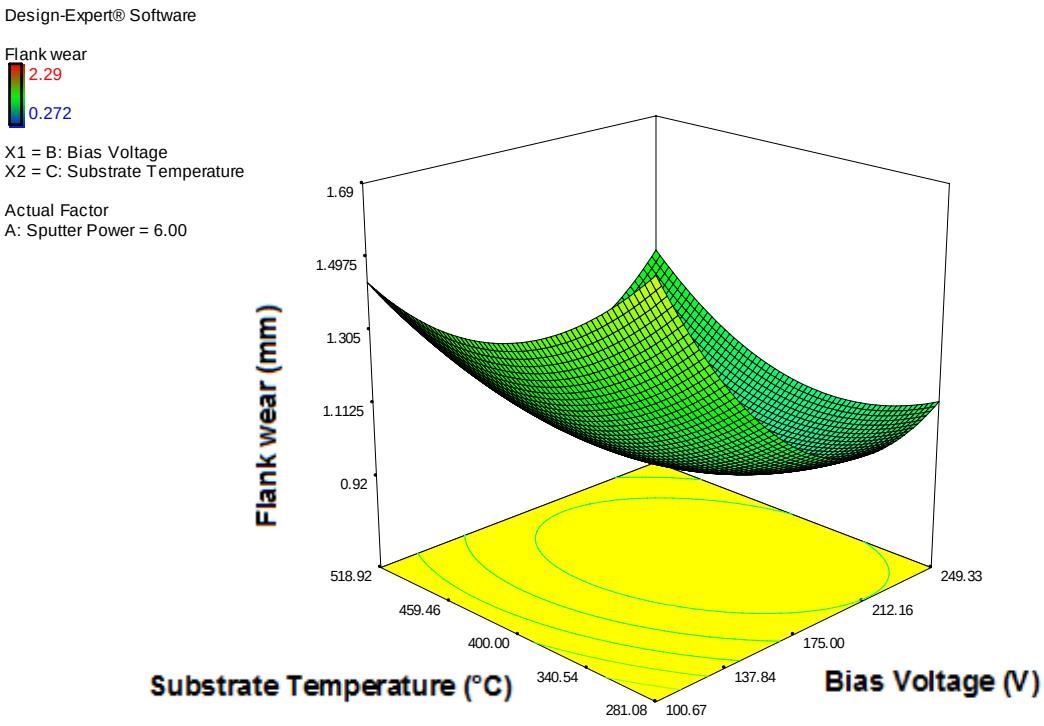

Figure 4.15: Response surface model for flank wear while holding sputtering power constant at 6 kW

Model validation

Validation of model to determine if the developed response surface model can predict the coating process behaviour was successfully done. The validation results of the three sets of parameter settings are shown in Table 4.17. As shown in Table 4.17 the actual flank wear of validation runs data fall within the 90% prediction interval and the residual errors are ranging between 4.23% to 9.88% in absolute value which are less than 10%. This indicates that the model is accurate enough to predict the resultant coating hardness within 90% CI and the residual error relative to predicted values are less than 10%.

Table 4.17: Summary of validation run for coating wear performance

Validation run	Input parameters			Prediction	Prediction interval		Validation	Residual Error (%)
	Sputter Power (kW)	Bias Voltage (V)	Substrate Temperature (C)	Flank wear (mm)	90% PI low	90% PI Hi	Flank wear (mm)	
1	5	-100	280	1.89	0.92	2.87	1.97	4.23
2	6.5	-150	350	1.02	0.2	1.83	0.97	-4.90
3	7	-145	450	0.81	0	1.67	0.73	-9.88

4.1.4 Modelling summary

- The relationship between PVD magnetron sputtering process parameters (substrate bias voltage, substrate temperature and sputter power) and developed TiAlN coating hardness, roughness and wear performance were successfully developed and validated. The models are represented as polynomial equations as shown in Table 4.18.

Table 4.18: Polynomial equations to represent the developed models.

Coating characteristics/ performance	**Polynomial models**
Hardness (Equation 1)	Roughness = +105.71410+18.30453P_s -0.41692V_s -0.26270T_s - 0.029133$P_s V_s$+ 0.051265$P_s T_s$ -4.01637E-004$V_s T_s$ -3.22349P_s^2 +2.16359E-003V_s^2+1.76509E-005T_s^2
Roughness (Equation 2)	Hardness = -65.04488-1.57702P_s +0.82486 V_s +0.29499T_s - 0.11702$P_s V_s$-0.030377$P_s T_s$ -1.59691E-003$V_s T_s$ +1.39684P_s^2 - 3.03132E-004V_s^2 -1.45081E- 04 T_s^2 +2.69721E-004$P_s V_s T_s$
Wear performance (Equation 3)	Flank wear =15.75645 - 0.99562P_s - 0.12889V_s - 0.043465T_s + 0.017406P_s V_s+ 5.39529 x10^{-3} P_s T_s + 2.61640 x10^{-4} V_s T_s - 0.11774P_s^2 + 4.94740 x10^{-3} V_s^2 + 1.10758 x 10^{-5} T_s^2 -4.15985 x10^{-5} P_s V_s T_s

- The process parameters that significantly influence the TiAlN coating hardness, roughness, and wear performance were also identified and summarized in Table 4.19.

Table 4.19: The PVD parameters and interactions that significantly influence the respective developed models.

Models	**Significant influencing parameters**	**Significant interaction factors**
Hardness	• Bias voltage, • Sputter power quadratic term • Substrate temperature quadratic term	interaction between sputter power substrate temperature
Roughness	• Sputter power • Substrate bias quadratic term	interaction between sputter power and substrate temperature
Wear performance	• Squared value of substrate bias voltage	interaction between sputter power and substrate temperature

- The models were successfully validated by the quantitative means of comparing the validation run results with the 90% PI of the model and assessing accuracy of the validation run results relative to predicted value by calculating residual error. All validation run results fell within the 90% PI of the models and the residual error for all runs were less than 10%. Qualitative validation was also performed by explaining the behaviour of the process parameters that significantly influenced the model using published work by other researchers and practitioners in this field.
- The RSM analysis also indicated there was strong interaction between substrate temperature and sputtering power that influenced coating hardness, roughness, and wear performance. There is lack of published study on this phenomenon by researchers and practitioners in this field.

4.1 Microstructure analysis of the developed TiAlN coating as a function of substrate bias voltage, substrate temperature and sputtering power variation.

To facilitate the discussion on the behaviour of the model based on the microstructure and of the developed coating, AFM, XRD, SEM and EDX analysis were carried out on specific coated specimens from selected experimental runs. The selected experimental runs represent the effect of varying a specific process parameter while the other two process parameters were held constant at the mid point of evaluated range. The selected sets of experimental runs to investigate the effect of varying substrate bias voltage, substrate temperature, and substrate bias voltage are tabulated in Table 4.20, Table 4.21 and Table 4.22 respectively.

Table 4.20: Experimental run with variation in substrate bias voltage and constant substrate temperature and sputtering power

Run	Sputtering Power	Bias Voltage	Substrate Temperature
	kW	V	°C
1	6	-50	400
19	6	-175	400
16	6	-300	400

Table 4.21: Experimental run with variation in substrate temperature and constant substrate bias voltage and sputtering power

Run	A:Sputtering Power	B:Bias Voltage	C:Substrate Temperature
	kW	Volts	°C
5	6	-175	200
19	6	-175	400
12	6	-175	600

Table 4.22: Experimental run with variation in sputtering power and constant substrate temperature and substrate bias voltage

Run	A:Sputtering Power	B:Bias Voltage	C:Substrate Temperature
	kW	Volts	°C
18	4	-175	400
19	6	-175	400
15	8	-175	400

Brief descriptions of the various microstructural analyses performed are as follows:

- AFM: The morphology of the developed TiAlN thin film coatings were analysed using Shimadzu SPM-9500J2 AFM apparatus. The detection mode used was contact mode using a commercial Si_3N_4 cantilever and the scanning area was set at 5x 5 microns (25 μm^2).
- XRD: The XRD analyses were performed using Bruker D-8 XRD apparatus. Due to the thin film sample, a grazing incidence angle (GIA) feature was utilized with a grazing angle of 1 degree. The analysis was done using CuKα radiation with λ = 0.15406 nm with Ni filter, operated at 40 kV and 40 mA. The 2θ scanning range was set between 30 to 60 degrees with a step size of 0.020 degree and a dwell time of 1 second. The 2θ scanning range was selected to capture two main peaks appeared for the developed coating, TiAlN (111) and (200)**.** The identification of TiAlN (111) and (200) peaks is based on standard JCPDS No: 37-1140; the peaks at 37.7° and 43.8° correspond to diffraction along 111 and 200 planes respectively. The quantitative data extracted from the XRD analysis are the I(111)/ I(200) and the grain size. The grain size (D_p) data was collected on dominant XRD peak of either (111) or (200) using Scherrer's equation $D_p = 0.9\ \lambda / \beta 2\theta \cos\theta$ (Culity 1972); Where λ is the wavelength of the X-ray, θ is the Bragg's angle and β2θ is the Full Width Half the Maximum (FWHM) intensity of 111 or 200 peak of the XRD pattern.
- EDX and SEM: The analyses were performed using SEM/EDX LEO-1525. SEM images captured the cross section view of fractured coating deposited on the WC substrate. The atomic percentage ratio of Al and Ti in the coating was

analysed by using EDX. The nitrogen content in the coating was not analysed due to limitation of EDX to light weight elements (Chen et al., 2008).

4.1.1 Analysis on the effect of substrate bias voltage variations

Based on the findings from the modelling work in the previous section, substrate bias voltage significantly influences the hardness, surface roughness, and also the tool wear performance as summarized in Figure 4.16.

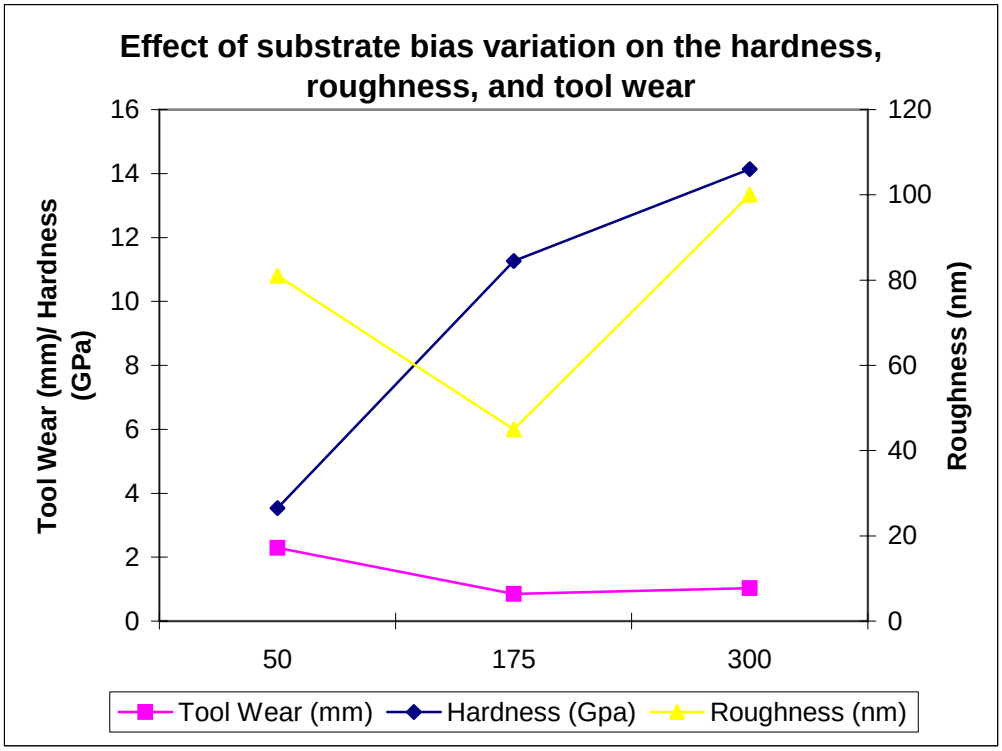

Figure 4.16: Effect of substrate bias variation on the hardness, roughness, and tool wear performance.

Table 4.23: TiAlN coating characteristics and microstructure data as substrate bias voltage varies

Run	Bias Voltage (V)	Hardness (GPa)	Roughness (nm)	Tool wear (mm)	Al/Ti	I111/I200	D_p (nm)
1	-50	3.54	81	2.29	1.88	2.43	59.30
19	-175	11.27	45	0.85	1.20	3.65	12.31
16	-300	14.14	100	1.03	1.02	3.84	10.66

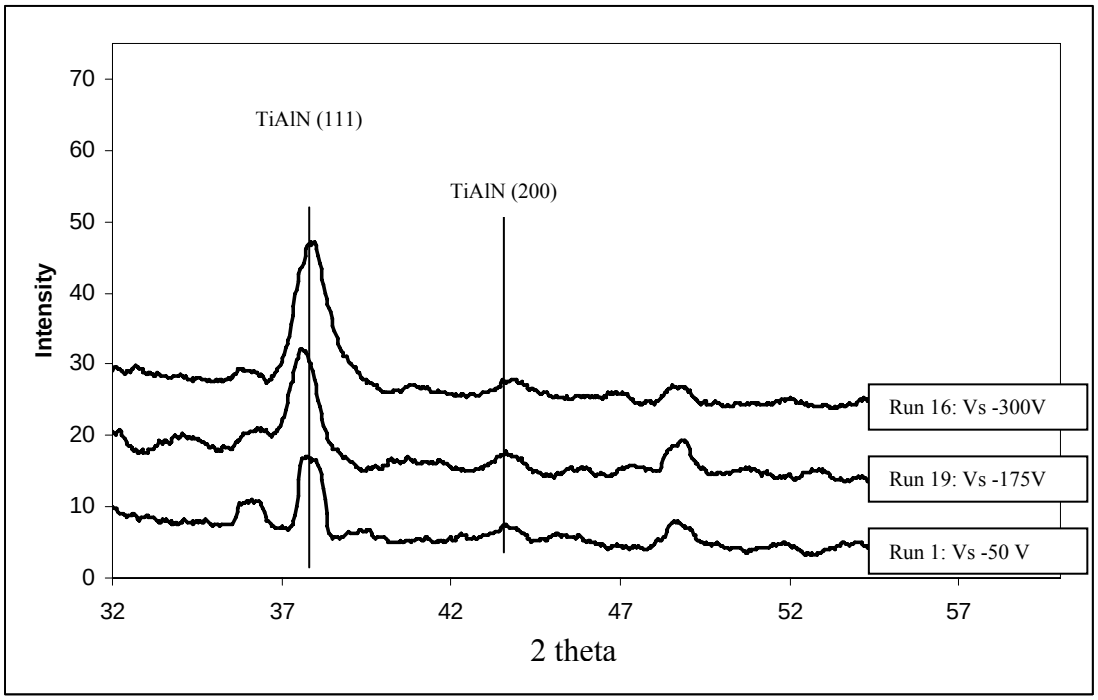

Figure 4.17: 2θ vs. intensity curves for the XRD analysis for substrate bias voltage of -50V, -175V and -300V

The 2θ vs. intensity curves for the XRD analysis for substrate bias voltage of -50V, -175V and -300V are shown in the Figure 4.17. Quantitative data from the XRD analysis such as I111/I200 and grain size are tabulated in Table 4.23.

The intensity ratio data indicates that as the substrate bias increases from -50V to -175V, the I111/I200 increases significantly from 2.429 to 3.654 reflecting shift in crystal orientation from (200) plane towards (111) plane. Subsequent incremental increases in substrate bias from -175 V to -300 V resulted in minimal changes in I111/I200 value. A similar trend in crystal orientation behavior under influence of substrate bias voltage variation was also reported in studies by Matsue et al. (2004) and Ahlgren and Blomqvist (2005).

Significant grain size reduction was observed from 59.299 nm to 12.309 nm as the voltage increased from -50V to -175 V. Further increase in substrate bias from -175V

to -300 V resulted less significant reduction in grain size. This finding (discussed below) is supported by results of a study performed by Barshilia and Rajam (2004).

The AFM images shown in Figure 4.18 provide visual evidence of the reduction of grain size and smoother surface morphology of TiAlN coating as the substrate bias voltage increases. The SEM images of fractured cross section also shown in Figure 4.18 indicate a reduction in porosity and formation of a dense columnar structure at higher bias voltage. The reduction in grain size can be attributed to increases in ion bombardment as a result from substrate bias incremental changes. This is due to higher nucleation density resulting in fine-grained morphology which in turn resulted in higher hardness (Barshilia and Rajam 2004). The energy impacted upon the growing coating, due to ion bombardment, also helps to anneal out imperfections in the coating. However above certain ion bombardment energy level, the damage induced by ion bombardment is more detrimental than the benefits (Hultman et al., 1987). Evidence of this can be observed in the hardness, roughness, and wear performance of the coating data plotted in figure 4.16. This plot indicates that above a certain bias voltage (-175 V) further increases in bias voltage cause a reduction in the rate of increase of hardness, a reversal of the previous reduction in roughness and a reduction in the rate of tool wear.

Influence of substrate bias on the composition of Ti and Al is indicated by the Al/Ti ratio in Table 4.23. The ratio of Al/Ti for substrate bias of -50V, -175V, and -300V are 1.88, 1.20, and 1.01 respectively. This indicates the reduction of Al atoms in the coating composition as the substrate bias increases. This can be attributed to higher levels of resputtering of Al compared to Ti during bombardment of ions onto the growing film due lower atomic mass of Al (Coll et al, 1991). TiAlN coating hardness

is greatly influenced by the Al/Ti ratio. It was reported that the hardness of $Ti_{1-x}Al_xN$ coating increased up to x=0.6 after which the hardness decreased (Ikeda and Satoh, 1991).

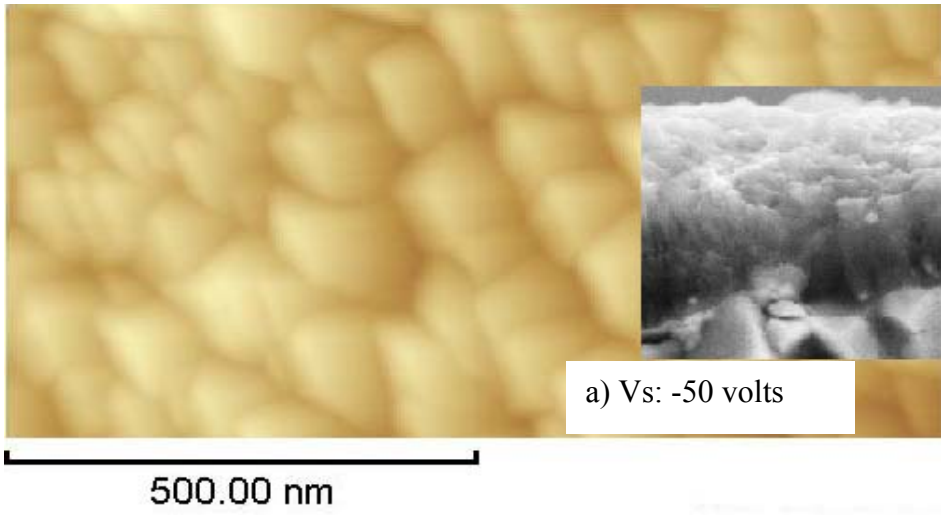

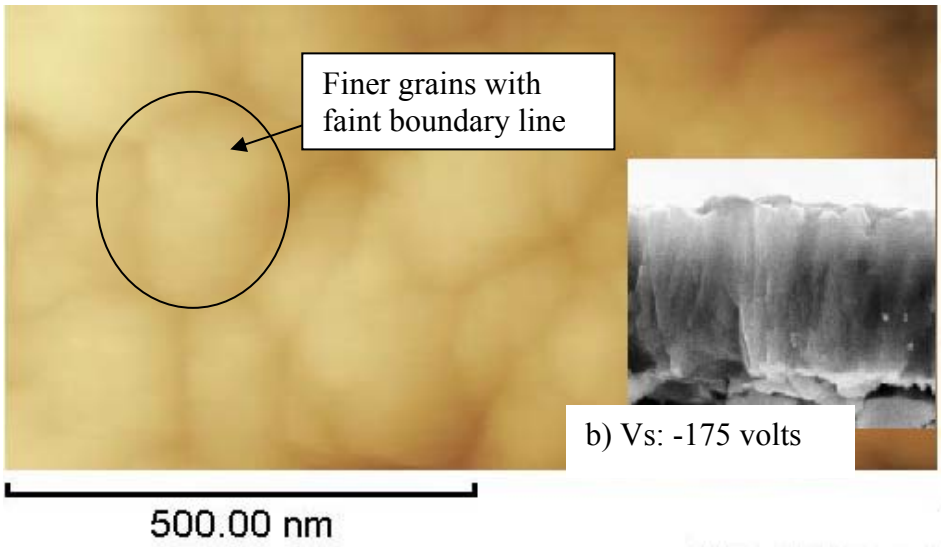

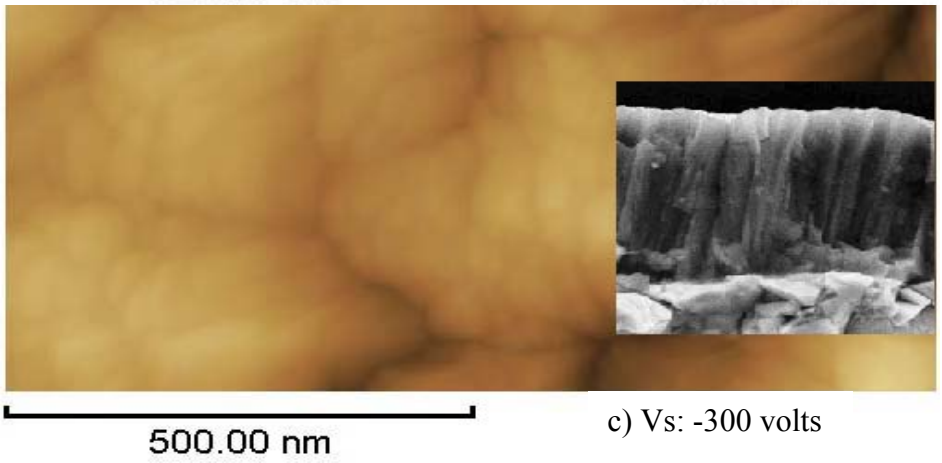

Figure 4.18: AFM image (with imbedded SEM image) indicating the transformation of grain size and morphology of TiAlN coating as the substrate bias increases.

4.1.2 Analysis on the effect of substrate temperature variations

Based on the findings of the modelling work in the previous section, substrate temperature significantly influences TiAlN coating hardness. Its influence on the roughness and wear performance is attributed to the interaction with sputtering power. In this section, the effect of substrate temperature on the developed TiAlN coating microstructure, with substrate bias and sputter power remaining constant at a mid-point settings is investigated.

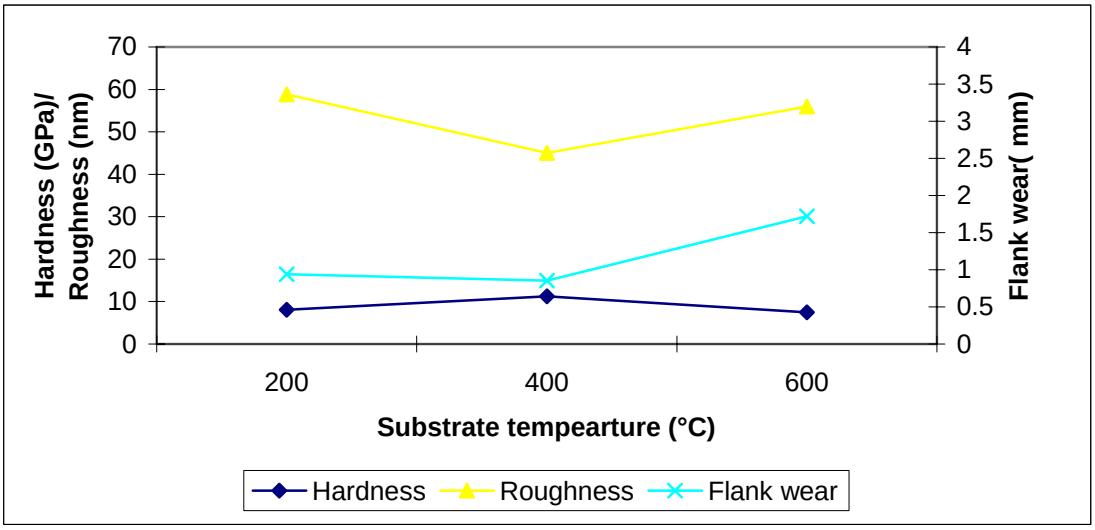

Figure 4.19: Effect of substrate temperature variation on the hardness, roughness, and tool wear performance.

Table 4.24: TiAlN coating characteristics and microstructure data as substrate temperature varies

Run	Substrate Temperature (°C)	Hardness (GPa)	Roughness (nm)	Flank wear (mm)	I111/I200	Al/Ti	Dp (nm)
5	200	8.05921	58.80	0.94	3.71	1.21	37.85
19	400	11.2656	45.00	0.85	3.65	1.20	12.31
12	600	7.4825	56.00	1.72	0.90	0.93	22.950

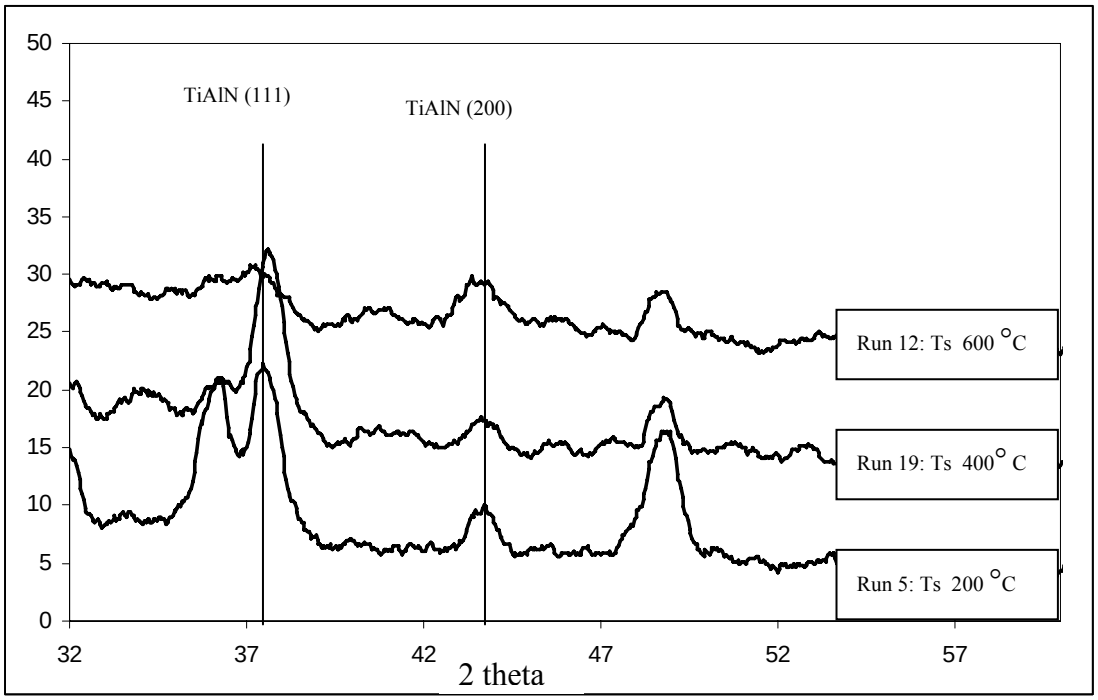

Figure 4.20: The 2θ vs. intensity XRD curves for substrate temperature of 200 °C, 400 °C and 600 °C

The 2θ vs. intensity XRD curves for substrate temperature of 200°C, 400°C and 600°C are shown in the Figure 4.20. Quantitative data from the XRD and EDX analysis such as I111/I200 and grain size and atomic number percentage ratio of Al/Ti are tabulated in Table 4.24.

The XRD curves in Figure 4.20 indicate that there is shift in peak value of TiAlN coating from (111) to (200) planes as the temperature increases. This shift is most apparent at the higher temperature of 600 °C. This is reflected by the change in I111/I200 shown in Table 4.24. A study on TiN coatings having same crystal structure as TiAlN by Xu et al. (2006) suggested the same trend, where at substrate temperatures of 200 °C both (111) and (200) peak exist and as the temperature increased to 500 °C, the (200) peak value became stronger while the (111) peak value almost disappeared.

The grain size determination based on XRD analysis was performed on the dominant peak crystal orientation and tabulated in Table 4.24. The data in Table 4.24 indicates the reduction in grain size as the temperature increases from 200 °C to 400 °C; however as the substrate temperature further increases to 600 °C the grain size increases. Study by González et al. (2007) on TiAlN reported the reduction of grain size as the substrate temperature increased from 50 °C to 150°C. However due to the narrower evaluation window compared to this study, the growth in grain size as the temperature increased was not observed. The increase in grain size as a function of temperature was reported by Subramanian et al. (2008) in the annealing study of TiAlN coating from 500 °C to 700 °C; as substrate temperature increases, growth on existing nuclei become thermodynamically more favorable compared to further nucleation. The change of grain size as a function of substrate temperature can be seen qualitatively in AFM images in Figure 4.21.

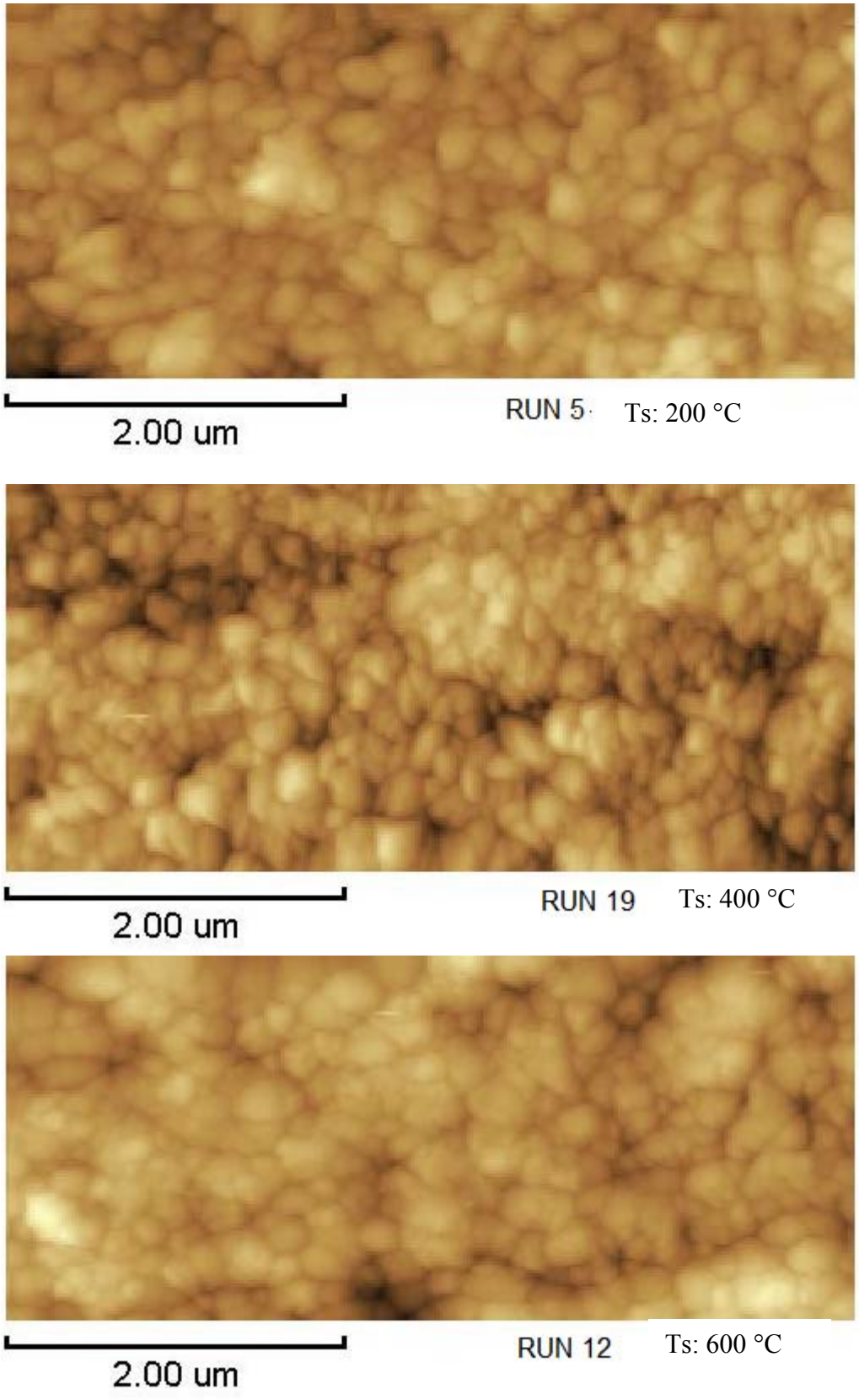

Figure 4.21: AFM images reflecting the change in grain size as the substrate temperature (Ts) changes from 200 °C to 600 °C

The increase in substrate temperature resulted in the reduction of atomic % ratio between Al and Ti as shown in Table 4.24 where the ratios are 1.21, 1.20, and 0.93 for the corresponding substrate temperature of 200 °C, 400 °C and 600 °C. The same observation was reported by Irudayaraj and Kalainathan (2008) on the study of TiAlN coatings deposited using the magnetron sputtering technique.

4.1.3 Analysis on the effect of sputtering power variations on TiAlN coating microstructure

Based on the modelling result, sputtering power and its quadratic term significantly influenced the roughness and hardness of the TiAlN coating respectively. Sputtering power also has a strong interaction with substrate temperature which influences tool wear, hardness, and roughness of the coating. The influencing behaviour of sputtering power at the mid-range setting of both substrate temperature and substrate bias voltage is shown in Figure 4.22.

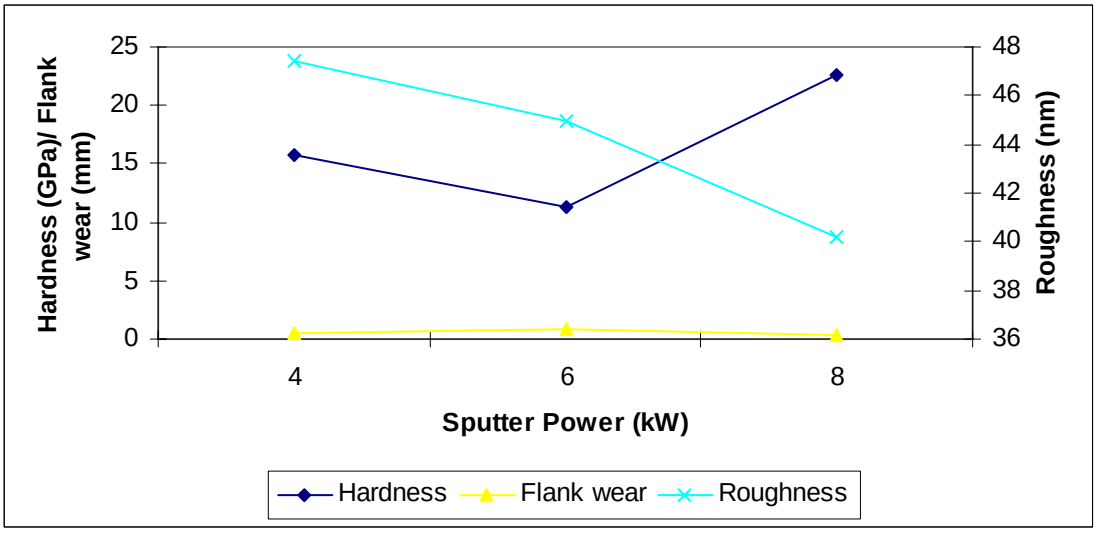

Figure 4.22: Effect of sputtering power variation on the hardness, roughness, and tool wear performance

The 2θ vs. intensity XRD curves for sputter power of 4kW, 6kW and 8kW are shown in Figure 4.23. The quantitative data from the XRD and EDX analysis such as

I111/I200 and grain size and atomic number percentage ratio of Al/Ti are tabulated in Table 4.25.

The XRD curves in Figure 4.23 indicates the shift in dominant peak of crystal orientation from (111) to (200) as the sputter power increases from 4kW to 8 kW. This is also reflected by the peak intensity ratio of the two, I111/I200, in Table 4.25. The I111/I200 ratio indicates that no significant peak of (200) can be found at the low sputter power of 4 kW. However the (200) peak becomes dominant at the sputter power of 8kW level. This trend was also reported by Xu et al. (2006) and Wuhrer and Yeung (2002) based on their study of TiN coating and TiAlN coating deposited using the same PVD sputtering technique. The grain size of the deposited TiAlN coating decreases as the sputter power increases as reflected in Table 4.25. The decrease in grain size can be attributed to higher number and greater energy of the depositing atoms onto the substrate surface. This condition is more favourable for the nucleation of new grains than the growth of existing ones (Wuhrer and Yeung, 2002). The AFM images of TiAlN the surface morphology for various sputter power settings are shown in Figure 4.24. The EDX analysis result in Table 4.25 indicates that the Al/Ti ratio increases as sputter power increases from 4kW to 6kW and decreases as the sputter power further increases from 6kW to 8kW.

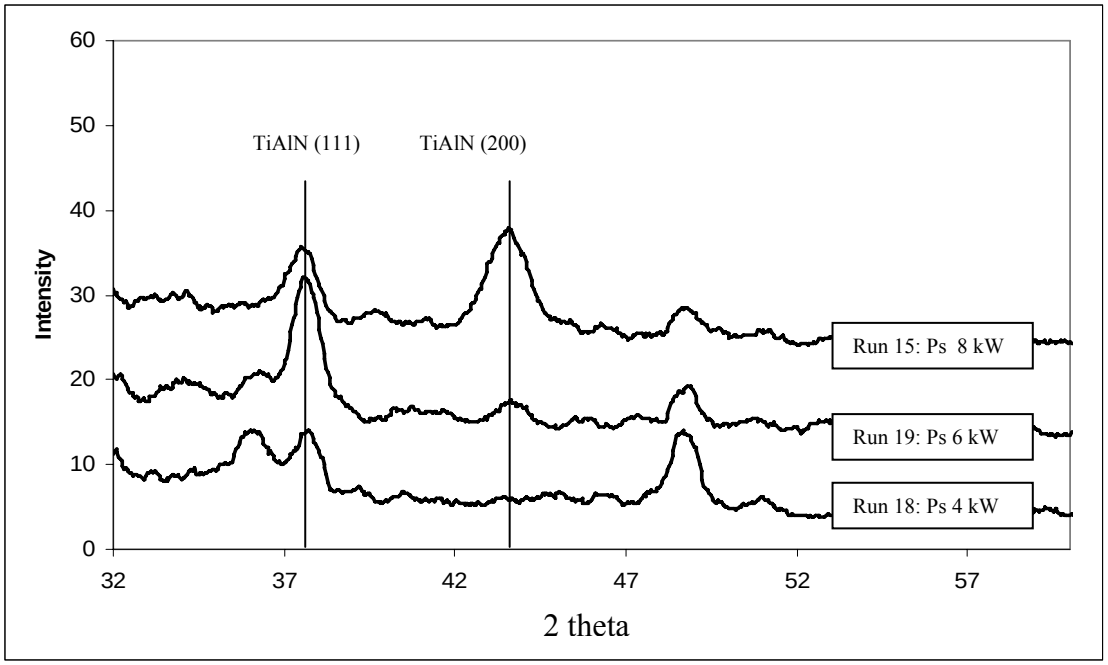

Figure 4.23: The 2θ vs intensity XRD curves for sputtering power of 4kW, 6kW and 8kW.

Table 4.25: The quantitative data from the XRD and EDX analysis for TiAlN coating as the sputtering power increases.

Run	Sputtering Power (kW)	Hardness (GPa)	Roughness (nm)	Flank wear (mm)	I111/I200	Al/Ti	Dp (nm)
18	4	15.6859	47.4	0.56	*	0.78	24.59
19	6	11.2656	45	0.854	3.65	1.20	12.31
15	8	22.6371	40.2	0.272	0.78	0.86	8.75
* No I200 peak							

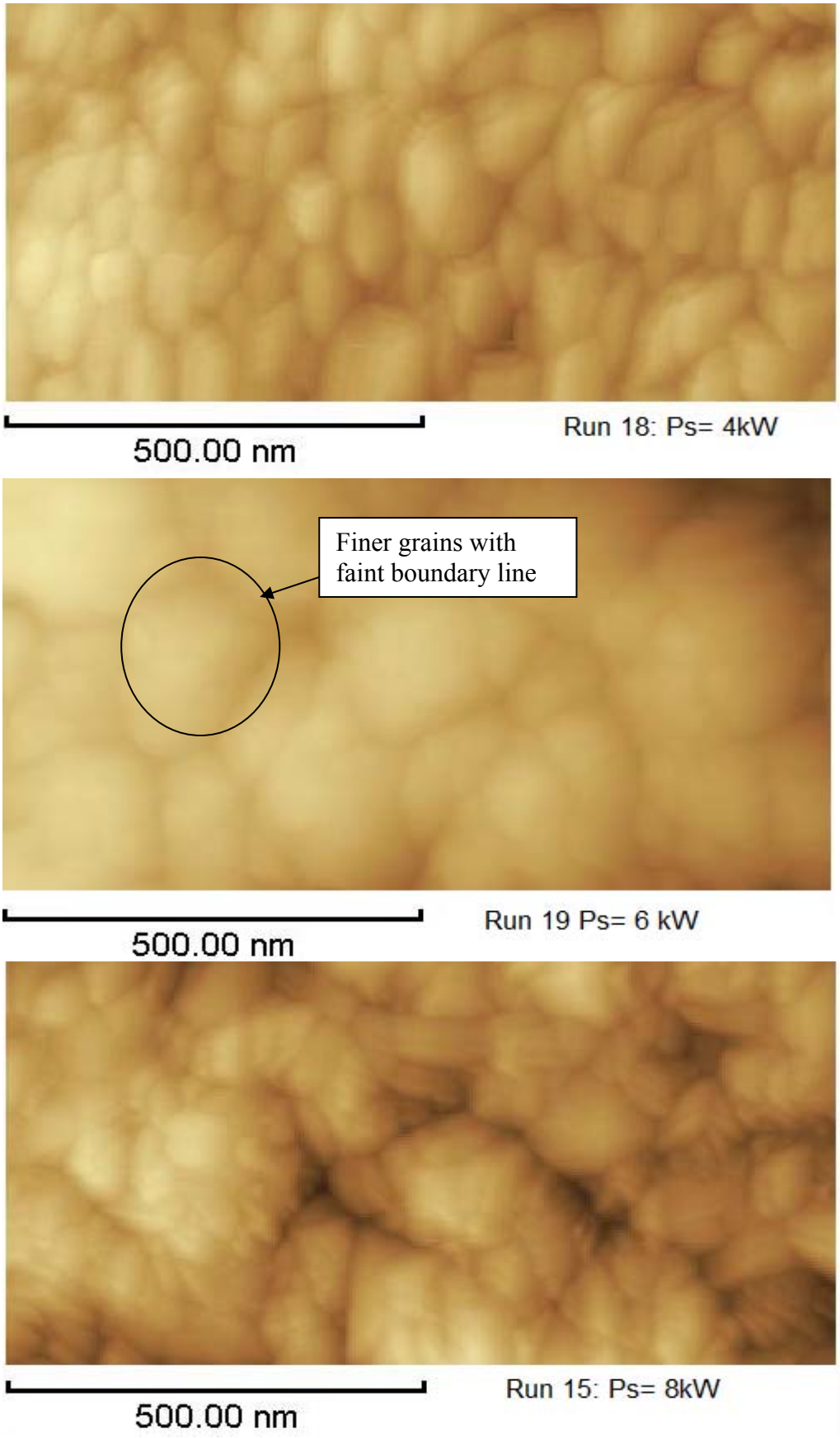

Figure 4.24: AFM images reflecting the reduction in grain size as the sputtering power (Ps) changes from 4 kW to 8 kW.

4.3 The interaction between sputtering power and substrate temperature

The modelling study reported in section 4.1 indicated that there was strong interaction between substrate temperature and sputtering power that influenced all three models; roughness, hardness and wear performance of the TiAlN coating. The interaction behaviour for those models is summarized in Figure 4.25. For both hardness and wear performance models, at low temperature, the changes in sputtering power results in small reduction in hardness and increase in flank wear value. However, at high substrate temperature, changes in sputter power resulted in significant changes in both hardness and flank wear.

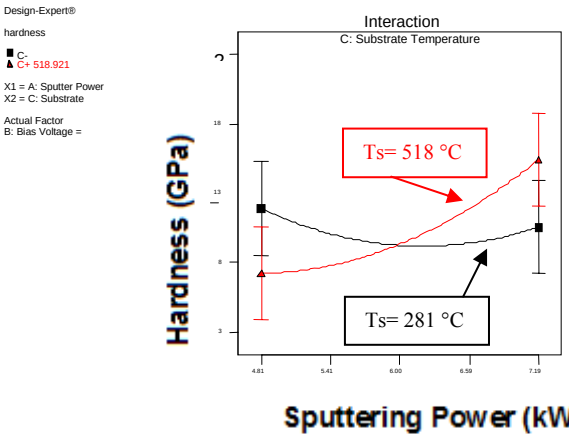

(a) Interaction of substrate temperature and sputtering power effect on coating hardness

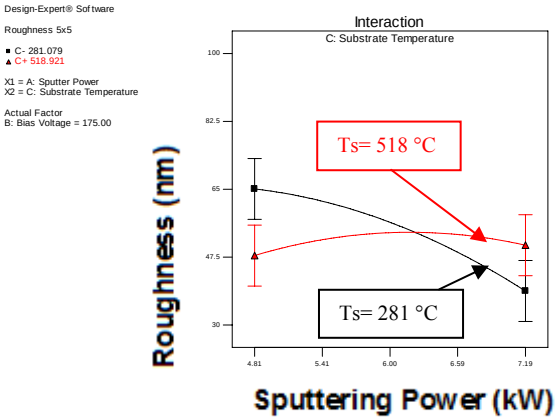

(b) Interaction of substrate temperature and sputtering power effect on coating roughness

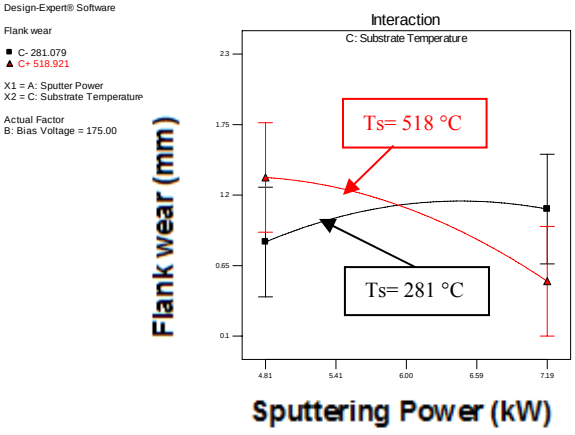

(c) Interaction of substrate temperature and sputtering power effect on flank wear

Figure 4.25: Interaction behavior of substrate temperature and sputtering power

High substrate temperature provides high kinetic energy to the depositing particle resulted in better atomic surface mobility. The particles can then reach lower potential energy before another particle deposited onto them (Mattox, 1998). This is

indicated by the shift in preferred crystallographic orientation peak from (111), for the low temperature condition, to (200) for the high temperature conditions shown in Figure 4.26. TiAlN is a rocksalt-structure (NaCl structure) of which the (200) planes having the lowest surface energy; the competitive planes (111) possess the highest strain energy. Due to high substrate temperature, the surface energy of deposited TiAlN coating reduces layer by layer such that the (200) plane becomes the primary crystallographic orientation parallel to the substrate surface (Banerjeeet al., 2002).

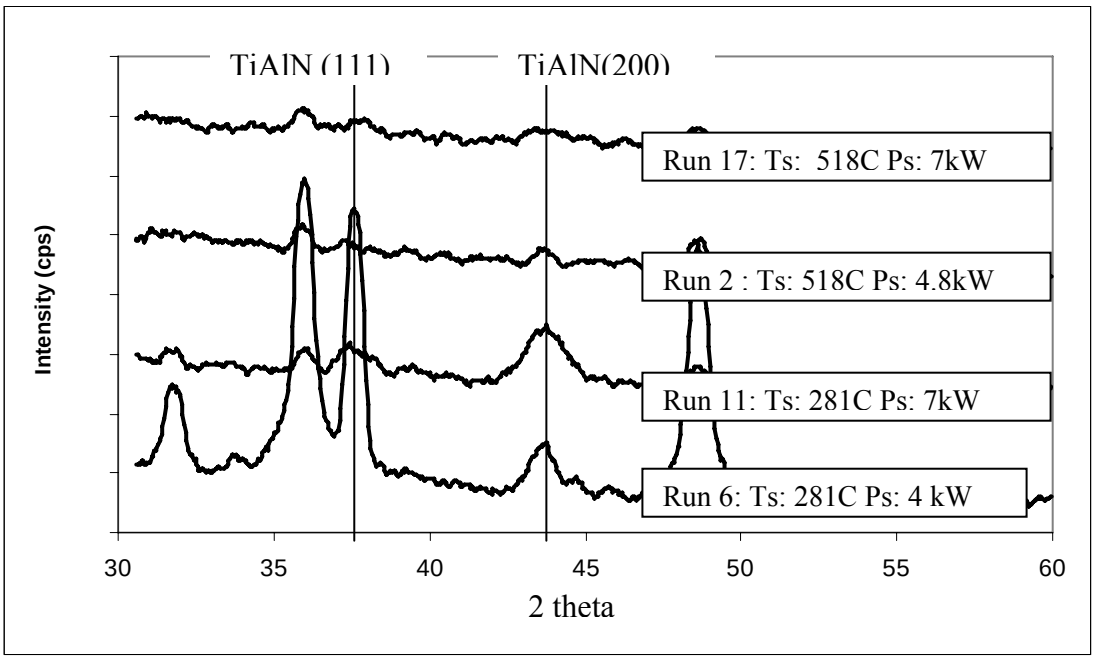

Figure 4.26: XRD curves to compare the effect of interaction between sputtering power and substrate temperature

At the high substrate temperature condition, lower sputtering power resulted in lower hardness and high flank wear. This can be attributed to the growth of deposited particles before another particles deposited on them. Sputtering power influences the sputter rate, higher sputtering power translates to higher sputter rate (Wuhrer and Yeung, 2004). At high sputtering power, the number of atoms arriving at the substrate in unit time is higher than that of at the lower sputtering power. Due to this the atoms deposited at the higher sputtering power and high temperature have more

time to migrate and be incorporated into an existing growth centre due to high temperature but do not have enough time to grow due to higher deposition rate compared to atoms deposited at low sputtering power and high temperature. This is evident on the XRD curves in Figure 4.26, where the broadening of (200) peak can be observed comparing "Run 2" and " Run 17 " curves. The broadening of the (200) peak is indicative of finer crystal grain size which increase the hardness and resulted in better tool wear performance (Bobzin et al. 2007).

The interaction between substrate temperature and sputtering power also influenced the roughness of deposited coating. As indicated in Figure 4.25 (b), at high substrate temperate the change in sputtering power has an insignificant effect on the roughness of the TiAlN coating because it suppressed preferential crystal growth which resulted in smoother surfaces (Lugscheider et al. 1996). The lack of preferential growth can be observed in Figure 4.26 where the peaks for high temperature XRD curves (Run 2 and Run 17) are much less pronounced compared to that of the lower temperature level (Run 11 and Run 6). The AFM images in Figure 4.27 shows the TiAlN coating morphology where the coating with high substrate temperature level, Run 2 and Run 17, has a rounded and smoother surface compared to the coating of lower substrate temperature level, Run 6 and Run 11.

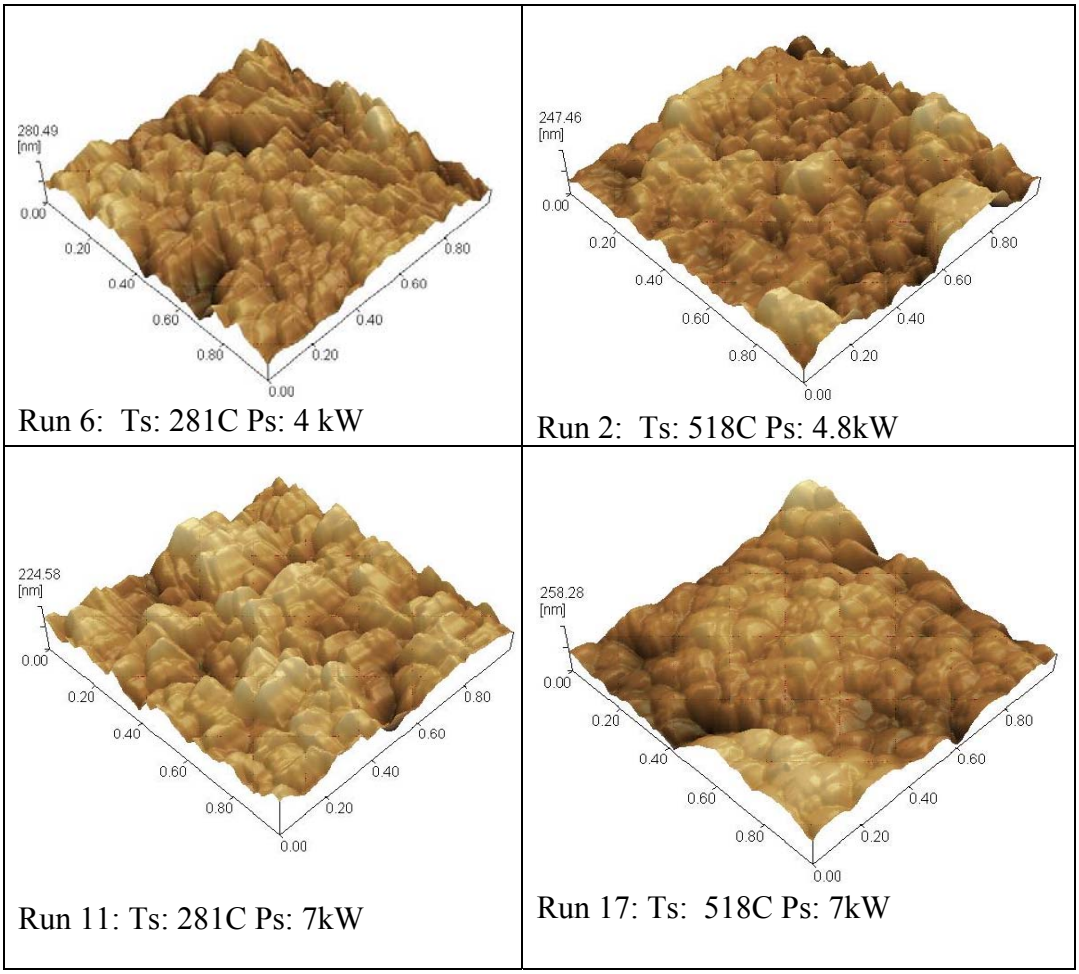

Figure 4.27: Interaction effect between substrate temperature and sputtering power on the TiAlN coating morphology.

At lower substrate temperature, the increase in sputtering power resulted in lower surface roughness as indicated in Figure 4.25(b). The increase in sputtering rate increases the nucleation rate and reduces the self-shadowing effect. Self–shadowing effect restricts deposition of particles on specific area due to oblique impingement of depositing particles; and this resulted in rougher coating surface morphology. The increase in sputtering rate increases the chances of particle depositions of different impingement angles, resulting in smoother morphology (Smith 1995, Wuhrer and Yeung 2004).

4.4 Correlation between coating performance, coating characteristics and microstructures

One of the objectives of this study is to establish if there is any correlation between coating performance (flank wear) and coating characteristics and microstructures. The method selected to accomplish this is by calculating the coefficient of determination, R^2, based on Pearson product moment correlation coefficient method, R. The R^2 value indicates of how well a regression line represents the data. If the regression line passes exactly through every point on the scatter plot, it would be able to explain all of the variation. The further the line is away from the points, the less it is able to explain. The coefficient of determination value will be in the range of $0 < R^2 < 1$. R^2 value of 1 means the regression line passes exactly through all points; R^2 value of 0 means denotes that no correlation at all between the two variables being investigated (Milton et al., 1997).

All the data obtained from the modelling experimental runs were compiled for the use of this correlation study. This data is tabulated in Table 4.26. Respective coating characteristics and microstructure data were plotted against flank wear in form of scatter plot using EXCEL software. The regression line to best fit the data and the R^2 were also generated using the EXCEL software and shown in Figure 4.28 to Figure 4.32.

Table 4.26: Compilation of TiAlN coating performance, characteristics, and microstructure data for correlation study.

Run	Flank wear (mm)	Al/Ti	Hardness (Gpa)	Roughness (nm)	Dp (nm)	I111/I200
1	2.29	1.88	3.54	81.00	59.30	2.43
2	1.08	1.25	5.27	65.60	38.83	1.80
3	0.73	1.13	13.17	81.90	29.01	1.55
4	1.40	0.81	10.96	70.30	26.71	0.21
5	0.94	1.21	8.06	58.80	37.85	3.71
6	2.01	1.46	4.33	75.60	41.19	9.12
7	1.92	1.26	4.04	44.30	25.68	2.05
8	0.57	1.09	16.12	48.10	11.52	10.57
9	1.26	1.21	7.77	43.70	9.45	0.16
10	1.97	1.38	3.53	56.10	27.81	2.41
11	1.18	1.34	9.76	49.90	14.78	0.92
12	1.72	0.93	7.48	56.00	22.95	0.90
13	0.35	0.68	15.26	49.10	38.07	1.95
14	0.86	1.10	8.91	57.90	11.63	0.32
15	0.27	0.86	22.64	40.20	8.75	0.78
16	1.03	1.02	14.14	100.00	10.66	3.84
17	0.93	0.73	8.88	67.30	14.08	1.64
18	0.56	0.78	15.69	47.40	24.59	*
19	0.85	1.20	11.27	45.00	12.31	3.65
20	0.83	1.11	12.34	63.60	10.14	2.75

*Data not obtainable, (200) peak cannot be detected from XRD analysis

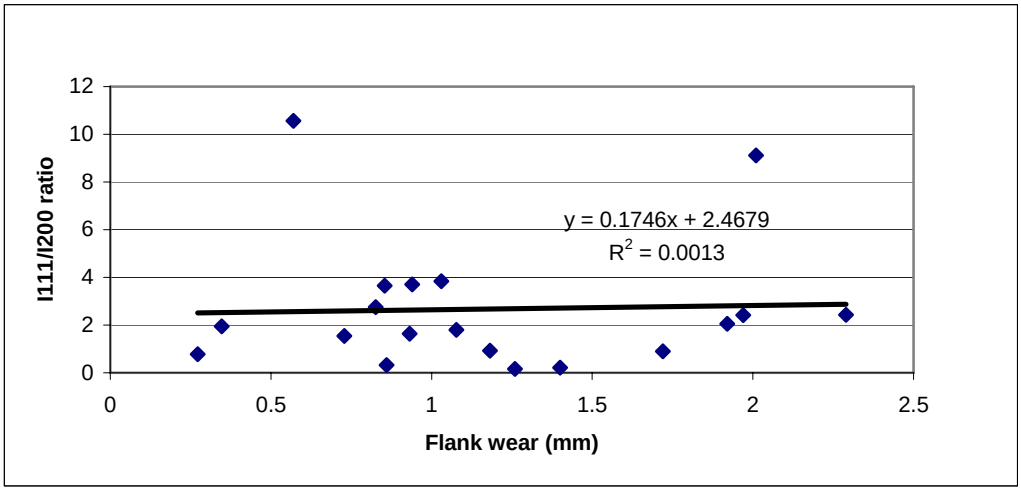

Figure 4.28: Correlation between flank wear and I111/1200 ratio.

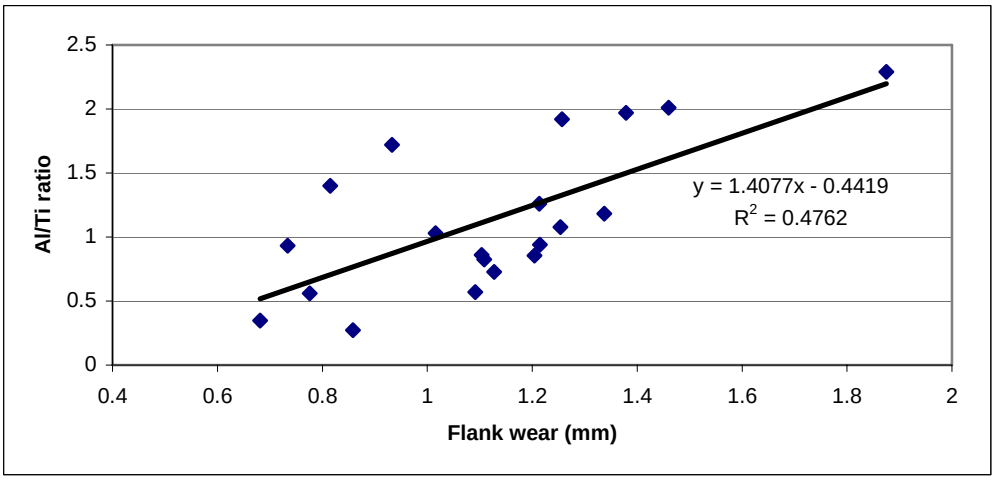

Figure 4.29: Correlation between flank wear and atomic percentage ratio of aluminum and titanium of TiAlN coating.

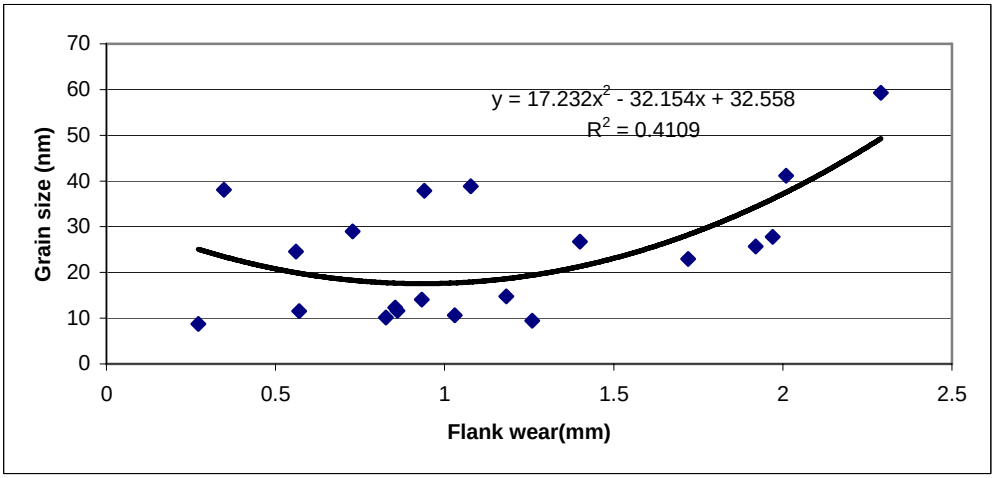

Figure 4.30: Correlation between flank wear and grain size of TiAlN coating

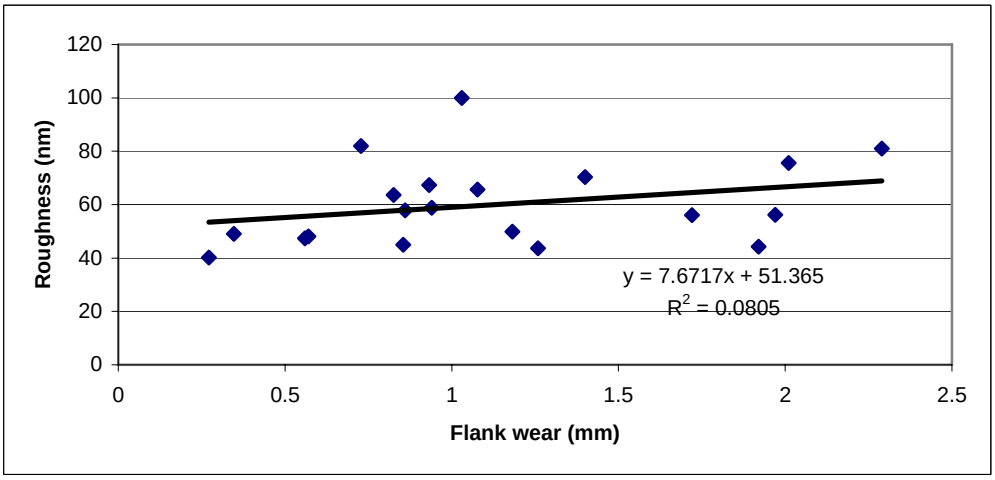

Figure 4.31: Correlation between flank wear and roughness of TiAlN coating.

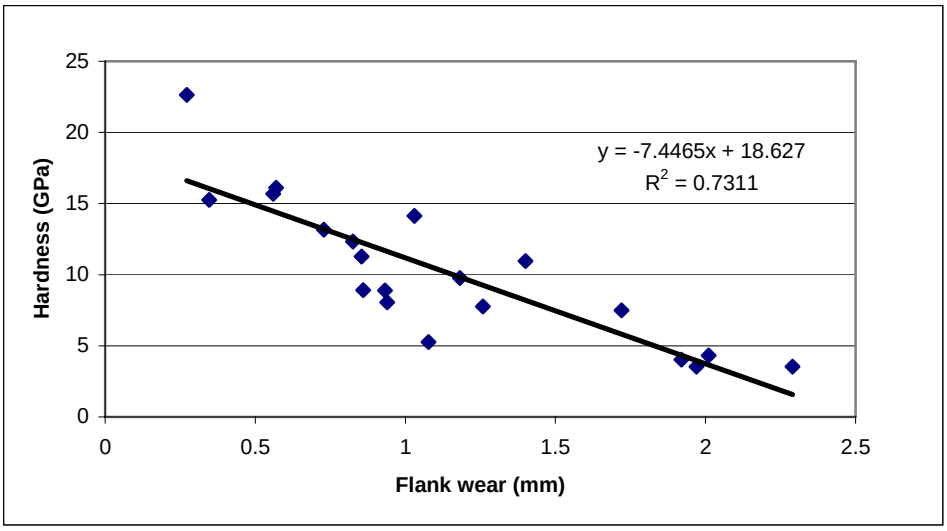

Figure 4.32: Correlation between flank wear and TiAlN coating hardness

To ease the comparison by which coating characteristics or microstructure data can be used to predict the performance of the TiAlN coating, the R^2 for each correlation study is tabulated in Table 4.27.

Table 4.27: Summary of coefficient of determination value for the correlation studies between flank wear and coating characteristic/ microstructure data.

Correlation study	Coefficient of Determination (R^2)
Flank wear and I111/1200 ratio	0.0013
Flank wear and atomic percentage ratio of Al/Ti	0.4762
Flank wear and grain size	0.4109
Flank wear and coating roughness	0.0805
Flank wear and coating hardness	0.7311

Data in Table 4.27 indicates that the performance of cutting tools (flank wear) has the strongest correlation with the coating hardness, with R^2 value of 0.7311. This R^2 value indicates that 73.11% of variability in the value of flank wear can be associated with the variation on coating hardness. Only 26.89% of the variability in flank wear data is influenced by unidentified factors. The atomic percentage of Al/Ti and grain size indicate some correlation with the flank wear with R^2 values of 0.4762 and

0.4109 respectively; and the peak intensity ratio of I111/I200 and coating roughness R^2 values are less than 0.1, indicating insignificant correlation with the flank wear.

The strong correlation between coating performance (flank wear) and the hardness was expected due to many reports and publication supporting that fact (Fox-Rabinovich et al. 2006, Trent and Wright 2000, Musil 2000). The effect of grain size and the Al/Ti ratio on the flank wear can be correlated to the effect of these two microstructural phenomena on the hardness of the coating (Bobzin et al., 2007; Park et al., 2009; Xu et al., 2006).

The lack of correlation, R^2 value of 0.0805, between the surface roughness and flank wear can be explained by the wear mechanism seen on some of the cutting tool inserts. Shown in Figure 4.33 is a typical flank wear image from this experimental run.

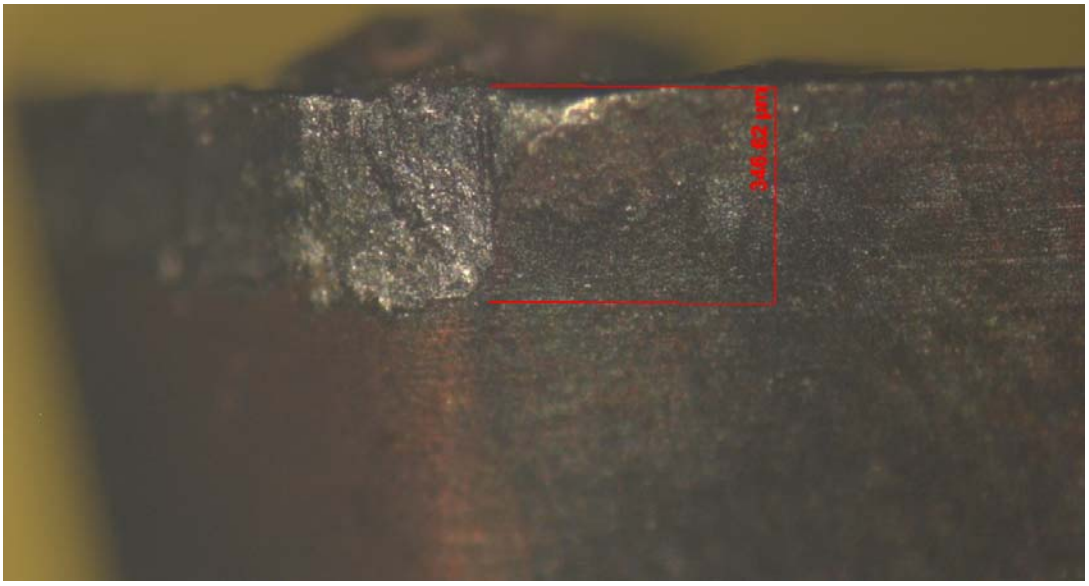

Figure 4.33: A typical flank wear image from the experiment

However, for samples displaying flank wear of more than 1 mm, the majority indicated presence of diffusion wear on the minor cutting edge of the cutting tool in Figure 4.34.

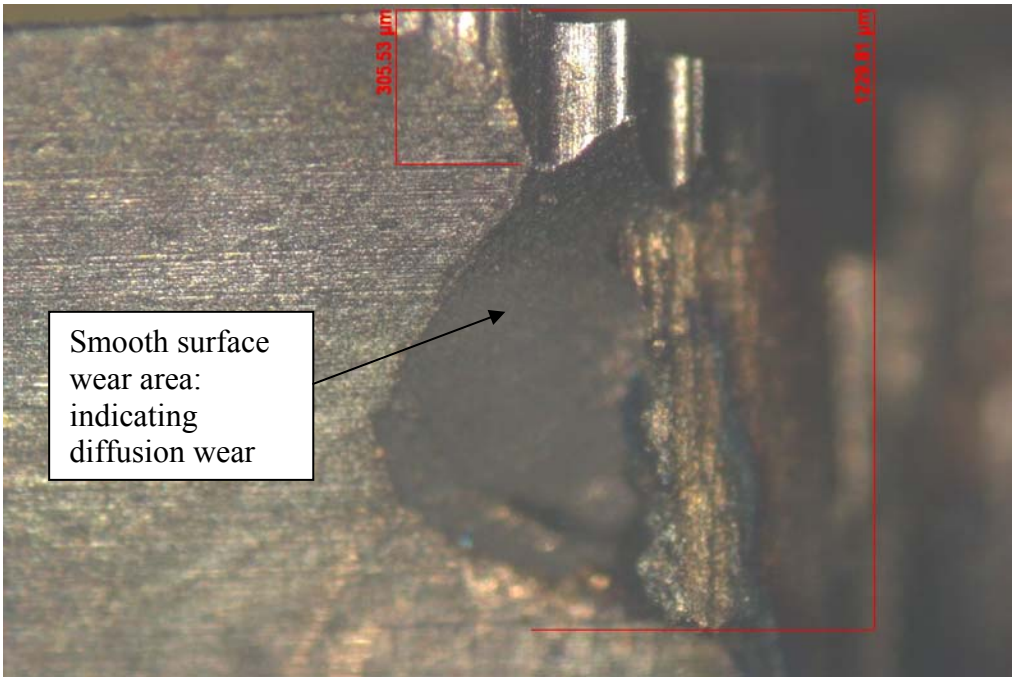

Figure 4.34: Diffusion wear on the minor cutting edge of the cutting tool.

SEM and EDX analysis performed on the diffusion wear area indicates clean tungsten carbide surface without trace of workpiece debris or coating as shown in Figure 4.35. A typical tool wear through friction usually leaves trace of workpiece material adhered on the worn surface as indicated by SEM and EDX analysis of a typical flank wear shown in Figure 4.36 which shows trace of Fe, Cr, and C which are some of the elements of the workpiece material.

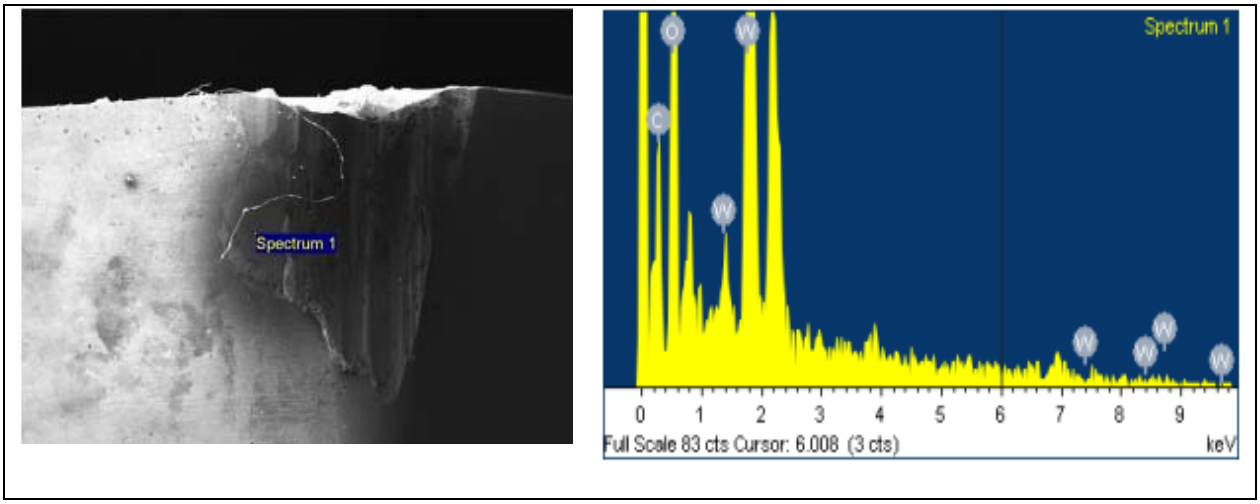

Figure 4.35: SEM and EDX analysis done on the diffusion wear area.

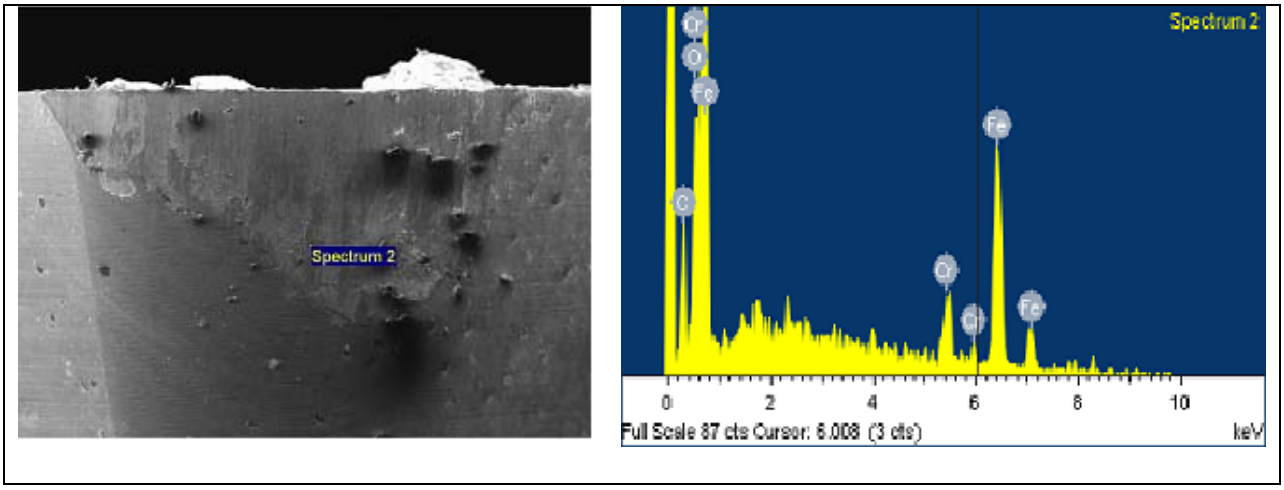

Figure 4.36: SEM and EDX analysis done on wear area associated to friction.

The diffusion wear was usually associated with high temperature conditions. This indicates the cutting process might generate high temperature condition at the cutting area. At high temperature cutting conditions the formation of a protective layer enriched in Al_2O_3 is more important for cutting tool performance than the friction between the coating and the work-piece (Bobzin et al., 2007; Park et al., 2009). The formation of Al_2O_3 in the TiAlN coating is influenced by the Al/Ti ratio which reflected by the experimental data in Figure 4.29. Study by Witthaut et al.(1998) indicated that the optimum ratio of Al/Ti was around 0.6, beyond which the coating

tends to form cracks during Al_2O_3 formation. If the crack formed in the TiAlN coating due to high temperature condition, the uncoated cutting tool area can experience high flank wear. This reasoning explained the better correlation between flank wear and the Al/Ti ratio compared to the coating roughness.

4.5 Summary of experimental results

This section summarizes the findings from the experiments. The summary is categorized into four sections, the modelling, the microstructure analysis, the interaction between process parameters, and the correlation between coating performance and the coating characteristics and microstructures.

- Modelling summary

The relationship between substrate bias (Vs), substrate temperature (Ts), and sputtering power (Ps) and the deposited TiAlN coating hardness, roughness, and performance (flank wear) were successfully defined as polynomial equations (models). These models were successfully validated by qualitative and quantitative methods. The significant parameters that influenced the deposited TiAlN coating hardness, roughness, and performance were also identified. Detail summary of modelling work is explained in chapter 4.1.4.

- Microstructure analysis summary

The effect of changes in process parameters on the microstructure of the deposited TiAlN coating is summarized in Table 4.28. These behaviours were also supported by published work by researchers in this field.

Table 4.28 : Summary of the behaviour of the deposited TiAlN coating with changes PVD process parameters

PVD Parameter	**Substrate temperature**	
	200° C to 400° C	**400 °C to 600° C**
I111/I200	Insignificant (3.71 to 3.65)	Decrease (3.65 to 0.9)
Al/Ti	Insignificant (1.21 to 1.20)	Decrease (1.2 to 0.93)
Dp (nm)	Decrease (37.85 to 12.31)	Increase (12.31 to 22.95)
PVD Parameter	**Substrate bias voltage**	
	-50V to -175V	**-175V to -300 V**
I111/I200	Increase (2.43 to 3.65)	Insignificant (3.65 to 3.84)
Al/Ti	Decrease (1.88 to 1.2)	Decrease (1.2 to 1.02)
Dp (nm)	Decrease (59.30 to 12.31)	Insignificant (12.31- 10.66)
PVD Parameter	**Sputtering Power**	
	4kW to 6kW	**6kW to 8kW**
I111/I200	Increase (No 200 peak to 3.65)	Decrease (3.65 to 0.78)
Al/Ti	Increase (0.78 to 1.2)	Decrease (1.2 to 0.86)
Dp (nm)	Decrease (24.59 to 12.31)	Insignificant (12.31 to 8.75)

- Interaction between process parameters summary

The ANOVA analysis indicated strong interaction between sputter power (Ps) and substrate temperature (Ts) that influenced the deposited coating hardness, roughness, and performance. The interaction behaviour can be summarized as the following:

- Coating hardness:

  At low Ts (281 ° C), changes in Ps do not have significant influence on TiAlN hardness. At high Ts (518 ° C), low Ps (4.8 kW) resulted in low hardness and high Ps (7.2 kW) resulted in high hardness.

- Coating roughness:

  At high Ts (518 ° C), changes in Ps do not have significant influence on TiAlN roughness. At low Ts (281 ° C), low Ps (4.8 kW) resulted in high roughness and high Ps (7.2 kW) resulted in low roughness.

- Coating performance:

  At Low Ts (281 ° C), the flank wear increases as the Ps increases from 4.8kW to 7.2kW. However, at high Ts (518 ° C), the flank wear decreases as the Ps increases from 4.8kW to 7.2kW.

- Correlation study summary

Correlation study between coating performance (flank wear) and coating characteristics and microstructures (hardness, Al/Ti, roughness, grain size, and I111/I200) indicated that flank wear has the strongest correlation with coating hardness with coefficient of determination, R^2 ,value of 0.7311. The study also indicated that flank wear has some correlation with grain size and Al/Ti with R^2 value of 0.4109 and 0.4762 respectively.

CHAPTER 5

CONCLUSIONS

5.0 Conclusions

- The research findings suggest that RSM can be used to model the PVD magnetron sputtering process as applied to the deposition of TiAlN hard coatings on tungsten carbide tool tip substrates.
- Three separate models in the form of polynomial equations were successfully developed to relate the relationships between PVD sputtering input process parameters (substrate temperature, substrate bias, and sputter power) and three output responses (coating hardness, coating roughness, and flank wear).
- The coating hardness, roughness, and flank wear outputs of the modelling validation runs were within the 90% prediction interval of the developed models and their residual errors, compared to the predicted values, were less than 10%.
- The models were also qualitatively validated by justifying the behaviour of the output responses (hardness, roughness, and flank wear) and microstructures (Al/Ti ratio, crystallographic peak ratio I111/1200, and grain size) with respect to variation of input variables, based on published work by researchers and practitioners in this field.
- This study also identified the significant parameters that influenced the coating hardness, roughness, and performance (flank wear) through ANOVA analysis during the development of the models. Coating hardness was influenced by the bias voltage, sputtering power, and substrate temperature; coating roughness was influenced by sputtering power and substrate bias and coating

performance was influenced by substrate bias. These findings were aligned with published work by other researchers.

- The ANOVA analysis also suggested that there was a significant interaction between the substrate temperature and the sputtering power which cannot be ignored and has not been reported in published journals. The ANOVA analysis indicated that the interaction between substrate temperature and sputtering power significantly influenced the resultant coating hardness, roughness, and performance.
- The correlation study between coating characteristics and microstructures and the coating performance (flank wear) suggested that the coating performance correlated most significantly to the coating hardness with R^2 value (coefficient of determination) of 0.7311. The study also suggested some correlation between coating performance with atomic percentage ratio of Al/Ti and grain size with R^2 value of 0.4762 and 0.4109 respectively.

5.1 New contributions to body of knowledge

Throughout this research, the author believes there are two new contributions to the body of knowledge:

- The development of PVD magnetron sputtering process model for the application of hard coating, specifically TiAlN coating on the WC substrate, using Response Surface Methodology.
- The establishment of a significant interaction between substrate temperature and the sputtering power during PVD magnetron sputtering process that influenced coating hardness, roughness, and performance.

5.2 Future work

- Coating adhesion is one of the important factors that can influence the performance of cutting tool. Assessment of coating adhesion was not included in this research due to unavailability of scratch adhesion testing equipment. Future research in this area should include this measurement as on of the output response of the modelling work. Aside from that, other machining characteristics such as workpiece surface finish and crater wear should also be included in as part of cutting tool performance measurement.
- One of the difficulties faced during the experiment was to maintain some level of consistency in coating thickness for all the experimental runs. This can be achieved if the PVD machine itself has in-situ thickness measurement capability. In order to ensure non-bias data due variation of coating thickness, future work of this nature should be carried out using equipment with such capability.
- The research findings suggested that RSM can be used to model PVD magnetron sputtering process for deposition of single layer hard coating. However, more research is needed to ascertain that the methodology is applicable for deposition of multi layer coatings.
- The interaction phenomena during the coating hardness modelling work suggested that at high substrate temperature, the increase in sputtering power resulted in a significant increase in coating hardness. Due to equipment capability limitation, this research was not able to identify the sputtering power limit beyond which no significant increase in coating hardness can be gained. Since hardness is strongly correlates with the coating performance, further research in this area can possibly improve coating performance.

REFERENCES

Adamczyk J., Horny N. , Tricoteaux A. , Jouan P.-Y. , Zadam M. (2008) 'On the use of response surface methodology to predict and interpret the preferred c-axis orientation of sputtered AlN thin films' *Applied Surface Science* 254, 1744–1750

Ahlgren M. and Blomqvist H. (2005) 'Influence of bias variation on residual stress and texture in TiAlN PVD coatings' *Surface & Coatings Technology* 200, 157– 160

Ahmad A.L., Low S.C., Abd Shukor S.R., Ismail A. (2009) 'Optimization of membrane performance by thermal-mechanical stretching process using responses surface methodology (RSM)' *Separation and Purification Technology* 66, 177–186

Aktas Nahit, I. Boyacı Hakkı, Mutlu Mehmet, Tanyolac Abdurrahman (2006) 'Optimization of lactose utilization in deproteinated whey by Kluyveromyces marxianus using response surface methodology (RSM)' *Bioresource Technology* 97, 2252–2259

Anderson Mark J. and Whitcomb Patrick J. (2005) *RSM Simplified: Optimizing Processes Using Response Surface Methods for Design of Experiments*, Productivity Press

Anon (2006) *Design-Expert Software, Version 7.0.3, User's Guide, Technical Manual*, Minneapolis :Stat-Ease Inc.,

Anon (1983) 'Metallurgical Coatings' *Proceedings of the international conference, San Diego California USA*, April 18-22 Vol. 1 & 2.

Axelevitch A. and Golan G. (2007) 'Modeling and Optimization of Film Deposition by Magnetron Sputtering' *Journal of Uncertain Systems* 1, (4) 277-290

Banerjee, R., Chandra, R., Ayyub, P. (2002) 'Influence of the sputtering gas on the preferred orientation of nanocrystalline titanium nitride thin films' *Thin Solid Films* 405, (1-2) 64-72

Barshilia Harish C. and Rajam K. S. (2004) ' Nanoindentation and atomic force microscopy measurements on reactively sputtered TiN coatings' *Bull. Mater. Sci*. 27, (1) 35–41

Benyounis K.Y. , Olabi A.G., Hashmi M.S.J. (2005) 'Optimizing the laser-welded butt joints of medium carbon steel using RSM' *Journal of Materials Processing Technology* 164–165, 986–989

Berg S. and Nyberg T. (2005) 'Fundamental understanding and modeling of reactive sputtering processes' *Thin Solid Films* 476, 215– 230

Bisgaard S. and Diamond N. (1990) 'An analysis of Taguchi's method of confirmatory trials' *CQPI Report no. 60, Centre of Quality and Productivity Improvement University of Wisconsin*.

Bobzin K., Lugscheider E., Maes M., Immich P., Bolz S. (2007) 'Grain size evaluation of pulsed TiAlN nanocomposite coatings for cutting tools' *Thin Solid Films* 515, 3681–3684

Bouzakis K.D. , Skordaris G., Michailidis N., Mirisidis I., Erkens G., Cremer R., (2007) 'Effect of film ion bombardment during the pvd process on the mechanical properties and cutting performance of TiAlN coated tools' *Surface & Coatings Technology* 202, 826–830

Box, G., W. Hunter and J. Hunter (1978) *Statistics for Experimenters: An Introduction to Design, Data Analysis, and Model Building*, N.Y.: John-Wiley

Bradbury S. R. and Huyanan T. (2000) 'Challenges facing surface engineering technologies in the cutting tool industry' *Vacuum* 56, (3) 173-177

Brundle C.R., Evans C.A., Wilson S. (1992) *Encyclopedia of Materials Characterization*, Stoneham, MA: Butterworth-Heinemann

Bunshah Rointan F. (1994) *Handbook of deposition technologies for films and coatings, second edition,* New Jersey: Noyes Publication

Byrne G. and Scholta E. (1993) 'Environmentally clean manufacturing processes—a strategic approach' *Ann. CIRP* 42, 471–474

Chen J.T., Wang J., . Zhang F., Zhang G.A., Fan X.Y., Wu Z.G., Yan P.X. (2008) 'Characterization and temperature controlling property of TiAlN coatings deposited by reactive magnetron co-sputtering' *J. Alloys Compd.* 472, (1-2) 91-96

Chen M.J., Chen K.N., Lin C.W.(2005) 'Optimization on response surface models for the optimal manufacturing conditions of dairy tofu' *J. Food Eng*. 68, 471–480

Cheng Y. H., Tay B. K. and Lau S. P. (2002) 'Substrate bias dependence of the structure and internal stress of TiN films deposited by the filtered cathodic vacuum arc' *J. Vac. Sci. Technol. A* 20, (4) 1327-1331

Choi Sung Ryong, Parka In-Wook, Kimb Sang Ho, Kima Kwang Ho (2004) 'Effects of bias voltage and temperature on mechanical properties of, Ti–Si–N coatings deposited by a hybrid system of arc ion plating and sputtering techniques' *Thin Solid Films* 447 –448, 371–376

Chou Wen-Jun, Sun Chun-Hsing, Yu Ge-Ping, Huang Jia-Hong (2003) 'Optimization of the deposition process of ZrN and TiN thin films on Si(1 0 0) using design of experiment method' *Materials Chemistry and Physics* 82, 228–236

Coll B.F., Fontana R., Gates A., Sathrum P. (1991) '(Ti---Al)N advanced films prepared by arc process' *Materials Science and Engineering: A* 140, 816-824

Criegern Rolf Von, Klaus Budde, Wolfgang Hoesler, Winfried Holzapfel (1997) 'Recent Advances in Surface and Thin Film Analysis Methods for Application to Packaging Problems' *IEEUCPMT Electronic Packaging Technology Conference*

Cullity B. D. (1972) *'Elements of X-ray diffraction'* MA: Addison-Wesley

Deng Y., Guan Y.F. and Rack P.D. (2006) 'Combinatorial synthesis and sputter parameter optimization of chromium-doped yttrium aluminum garnet photoluminescent thin films' *Thin Solid Films Volume* 515, (4) 1721-1726

Deshpande R.P., Chinnan M.S., McWatters K.H. (2008) 'Optimization of a chocolate-flavored, peanut–soy beverage using response surface methodology (RSM) as applied to consumer acceptability data' *LWT* 41, 1485–1492

Ding Xing-zhao , Tan A.L.K., Zeng X.T. , Wang C. , Yue T. , Sun C.Q. (2008) Corrosion resistance of CrAlN and TiAlN coatings deposited by lateral rotating cathode arc, *Thin Solid Films* 516, 5716–5720

Evans R.D., Doll G.L., Meng W.J, Mei F., Glass J.T. (2007) 'Effects of applied substrate bias during reactive sputter deposition of nanocomposite tantalum carbide/amorphous hydrocarbon thin films' *Thin Solid Films* 515, 5403–5410

Farooq M. and Lee Z. H. (2002) 'Optimization of the Sputtering Process for Depositing Composite Thin Films' *Journal of the Korean Physical Society* 40, (3) 511_515

Fox-Rabinovich G.S., Beake B.D., Endrino J.L., Veldhuis S.C., Parkinson R., Shuster L.S. and Migranov M.S. (2006) 'Effect of mechanical properties measured at room and elevated temperatures on the wear resistance of cutting tools with TiAlN and AlCrN coatings' *Surface and Coatings Technology* 200, (20-21) 5738-5742

Gekonde Haron O. and Subramanian S. V. (2002) 'Tribology of tool–chip interface and tool wear mechanisms' *Surface and Coatings Technology* 149, (2-3) 151-160

González García L., Garnica-Romo M. G., Hernández-Torres J., and Espinoza-Beltrán F. J., (2007) 'A study of TiAlN coatings prepared by RF co-sputtering' *Brazilian Journal of Chemical Engineering* 24, (02) 249 – 257

Grasserbauer M. and Werner H. W. (1995) *Analysis of Microelectronic Materials and Devices*, N.Y.: John Wiley & Sons

Gredic T and Zlatanovic M. (1991) 'Plasma deposition of (Ti,Al)N coatings at various magnetron discharge power levels' *Surface & coatings technology* 48, 25-30

Hainsworth S. V. and Soh W. C. (2003) 'The effect of the substrate on the mechanical properties of TiN coatings' *Surface and Coatings Technology* 163-164, 515-520

Han H.W., Lee N.E. (2005) 'Sputter deposition modeling of Ti thin film on a sharp tip' *Thin Solid Films* 475, (1-2) 144-149

Hewidy M.S., El-Taweel T.A., El-Safty M.F. (2005) ' Modelling the machining parameters of wire electrical discharge machining of Inconel 601 using RSM' *Journal of Materials Processing Technology* 169, 328–336

Hultman L., Helmersson U., Barnett S. A., Sundgren J. E. and Greene J. E. (1987) ' Low-energy ion irradiation during film growth for reducing defect densities in epitaxial TiN(100) films deposited by reactive-magnetron sputtering' *J. Appl. Phys.* 61, 552

Ikeda T. and Satoh H. (1991) 'Phase formation and characterization of hard coatings in the Ti---Al---N system prepared by the cathodic arc ion plating method' *Thin Solid Films* 195, (1-2) 99-110

Irudayaraj A. Albert and Kalainathan S. (2008) 'The influence of N2 flow rate and substrate temperature on Ti1-xAlxN thin films' *Cryst. Res. Technol*. 43, (7) 709 – 712

Kalavathy M Helen., Regupathi Iyyaswami, Pillai Magesh Ganesa, Miranda Lima Rose, (2009) 'Modelling, analysis and optimization of adsorption parameters for H3PO4 activated rubber wood sawdust using response surface methodology (RSM)' *Colloids and Surfaces B: Biointerfaces* 70, 35–45

Karacan F., Ozden U., Karacan S. (2007) 'Optimization of manufacturing conditions for activated carbon from Turkish lignite by chemical activation using response surface methodology' *Appl. Therm. Eng*. 27, 1212–1218

Keles, O., Taptik, Y., Eryilmaz, O. L., Urgen, M., Çakir, A. F. (1999) 'Optimization of Arc-PVD TiN Coating Process Parameters by Taguchi Technique' *Quality Engineering* 12, (1) 29-36

Keles Ozgul, Aykac Gokcen, Inal Osman T. (2003) 'The role of parameters in plasma assisted vapour deposition of tinytin-oxide coatings' *Surface and Coatings Technology* 172, 166–175

Kim Jae-keun and Jeong Sang-hun (2001) 'Effects of Deposition Parameters on AlN Film Growth Using Reactive DC Magnetron Sputtering' *Journal of the Korean Physical Society* 38, (1) 19-24

Laing K., Hampshire J., Teer D., and Chester G.(1999) 'The effect of ion current density on the adhesion and structure of coatings deposited by magnetron sputter ion plating' *Surf. Coat. Technol.* 112, 177–180

Lugscheider E. , Barimani C., Wolff C., Guerreiro S., Doepper G. (1996) 'Comparison of the structure of PVD-thin films deposited with different deposition energies' *Surface and Coatings Technology* 86-87, 177-183

Matsue Tatsuya, Hanabusa Takao, Ikeuchi Yasukazu (2004) 'Dependence to processing conditions of structure in TiN filmsdeposited by arc ion plating' *Vacuum* 74, 647–651

Mattox, D. M. (1998) *Handbook of physical vapour deposition (PVD) processing*, N.Y. : Noyes Publications.

Mattox D.M. (2003) *The Foundation of Vacuum Technology*, New York: Noyes/ William Andrew

Mayrhofer Paul H., Mitterer Christian, Hultman Lars, Clemens Helmut (2006) 'Microstructural design of hard coatings', *Progress in Materials Science* 51, 1032-1114

Medjani F., Sanjinés R., Allidi G., Karimi (2006) 'A. Effect of substrate temperature and bias voltage on the crystallite orientation in RF magnetron sputtered AlN thin films' *Thin Solid Films* 515, (1) 25 260-265

Milton S. J., McTeer P. M., Corbet J. J. (1997) *Introduction to Statistics*, Boston: McGraw-Hill

Montgomery D.C. (2005) *Design and Analysis of Experiments*, 6th edition, New York: John Wiley

Mubarak A., Hamzah E., Toff M.R.M. (2006) Influence of nitrogen gas flow rate on the microstructural and mechanical properties of TiN deposited carbon steel synthesized by CAE PVD technique, *AJSTD* 23, (4) 239-251

Musil J and Vlcek J. (1998) 'Magnetron sputtering of films with controlled texture and grain *size' Materials Chemistry and Physics* 54, 116-122

Musil J. (2000) 'Hard and superhard nanocomposite coatings' *Surface and Coatings Technology* 125, 322–330

Nambiar E.K. Kunhanandan and Ramamurthy K. (2006) 'Models relating mixture composition to the density and strength of foam concrete using response surface methodology' *Cement & Concrete Composites* 28, 752–760

Nissim A., Raveh A., Sariel J., Mintz M.H. (2007) 'Effect of substrate bias voltage on the properties of magnetron-sputtered gadolinium layers' *Surface and Coatings Technology* 201, (16-17) 7054-7059

Oliver W.C. and Pharr G.M. (1992) 'Improved technique for determining hardness and elastic modulus using load and displacement sensing indentation experiments' *J Material Res.* 7, 1564-1580

Park Jong-Keuk, Park Hyun-Jin, Ahn Jin-Ho , Baik Young-Joon (2009) 'Effect of Ti to Al ratio on the crystalline structure and hardening of a Ti1−xAlxN/CrN nanoscale multilayered coating' *Surface & Coatings Technology* 203, 3099–3103

Patsalas P., Charitidis C., Logothetidis S. (2000) 'The effect of substrate temperature and biasing on the mechanical properties and structure of sputtered titanium nitride thin films' *Surface and Coatings Technology* 125, (1-3) 335-340

Petrov I. , Barna P.B., Hultman L., Greene J.E. (2003) 'Microstructural evolution during film growth' *J Vac Si Technol A* 21, (5) 117-128

Razali M. Mohd., Esmar B., Sivarao P.S., Hadzley A.B. Mohd.,and Nizam A.R. Md., I. Ismawati, (2006) 'PROPERTIES OF PVD TIALN COATINGS: A SURVEY' *Proceeding of ICOMAST2006 International Conference on Manufacturing Science and Technology August 28-30, 2006, Melaka, Malaysia*

Razali M. Mohd., Esmar B., and Nizam A.R. Md. (2009) 'Optimization of flank wear in dry turning of AISI D2 steel with PVD TiAlN- coated WC inserts using response surface methodology' *International Journal of Materials Engineering and Technology* 2, (1) 17-27

Safi I. (2000) 'Recent aspects concerning DC reactive magnetron sputtering of thin films: a review' *Surface and Coatings Technology* 127, (2-3) 203-218

Schramm B.C., Scheerer H., Hoche H., Broszeit E., Abele E., Berger C. (2004) 'Tribological properties and dry machining characteristics of PVD-coated carbide inserts' *Surface and Coatings Technology* 188-189, 623-629

Schneider Jochen M, Rohde Suzanne, Sproul William D., and Matthews Allan (2000) 'Recent developments in plasma assisted physical vapour deposition' *J. Phys. D: Appl. Phys*. 33, 173–186

Settineri L. and Faga M.G. (2006) 'Laboratory tests for performance evaluation of nanocomposite coatings for cutting tools' *Wear* 260, 326–332

Sharma Shweta, Malik Anushree, Satya Santosh (2009) 'Application of response surface methodology (RSM) for optimization of nutrient supplementation for Cr (VI) removal by *Aspergillus lentulus* AML05' *Journal of Hazardous Materials* 164, 1198–1204

Shokuhfar A.S.M.R. Khalili, F. Ashenai Ghasemi , K. Malekzadeh , S. Raissi, (2008) Analysis and optimization of smart hybrid composite plates subjected to low-velocity impact using the response surface methodology (RSM), Thin-Walled Structures 46, 1204– 1212

Smith D.L.(1995) *Thin Film Deposition: Principle & Practice*, New York: McGraw Hill

Song Hongwei, Ilegbusi Olusegun J., Trakhtenberg L.I. (2005) 'Modeling vapor deposition of metal/semiconductor-polymer nanocomposite' *Thin Solid Films* 476, (1) 190-195

Steppan D.D., Werner J., Yeater R.P. (1998) 'Essential regression and experimental design for chemists and engineers' [online] available from <http://geocities.com/SiliconValley/Network/1032/CGPage1.html> [20th April 2008]

Subramanian B., Ashok K., Kuppusami P., anjeevirajaC. S, and Jayachandran M.(2008) 'Characterization of reactive DC magnetron sputtered TiAlN thin films' *Cryst. Res. Technol*. 43, (10) 1078 – 1082

Trent E.M. and Wright P.K. (2000) *Metal Cutting (4th ed.)*, Woburn MA,: Butterworth-Heinemann

Tuffy K., Byrne G. and Dowling D. (2004) 'Determination of the optimum TiN coating thickness on WC inserts for machining carbon steels' *Journal of Materials Processing Technology* 155-156, 1861-1866

Voznesensky, V. A.(1974) *Experiment Planning Statistical Methods for Technical and Economical Investigations*, Moscow: Statistics.

Wachter R., Cordery A.(1999) 'Response surface methodology modelling of diamond like carbon film deposition' *Carbon* 37, 1529

Wang Da-Yung, Li Yen-Way, Chang Chi-Long, Ho Wei-Yu (1999) 'Deposition of high quality (Ti,Al)N hard coatings by vacuum arc evaporation process' *Surface and Coatings Technology* 114, 109–113

Wasa K., Kitabatake M., Adachi H. (2004) *Thin film materials technology: sputtering of compound materials, 2nd Edition*, New York: Elsevier Science & Technology Books

Weber F.-R., Fontaine F., Scheib M., Bock W. (2004) 'Cathodic arc evapouration of (Ti,Al)N coatings and (Ti,Al)NyTiN multilayer-coatings—correlation between lifetime of coated cutting tools, structural and mechanical film properties' *Surface and Coatings Technology* 177 –178, 227–232

Witthaut Mirjam , Cremer Rainer, Alexander von Richthofen , Neuschütz Dieter (1998) 'Improvement of the oxidation behavior of Ti1-xAlxN hard coatings by optimization of the Ti/Al ratio' *Fresenius J Anal Chem* 361, 639–641

Wuhrer R. and Yeung W. Y. (2002) 'A study on the microstructure and property development of d.c. magnetron co-sputtered ternary titanium aluminium nitride coatings' *Jornal of Materials Science* 37, 3477 – 3482

Wuhrer R. and Yeung W. Y. (2004) 'Grain refinement with increasing magnetron discharge power in sputter deposition of nanostructured titanium aluminium nitride coatings' *Scripta Materialia* 50, 813–818

Xu Xuan-qian, Ye Hui, Zou Tong (2006) 'Characterization of DC magnetron sputtering deposited thin films of TiN for SBN/MgO/TiN/Si structural waveguide' *J Zhejiang Univ SCIENCE A* 7, (3) 472-476

Yu Donghai, Wang Chengyong, Cheng Xiaoling and Zhang Fenglin (2008) 'Optimization of hybrid PVD process of TiAlN coatings by Taguchi method' *Applied Surface Science* 255, (5) 1865-1869

Zinatizadeh A.A.L., Mohamed A.R., Abdullah A.Z., Mashitah M.D., Isa M. Hasnain, Najafpour G.D. (2006) 'Process modeling and analysis of palm oil mill effluent treatment in an up-flow anaerobic sludge fixed film bioreactor using response surface methodology (RSM)' *Water Research* 40, 3193 – 3208

Bibliography

Maissel L. I. and Glang R.(1983) *Handbook of Thin Film Technology*, New York: McGraw-Hill

Bunshah R. F. (1994) *Handbook of Deposition Technologies for Films and Coatings Science, Technology and Applications*, New Jersey: Noyes Publications

Mattox D.M. (2003) *The Foundation of Vacuum Technology*, New York: Noyes/ William Andrew

Mattox, D. M. (1998) *Handbook of physical vapour deposition (PVD) processing*, N.Y.: Noyes Publications

Smith D.L. (1995) *Thin Film Deposition: Principle & Practice*, New York: McGraw Hill

APPENDICES

APPENDIX A

Nano-indenter hardness data

Average of six measurements

RUN	Hardness (GPa)	Reduced modulus of elasticity (Er) (GPa)
1	3.535069	290.1244
2	5.272038	331.6927
3	13.17336	320.078
4	10.96025	286.8991
5	8.059207	279.7471
6	4.329306	295.5836
7	4.039148	255.2914
8	16.11708	382.6003
9	7.768489	261.3774
10	3.532995	272.2843
11	9.763991	321.1017
12	7.482502	267.1579
13	15.25636	264.5339
14	8.908315	269.7343
15	22.63711	422.3693
16	14.14029	319.2773
17	8.883542	315.0782
18	15.68585	312.9719
19	11.26562	309.3299
20	12.33539	299.707

APPENDIX B

AFM coating surface roughness data

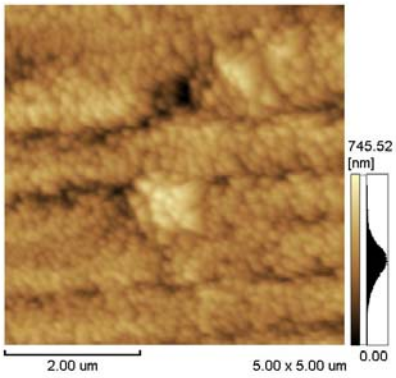

All Area		A		B	
LengthX	5.000[um]	LengthX		LengthX	
LengthY	5.000[um]	LengthY		LengthY	
Area	25.000[(um)2]	Area		Area	
Ra	62.122[nm]	Ra		Ra	
Ry	700.817[nm]	Ry		Ry	
Rz	380.421[nm]	Rz		Rz	
Rms	81.024[nm]	Rms		Rms	
Rp	336.177[nm]	Rp		Rp	
Rv	364.640[nm]	Rv		Rv	

Run 1

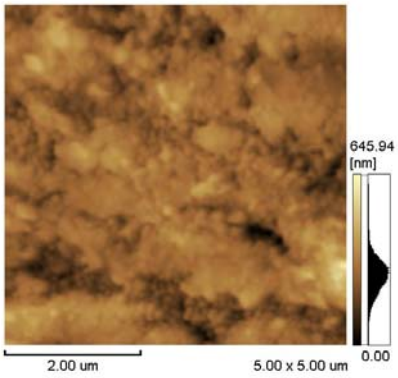

All Area		A		B	
LengthX	5.000[um]	LengthX		LengthX	
LengthY	5.000[um]	LengthY		LengthY	
Area	25.000[(um)2]	Area		Area	
Ra	51.063[nm]	Ra		Ra	
Ry	612.813[nm]	Ry		Ry	
Rz	264.833[nm]	Rz		Rz	
Rms	65.594[nm]	Rms		Rms	
Rp	351.146[nm]	Rp		Rp	
Rv	261.667[nm]	Rv		Rv	

Run 2

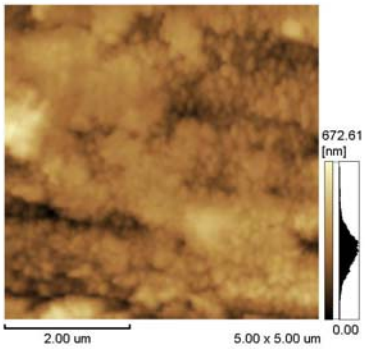

All Area		A		B	
LengthX	5.000[um]	LengthX		LengthX	
LengthY	5.000[um]	LengthY		LengthY	
Area	25.000[(um)2]	Area		Area	
Ra	63.636[nm]	Ra		Ra	
Ry	652.599[nm]	Ry		Ry	
Rz	279.336[nm]	Rz		Rz	
Rms	81.954[nm]	Rms		Rms	
Rp	353.447[nm]	Rp		Rp	
Rv	299.152[nm]	Rv		Rv	

Run 3

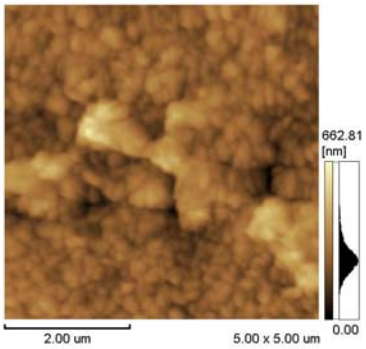

All Area		A		B	
LengthX	5.000[um]	LengthX		LengthX	
LengthY	5.000[um]	LengthY		LengthY	
Area	25.000[(um)2]	Area		Area	
Ra	52.175[nm]	Ra		Ra	
Ry	626.454[nm]	Ry		Ry	
Rz	246.871[nm]	Rz		Rz	
Rms	70.345[nm]	Rms		Rms	
Rp	367.331[nm]	Rp		Rp	
Rv	259.123[nm]	Rv		Rv	

Run 4

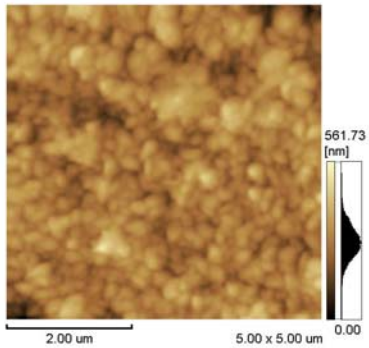 All Area A B LengthX 5.000[um] LengthX LengthX LengthY 5.000[um] LengthY LengthY Area 25.000[(um)2] Area Area Ra 46.421[nm] Ra Ra Ry 522.406[nm] Ry Ry Rz 420.528[nm] Rz Rz Rms 58.791[nm] Rms Rms Rp 246.954[nm] Rp Rp Rv 275.452[nm] Rv Rv	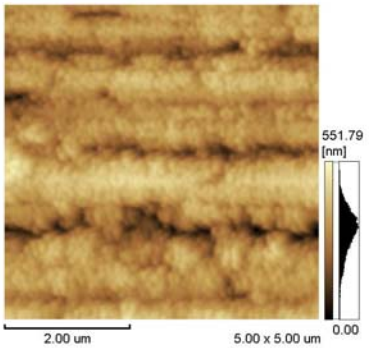 All Area A B LengthX 5.000[um] LengthX LengthX LengthY 5.000[um] LengthY LengthY Area 25.000[(um)2] Area Area Ra 59.558[nm] Ra Ra Ry 523.466[nm] Ry Ry Rz 255.027[nm] Rz Rz Rms 75.563[nm] Rms Rms Rp 215.408[nm] Rp Rp Rv 308.058[nm] Rv Rv
Run 5	Run 6
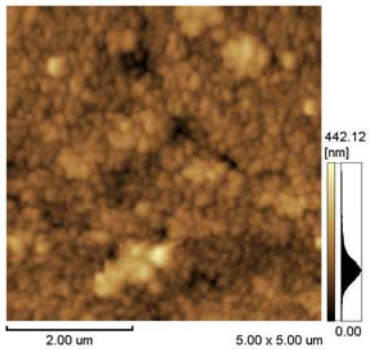 All Area A B LengthX 5.000[um] LengthX LengthX LengthY 5.000[um] LengthY LengthY Area 25.000[(um)2] Area Area Ra 32.362[nm] Ra Ra Ry 420.803[nm] Ry Ry Rz 237.018[nm] Rz Rz Rms 44.323[nm] Rms Rms Rp 271.645[nm] Rp Rp Rv 149.158[nm] Rv Rv	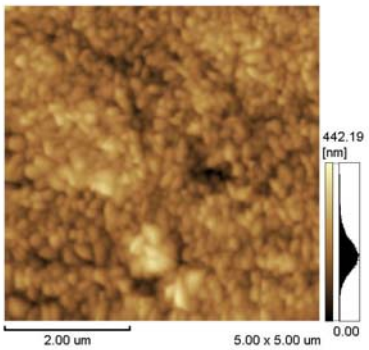 All Area A B LengthX 5.000[um] LengthX LengthX LengthY 5.000[um] LengthY LengthY Area 25.000[(um)2] Area Area Ra 37.193[nm] Ra Ra Ry 411.317[nm] Ry Ry Rz 242.550[nm] Rz Rz Rms 48.131[nm] Rms Rms Rp 224.187[nm] Rp Rp Rv 187.130[nm] Rv Rv
Run 7	Run 8

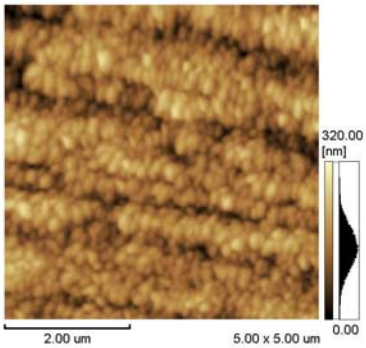 All Area A B LengthX 5.000[um] LengthX LengthX LengthY 5.000[um] LengthY LengthY Area 25.000[(um)2] Area Area Ra 35.056[nm] Ra Ra Ry 288.583[nm] Ry Ry Rz 230.461[nm] Rz Rz Rms 43.722[nm] Rms Rms Rp 143.421[nm] Rp Rp Rv 145.162[nm] Rv Rv	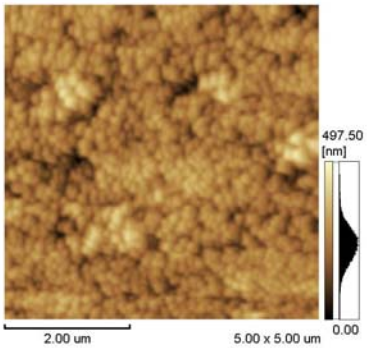 All Area A B LengthX 5.000[um] LengthX LengthX LengthY 5.000[um] LengthY LengthY Area 25.000[(um)2] Area Area Ra 44.144[nm] Ra Ra Ry 459.585[nm] Ry Ry Rz 361.638[nm] Rz Rz Rms 56.103[nm] Rms Rms Rp 223.726[nm] Rp Rp Rv 235.858[nm] Rv Rv
Run 9	Run 10
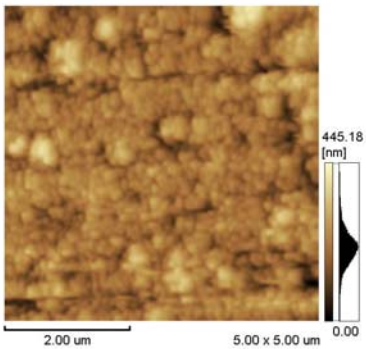 All Area A B LengthX 5.000[um] LengthX LengthX LengthY 5.000[um] LengthY LengthY Area 25.000[(um)2] Area Area Ra 38.115[nm] Ra Ra Ry 423.133[nm] Ry Ry Rz 373.872[nm] Rz Rz Rms 49.925[nm] Rms Rms Rp 214.614[nm] Rp Rp Rv 208.519[nm] Rv Rv	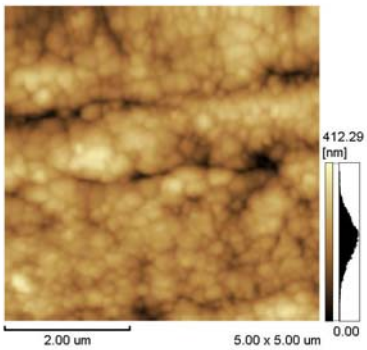 All Area A B LengthX 5.000[um] LengthX LengthX LengthY 5.000[um] LengthY LengthY Area 25.000[(um)2] Area Area Ra 44.250[nm] Ra Ra Ry 392.789[nm] Ry Ry Rz 240.453[nm] Rz Rz Rms 55.999[nm] Rms Rms Rp 178.112[nm] Rp Rp Rv 214.677[nm] Rv Rv
Run 11	Run 12

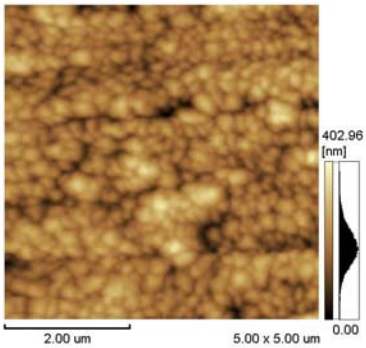

All Area	A	B
LengthX 5.000[um]	LengthX	LengthX
LengthY 5.000[um]	LengthY	LengthY
Area 25.000[(um)2]	Area	Area
Ra 38.746[nm]	Ra	Ra
Ry 379.483[nm]	Ry	Ry
Rz 249.822[nm]	Rz	Rz
Rms 49.106[nm]	Rms	Rms
Rp 192.971[nm]	Rp	Rp
Rv 186.512[nm]	Rv	Rv

Run 13

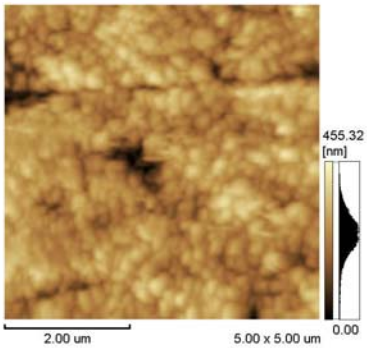

All Area	A	B
LengthX 5.000[um]	LengthX	LengthX
LengthY 5.000[um]	LengthY	LengthY
Area 25.000[(um)2]	Area	Area
Ra 45.038[nm]	Ra	Ra
Ry 422.104[nm]	Ry	Ry
Rz 312.042[nm]	Rz	Rz
Rms 57.870[nm]	Rms	Rms
Rp 175.374[nm]	Rp	Rp
Rv 246.730[nm]	Rv	Rv

Run 14

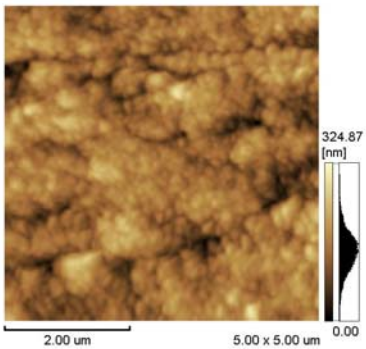

All Area	A	B
LengthX 5.000[um]	LengthX	LengthX
LengthY 5.000[um]	LengthY	LengthY
Area 25.000[(um)2]	Area	Area
Ra 31.809[nm]	Ra	Ra
Ry 302.275[nm]	Ry	Ry
Rz 158.129[nm]	Rz	Rz
Rms 40.190[nm]	Rms	Rms
Rp 158.552[nm]	Rp	Rp
Rv 143.723[nm]	Rv	Rv

Run 15

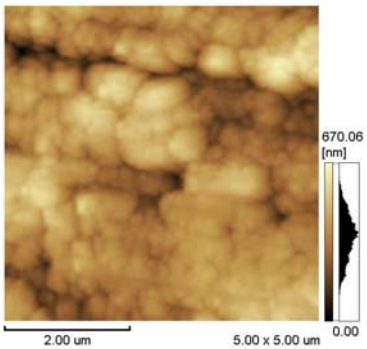

All Area	A	B
LengthX 5.000[um]	LengthX	LengthX
LengthY 5.000[um]	LengthY	LengthY
Area 25.000[(um)2]	Area	Area
Ra 80.517[nm]	Ra	Ra
Ry 650.977[nm]	Ry	Ry
Rz 309.435[nm]	Rz	Rz
Rms 100.018[nm]	Rms	Rms
Rp 287.500[nm]	Rp	Rp
Rv 363.477[nm]	Rv	Rv

Run 16

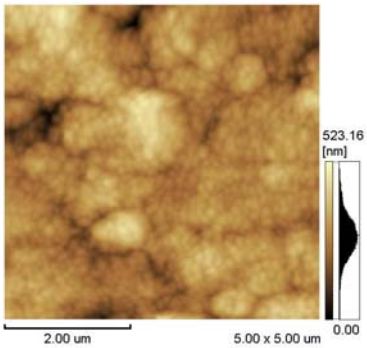

All Area	A	B
LengthX 5.000[um]	LengthX	LengthX
LengthY 5.000[um]	LengthY	LengthY
Area 25.000[(um)2]	Area	Area
Ra 52.697[nm]	Ra	Ra
Ry 500.690[nm]	Ry	Ry
Rz 385.160[nm]	Rz	Rz
Rms 67.318[nm]	Rms	Rms
Rp 222.789[nm]	Rp	Rp
Rv 277.902[nm]	Rv	Rv

Run 17

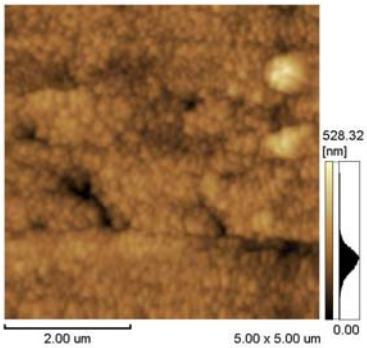

All Area	A	B
LengthX 5.000[um]	LengthX	LengthX
LengthY 5.000[um]	LengthY	LengthY
Area 25.000[(um)2]	Area	Area
Ra 34.906[nm]	Ra	Ra
Ry 491.802[nm]	Ry	Ry
Rz 253.016[nm]	Rz	Rz
Rms 47.368[nm]	Rms	Rms
Rp 294.204[nm]	Rp	Rp
Rv 197.598[nm]	Rv	Rv

Run 18

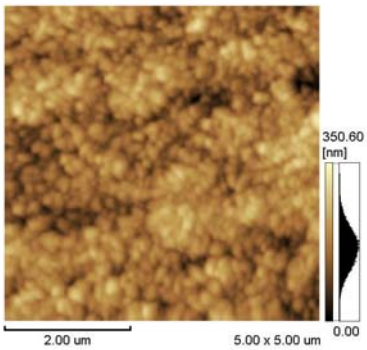

All Area	A	B
LengthX 5.000[um]	LengthX	LengthX
LengthY 5.000[um]	LengthY	LengthY
Area 25.000[(um)2]	Area	Area
Ra 36.174[nm]	Ra	Ra
Ry 329.596[nm]	Ry	Ry
Rz 162.758[nm]	Rz	Rz
Rms 45.035[nm]	Rms	Rms
Rp 166.084[nm]	Rp	Rp
Rv 163.511[nm]	Rv	Rv

Run 19

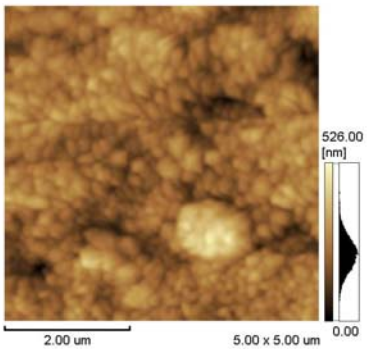

All Area	A	B
LengthX 5.000[um]	LengthX	LengthX
LengthY 5.000[um]	LengthY	LengthY
Area 25.000[(um)2]	Area	Area
Ra 49.009[nm]	Ra	Ra
Ry 506.750[nm]	Ry	Ry
Rz 311.075[nm]	Rz	Rz
Rms 63.594[nm]	Rms	Rms
Rp 280.273[nm]	Rp	Rp
Rv 226.476[nm]	Rv	Rv

Run 20

APPENDIX C

Flank wear measurement data

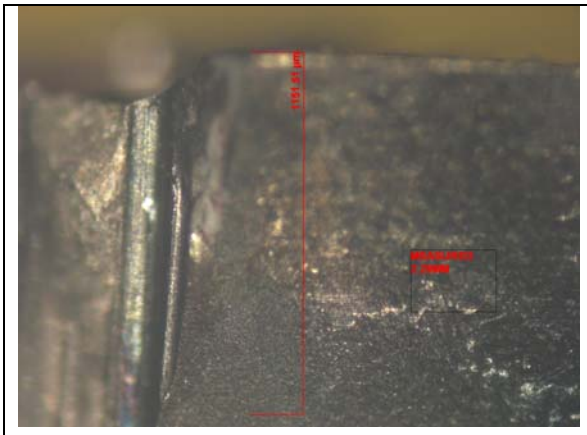	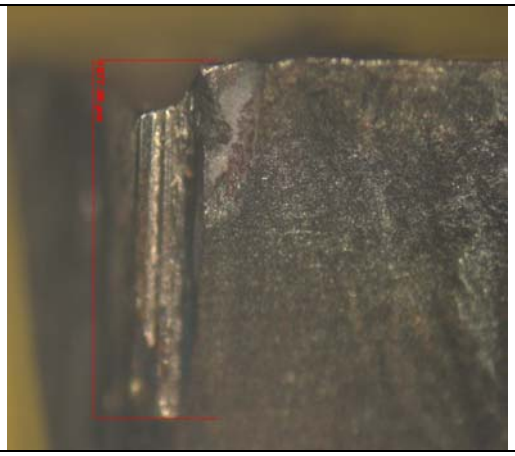
Run 1	Run 2
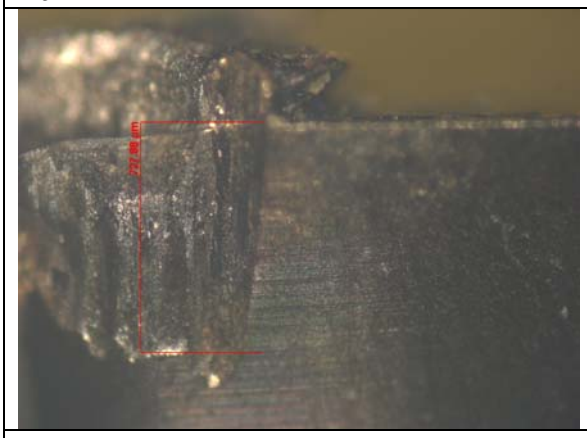	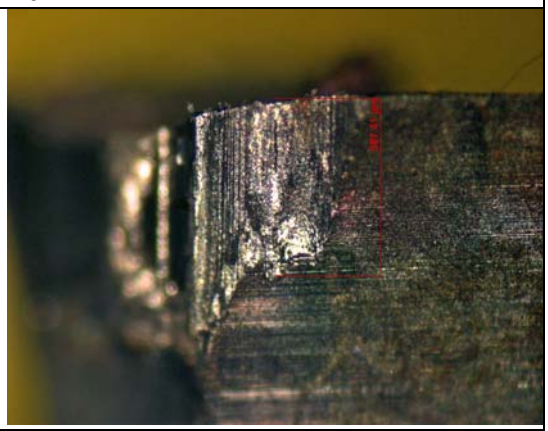
Run 3	Run 4
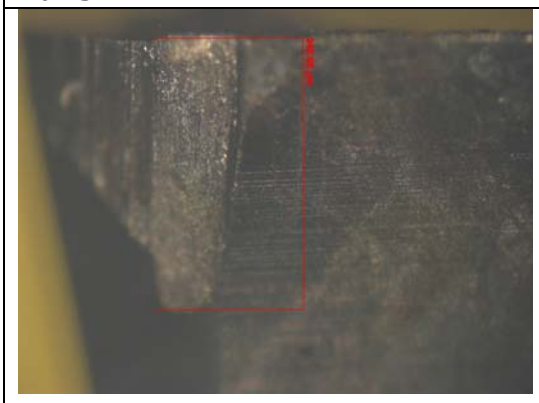	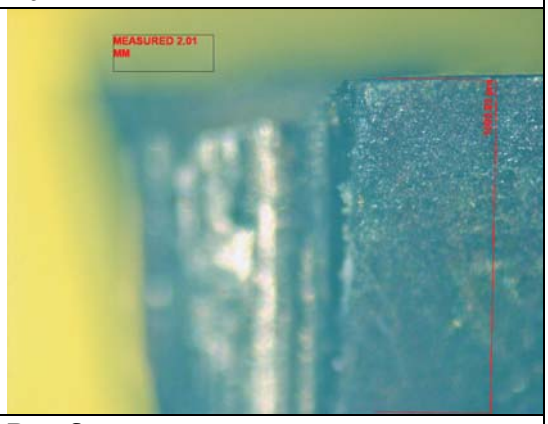
Run 5	Run 6

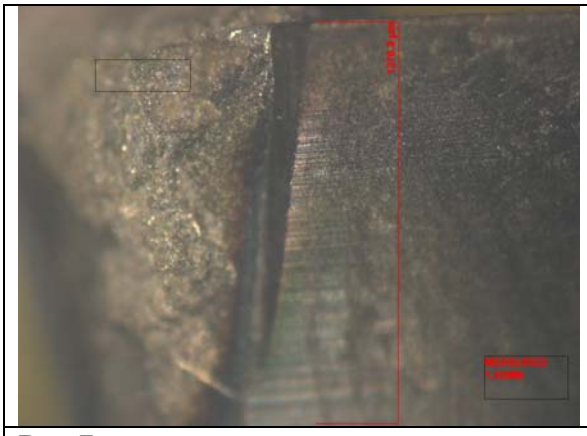	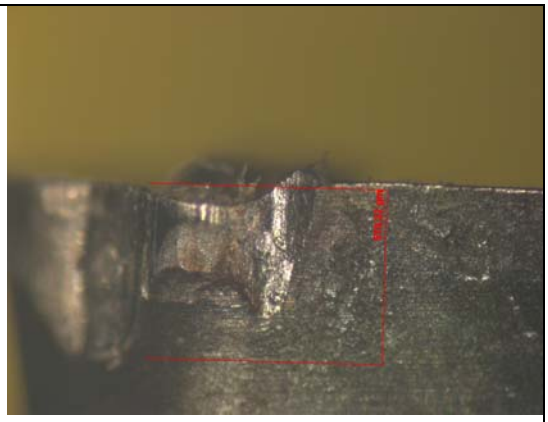
Run 7	Run 8
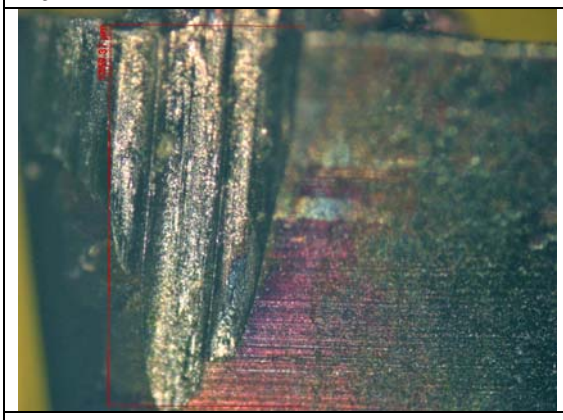	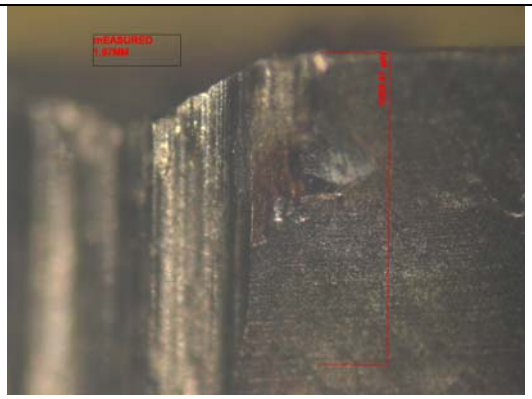
Run 9	Run 10
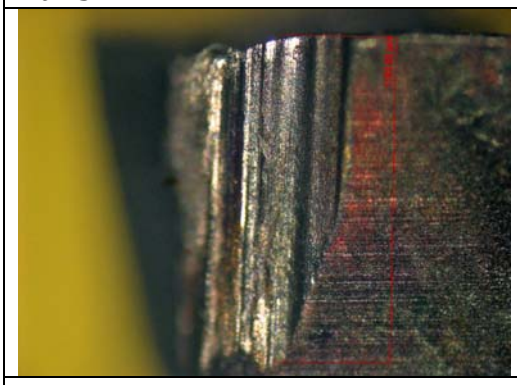	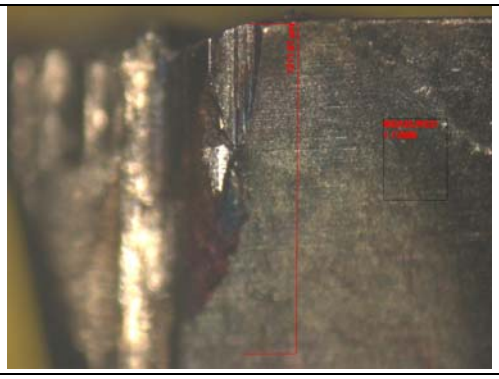
Run 11	Run 12

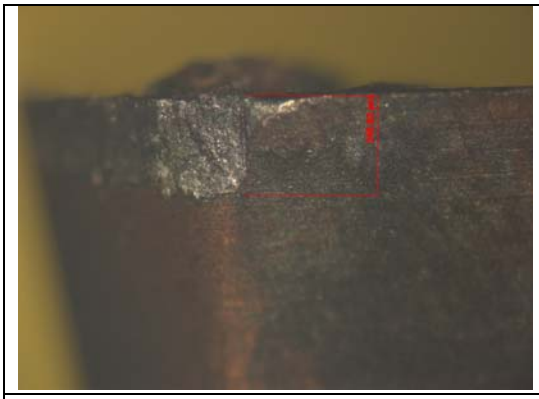	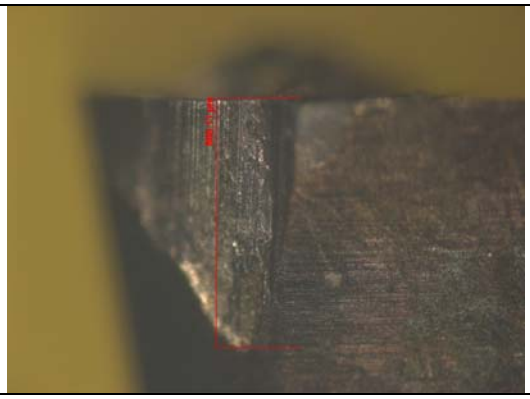
Run 13	Run 14
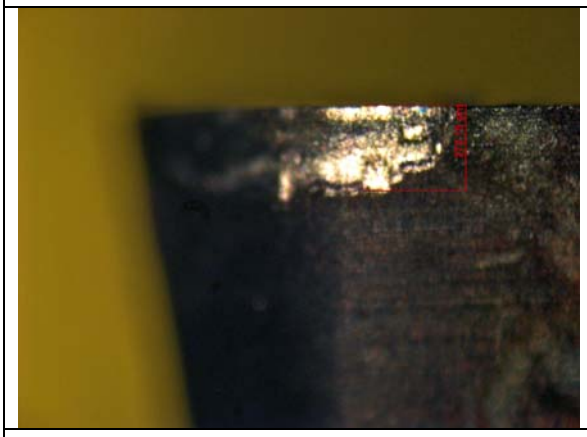	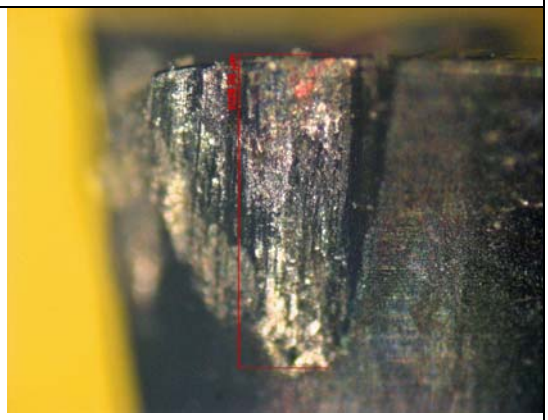
Run 15	Run 16
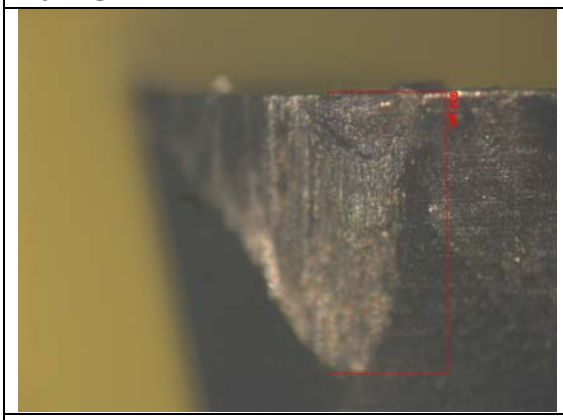	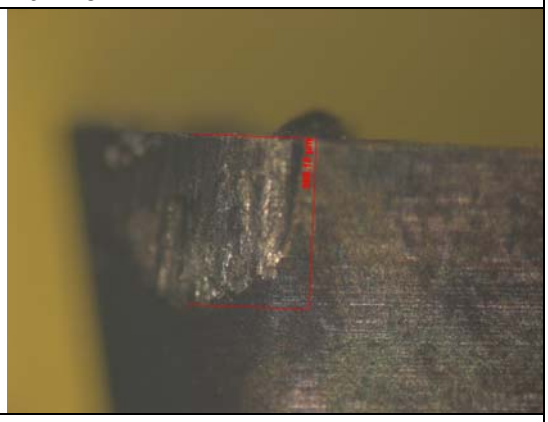
Run 17	Run 18

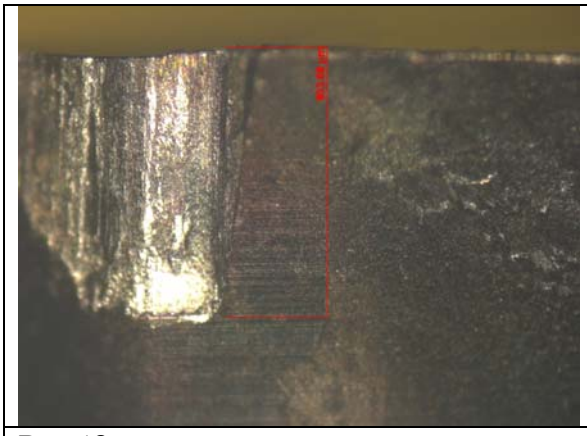	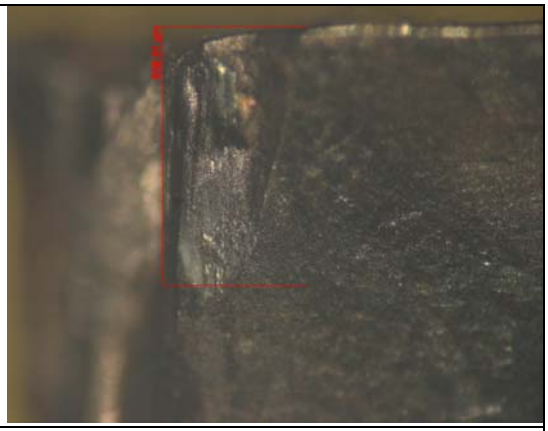
Run 19	Run 20

APPENDIX D

XRD DATA

	Crystal orientation	Pos. [°2Th.]	Height [cts]	FWHM [°2Th.]	d-spacing [Å]
Run 1	111	37.4997	40.65	0.1479	2.39841
	200	43.44	16.72	0.09	2.08321
Run 2	111	37.12	9	0.09	2.42206
	200	43.4	5	0.09	2.08504
Run 3	111	37.1631	54.91	0.3017	2.41935
	200	43.2766	35.4	0.1942	2.0907
Run 4	111	37.4628	17.7	0.3069	2.40069
	200	43.2607	84.8	0.3342	2.09143
Run 5	111	37.1662	33.48	0.2315	2.41916
	200	43.28	9	0.09	2.09054
Run 6	111	37.3221	127.7	0.2126	2.40941
	200	43.44	14	0.09	2.08321
Run 7	111	37.1916	34.92	0.3409	2.41756
	200	43.28	17	0.09	2.09054
Run 8	111	37.2967	52.85	0.7601	2.411
	200	43.56	5	0.09	2.07775

Run 9	Crystal orientation	Pos. [°2Th.]	Height [cts]	FWHM [°2Th.]	d-spacing [Å]
	111	37.08	3	0.09	2.42458
	200	43.3294	18.54	0.9446	2.08827
Run 10	Crystal orientation	Pos. [°2Th.]	Height [cts]	FWHM [°2Th.]	d-spacing [Å]
	111	37.2988	28.94	0.3149	2.41086
	200	43.4956	12	0.6822	2.08068
Run 11	Crystal orientation	Pos. [°2Th.]	Height [cts]	FWHM [°2Th.]	d-spacing [Å]
	111	37.1992	14.6	0.3881	2.41709
	200	43.4902	15.9	0.6043	2.08092
Run 12	Crystal orientation	Pos. [°2Th.]	Height [cts]	FWHM [°2Th.]	d-spacing [Å]
	111	37.28	12	0.9599	2.41204
	200	43.1629	13.3	0.3892	2.09594
Run 13	Crystal orientation	Pos. [°2Th.]	Height [cts]	FWHM [°2Th.]	d-spacing [Å]
	111	37.3004	10.7	0.1098	2.41076
	200	43.36	5.5	0.5042	2.08687
Run 14	Crystal orientation	Pos. [°2Th.]	Height [cts]	FWHM [°2Th.]	d-spacing [Å]
	111	37.3294	5.6	0.4603	2.40896
	200	43.4929	17.27	0.768	2.07908
Run 15	Crystal orientation	Pos. [°2Th.]	Height [cts]	FWHM [°2Th.]	d-spacing [Å]
	111	37.116	20.28	0.8672	2.42232
	200	43.3547	26.06	1.0209	2.08711
Run 16	Crystal orientation	Pos. [°2Th.]	Height [cts]	FWHM [°2Th.]	d-spacing [Å]
	111	37.4264	41.08	0.8227	2.40294
	200	43.4064	10.7	0.3309	2.08475
Run 17	Crystal orientation	Pos. [°2Th.]	Height [cts]	FWHM [°2Th.]	d-spacing [Å]
	111	37.4614	13.3	0.3643	2.40077
	200	43.6	8.1	0.6347	2.07594
Run 18	Crystal	Pos.	Height	FWHM	d-spacing

	orientation	[°2Th.]	[cts]	[°2Th.]	[Å]
	111	37.12	17.5	0.3562	2.42206
	200	*	*	*	*
Run 19	Crystal orientation	Pos. [°2Th.]	Height [cts]	FWHM [°2Th.]	d-spacing [Å]
	111	37.28	34.02	0.712	2.41204
	200	43.3436	9.31	0.4628	2.08762
Run 20	Crystal orientation	Pos. [°2Th.]	Height [cts]	FWHM [°2Th.]	d-spacing [Å]
	111	37.34	21.75	0.864	2.40631
	200	43.2479	7.91	0.482	2.09202

* No peak detected

APPENDIX E

EDX DATA

(% atomic number)

Run #	N	Al	Ti	Al/Ti
1	57.16	27.94	14.9	1.875168
2	56.99	23.93	19.085	1.253864
3	48.77	27.205	24.125	1.127668
4	40.54	26.69	32.76	0.814713
5	58.005	23.035	18.96	1.214926
6	58.21	24.8	16.99	1.459682
7	54.03	25.6	20.37	1.25675
8	42.26	30.13	27.61	1.091271
9	44.17	30.61	25.23	1.213238
10	44.9	31.93	23.16	1.37867
11	40.04	34.31	25.66	1.337101
12	47.07	25.54	27.39	0.932457
13	46.46	21.69	31.84	0.681219
14	49.96	26.25	23.79	1.103405
15	45.18	25.32	29.5	0.858305
16	43.93	28.26	27.82	1.015816
17	31.56	28.97	39.47	0.733975
18	50.71	21.51	27.73	0.775694
19	43.43	30.9	25.66	1.204209
20	43.18	29.87	26.95	1.108349